

Dissertation zur Erlangung des Doktorgrades
der Fakultät für Chemie und Pharmazie
der Ludwig-Maximilians-Universität München

Characterization of the SAM-key –
a conserved regulatory domain of the Fun30 nucleosome
remodeler



Leonhard Andreas Karl

aus

München, Deutschland

2022

Erklärung

Diese Dissertation wurde im Sinne von § 7 der Promotionsordnung vom 28. November 2011 von Frau Prof. Dr. Elena Conti betreut.

Eidesstattliche Versicherung

Diese Dissertation wurde eigenständig und ohne unerlaubte Hilfe erarbeitet.

München, 13.03.2023

Leonhard Karl

Dissertation eingereicht am 23.11.2022

1. Gutachterin: Frau Prof. Dr. Elena Conti
2. Gutachter: Herr Prof. Dr. Boris Pfander

Mündliche Prüfung am 01.03.2023

Substantial parts of this thesis are summarized and submitted for publication in Life Sciences Alliance:

Karl LA, Galanti L, Bantele SCS, Šafarić B, Rajappa L, Foster B, Bansal P, Metzner F, Chacin E, Basquin J, Duderstadt K, Kurat CF, Bartke T, Hopfner K, & Pfander B. **A SAM-key domain required for enzymatic activity and allosteric activation of the Fun30 nucleosome remodeler.** *Life Sci All (submitted)*

Contributions

This thesis comprises the work of my doctoral studies in the research group “DNA Replication and Genome Integrity” at the Max Planck Institute of Biochemistry (MPI-B, Martinsried), which was conducted between January 2018 and October 2022 under supervision of Prof. Dr. Boris Pfander.

The projects were performed in collaboration with other members of the research group and the MPI of Biochemistry Core Facilities.

Dr. Susanne C. S. Bantele (*Boris Pfander laboratory, MPI-B, Martinsried – present address: Jiri Lukas laboratory, Novo Nordisk Foundation Center for Protein Research, Copenhagen, Denmark*) laid the groundwork for this project and conducted the initial screening experiments for important parts of Fun30, including strain construction (see Table 3: *S. cerevisiae* strains), CPT spotting assays and ChIP-qPCR experiments (as seen in Fig. 6 A-C, 9 A-B, 10, 14).

Purification and labeling of histone octamers were performed by Lionel Rajappa and Barbara Šafarić (*Karl Duderstadt laboratory, MPI-B, Martinsried*) (used for preparing labelled nucleosomes, Fig. 11, 13, 15, 16, 23, 24). Nucleosome assembly and *in vitro* remodeling assays were carried out by myself.

Felix Metzner and Prof. Dr. Karl-Peter Hopfner (*Gene Center, LMU, Munich*) helped with structural overlays of Fun30 and other remodelers (Fig. 22).

The MPI-B Core Facilities (*MPI-B, Martinsried*) were involved in purification of SAM-key protein (Fig. 16, 24; Leopold Ulrich), performed the mass spectrometry and data analysis part of XL-MS (Fig. 12, 19, 20; Dr. Barbara Steigenberger), and helped with structure prediction using AlphaFold2 (Fig. 17, 18; Dr. Jérôme Basquin).

Table of Contents

SUMMARY	7
INTRODUCTION	8
1. Chromatin and nucleosome structure	8
How do nucleosomes form on DNA?	10
2. Nucleosome remodelers	10
3. Role of chromatin in the cellular response to a DNA double-strand break	12
4. Double-strand break repair pathways	13
5. DNA end resection	13
Chromatin in resection	14
6. Remodeling of DSBs	14
Early remodeling at DSBs	14
Late remodeling at DSBs.....	15
7. The Fun30-SMARCAD1-ETL family of nucleosome remodelers	15
8. Studying single-subunit remodelers	17
Objectives of the study	19
RESULTS	20
1. Multiple sequence alignment shows high conservation of the SNF2-type, two-lobed ATPase domain and another central region of Fun30	20
2. Region between 247-389 is crucial for Fun30 function	22
3. Structure prediction shows SAM-like helix bundle with elongated protruding alpha helix – termed SAM-key domain	23
4. Fun30 Δ SAM mutant (Fun30 Δ 275-436) generates a defect in resection and resistance to camptothecin	24
5. The SAM-key domain is required for Fun30's function in silencing	25
6. Establishment of a purification strategy for Fun30 from bacteria	26
7. Characterization of Fun30 Δ SAM mutant showed normal folding and stability	27
8. Fun30 Δ SAM is proficient in DNA and nucleosome binding	30
9. DDC1-Fun30 Δ SAM does not make cells hyper-resective	32
10. Fun30 Δ SAM is inactive	32
11. SAM-key <i>in trans</i> complementation is possible	35
12. AlphaFold2 modelling of Fun30 predicts hydrophobic interaction of SAM-key with ATPase domain – specifically with protrusion I	37
13. XL-MS data confirm AlphaFold2 model of Fun30 and position of the SAM-key close to protrusion I	38
14. Model comparison with other remodeler structures mostly lacks a structural analog for the SAM-key	42
15. Docking of the model to nucleosomes suggest SAM-key could be a functional and structural analog to post-HSA domain	44
16. The protrusion I-SAM-key interface is required for Fun30 remodeling activity	46
DISCUSSION	50
Mechanistic understanding of chromatin remodeling	50
Identification of the SAM-key as novel domain important for Fun30 function	50

SAM-like domain functions	51
Fun30 dimerization	51
Characterization of the Fun30 Δ SAM mutant	52
1. Folding and stability	52
2. DNA and nucleosome binding	53
3. Catalytic activity	53
3.1. The Fun30 SAM-key in nucleosome sliding and eviction	54
3.2. The Fun30 SAM-key in DNA-stimulated ATP hydrolysis	55
Structural analysis based on Fun30 AlphaFold2 model	56
1. Structural analogy of the SAM-key with post-HSA domains in other remodelers	56
2. A common structural regulatory hub in the catalytic subunits of chromatin remodelers	57
3. XL-MS confirms Fun30 model and suggests SAM-key interacts with protrusion I	58
4. Mutation of the SAM-key-protrusion I interface phenocopies Fun30 Δ SAM	59
5. Fun30 docking to the nucleosome according to nucleosome-remodeler co-structures	60
Model: Fun30 SAM-key allosterically activates ATPase domain	61
Beyond the scopes of the project	64
Application of knowledge from Fun30 regulation to improve genome editing	64
Application of knowledge from Fun30 regulation for development of disease and cancer treatments	64
 MATERIAL AND METHODS	 65
 REFERENCES	 93
 APPENDIX	 105
Abbreviations	105
Prefixes and units	106
Amino acid abbreviations	106
ACKNOWLEDGEMENTS	108
CURRICULUM VITAE	110

Summary

Cells need to constantly access their genetic material. However, in eukaryotic cells, DNA is compactly wrapped around nucleosomes and their presence poses a barrier for DNA transactions. To facilitate access, eukaryotes use ATP-driven molecular machines that dynamically shape chromatin structure, called nucleosome remodelers.

Budding yeast Fun30 is the prototype member of the Fun30-SMARCAD1-ETL sub-family of nucleosome remodelers important for DNA repair and gene silencing. While the catalytic mechanism has been elucidated for several remodelers, for this family of single-subunit remodelers we lack mechanistic understanding.

Here we report the discovery of the SAM-key, an evolutionary conserved domain with a sterile alpha motif (SAM)-like fold with one characteristic, long, protruding helix, using structure prediction, multiple sequence alignment and biochemical characterization.

The SAM-key is crucial for Fun30 function, as deletion of the SAM-key from *FUN30* in budding yeast leads to DNA repair and gene silencing defects similar to a deletion of *FUN30*. Biochemical and biophysical characterization of the SAM-key mutant *in vitro* showed similar folding and stability as wildtype Fun30 as well as wildtype-level binding to DNA and nucleosomes. However, the mutant is deficient in DNA-stimulated ATP hydrolysis as well as nucleosome sliding and eviction. Structure prediction using AlphaFold2 models interaction of the long helix of the SAM-key with protrusion I, a structural element of the conserved 2-lobed ATPase domain that controls catalytic activity in other remodelers. We verified the model and the interaction by crosslinking-mass spectrometry and mutation of the interface with a double point mutant Fun30-ICRR, which phenocopies the SAM-key deletion with defective ATPase activity and nucleosome remodeling. This confirms a regulatory role for the interaction of the SAM-key helix with protrusion I.

Our data thereby demonstrate a central role of the SAM-key domain in mediating the activation of Fun30 catalytic activity, a new insight into the biology of this protein and highlighting the importance of allosteric activation for nucleosome remodelers.

Introduction

1. Chromatin and nucleosome structure

In eukaryotic cells the genetic material is stored inside the nucleus. A diploid human genome with approximately 6 billion base pairs, each 0.34 nanometers long, corresponds to a total of about 2 meters of DNA, while the average nucleus of a human cell has a diameter of about 6 micrometers (Alberts et al., 2002). To achieve the necessary compaction, DNA forms a macromolecular complex with proteins called chromatin. It was discovered first in the late 19th century by Walther Flemming, one of the founders of the field of cytogenetics, and because of its propensity to strongly absorb basophilic dyes, he named the structure chromatin from chroma (Greek) for color.

Since then, we know much more about chromatin: A DNA macromolecule is complexed with specific proteins, called histones. Histones are small, positively charged proteins that form nucleosomes with DNA: Eight histones forming a histone octamer, consisting of two molecules of histones H2A, H2B, H3 and H4, and about 147 base pairs of DNA, that is wrapped 1.65 times around the octamer to form one nucleosome – the basic subunit of chromatin (Oudet et al., 1975). This basic subunit is repeated 100,000-fold along the DNA. Further compaction of the DNA is achieved by histone H1, that binds with about 20 bp of linker DNA – between two neighboring nucleosomes – and completes the second full turn of DNA around the histone octamer.

In vitro, short nucleosome strings (also termed 10-nm chromatin fibers) are folded into a spiral-fiber with diameter of 30 nanometers (Hansen, 2002; Tremethick, 2007). Based on this it has long been assumed that also *in vivo* this 30-nm fiber is formed first and this fiber twists to form bigger loops, which form even bigger spiral-fibers and in the end form the compact DNA-protein-complex that fits into the nucleus (Annunziato, 2008).

However, the existence of such 30-nm fibers could only be shown for certain cell types, like chicken erythrocytes (Nishino et al., 2012), but not for human mitotic chromosomes (Eltsov et al., 2008; Fussner et al., 2011; Maeshima et al., 2010; Nishino et al., 2012). The alternatively suggested model is packaging of 10-nm chromatin fibers in a fractal organization, a similar compaction mode, by forming larger loops and spirals out of smaller loops and spirals, but not relying on the existence of the 30-nm fiber (Fussner et al., 2011; Hansen, 2012; Nishino et al., 2012).

The first high-resolution X-ray structure of the nucleosome, the basic subunit of chromatin, was solved by Karolin Luger in 1997: It showed 146 bp of DNA wrapped around the histone octamer 1.65 times in a super-helix (Fig. 1 A-B, (Luger et al., 1997).

Therefore, DNA locations on the nucleosome are specified by their superhelical location (SHL), with SHL0 defined with the central base pair at the nucleosome dyad – a pseudo-symmetry axis (Fig. 1 C). Consecutive SHLs are each one superhelical turn (10bp) away from the dyad and range from SHL-7 (direction of entry DNA) to SHL7 (exit DNA).

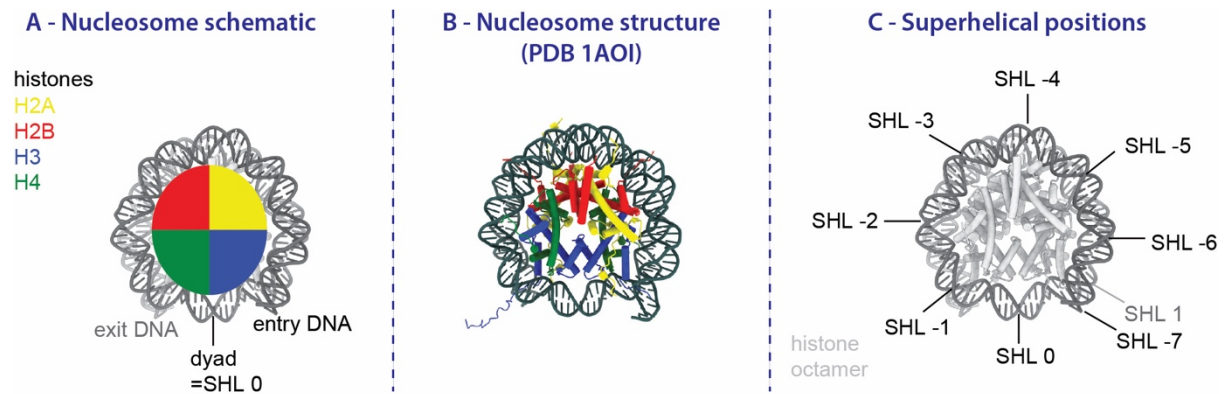


Figure 1: The nucleosome

A: Schematic of a nucleosome as a disc on which DNA is wrapped 1.65 times. Colors of the circle indicate the four different histones H2A in yellow, H2B in red, H3 in blue, H4 in green and their approximate position on the nucleosome surface. Entry DNA, nucleosome dyad and exit DNA indicated.

B: *Xenopus laevis* nucleosome structure (PDB 1AOI, (Luger et al., 1997)), histone colors as in A.

C: Superhelical positions on the nucleosome. Top view of a nucleosome structure (PDB 7OHC), histone octamer in grey. Superhelical locations (SHL) denominate DNA positions one full helical turn (10 bp) away from the pseudo-symmetry-axis at the dyad. Numbers indicate position relative to the nucleosome dyad (SHL 0) in direction of entry DNA with negative numbers (SHL -1 – SHL -7) and in direction of exit DNA with positive numbers (SHL 1 – SHL 7). For clarity only SHL -7 to SHL 1 are indicated.

This structure of a frog (*Xenopus laevis*) nucleosome core particle (PDB 1AOI) and later structures of yeast, fly and human nucleosomes (Clapier et al., 2008; Luger et al., 1997; Tsunaka et al., 2005; White et al., 2001) gave important insights:

First, size and shape of the nucleosome: It is overall disk-shaped with an overall diameter of approximately 100 Å and height ranging from ~25-60 Å, with one Ångström (Å) equal to 0.1 nanometer. However, the N-terminal tails of the histone proteins do not form part of the disk but protrude either from the surface outside the DNA (H2A, H4) or between the DNA (H2B, H3).

Second, surface area and charge: The DNA phosphate backbone presents a highly negative electrostatic surface. In addition to that the so-called acidic patch on the disk-surface of the nucleosome presents another negatively charged surface, consisting of acidic residues of histones H2A and H2B. In contrast, the protruding histone tails carry a strong positive charge.

Third, conservation: structural features and architecture are highly similar between nucleosomes from yeast, fly, frog or man.

Further research discovered that chromatin is by far not only important for packaging of DNA, but also for regulating DNA transactions: Pioneering studies by Vincent Allfrey showed that histones can be post-translationally modified (Allfrey et al., 1964), and the authors speculated about a role in regulating RNA synthesis.

Decades later, the nucleosome structure brought insights on how post-translational modifications (PTMs) could affect chromatin structure: 8 amino-(N)-terminal and 2 carboxy-(C)-terminal tails of the histone proteins protrude from the nucleosome structure at defined locations and contact other nucleosomes. Chemical modification of the properties of these tails would alter nucleosome-nucleosome interactions and thereby overall chromatin architecture (McGinty and Tan, 2015).

Aside from the core histones H2A, H2B, H3 and H4, there are several histone variants whose incorporation in the nucleosome change its properties. One example is histone H2A.Z, a variant of H2A, which has an

extended acidic patch and compared to a canonical nucleosome displays slight destabilization of the nucleosome (Santisteban et al., 2000).

How do nucleosomes form on DNA?

At physiological conditions, DNA and histones tend to form insoluble aggregates when mixed. So-called histone chaperones bind to free histones, histone dimers or tetramers and prevent their premature interactions with DNA.

In vivo, replication-coupled nucleosome assembly is suggested to work in two steps: (H3–H4)₂ tetramers are deposited onto DNA first, and then H2A–H2B dimers are added with help of so-called histone chaperones (Nap1) and chromatin assembly factors (CAF-1, ACF) (Nakagawa et al., 2001; Smith and Stillman, 1991).

In vitro, the salt-gradient dialysis method allows nucleosome reconstitution on DNA (Dyer et al., 2004; Luger et al., 1999). This method exploits the fact, that two H3–H4 dimers form a tetramer, both in presence and absence of DNA, and with two H2A–H2B dimers they form a histone octamer. However, the octamer is only stable in presence of DNA or when the charges are otherwise neutralized, in this case using high salt conditions. Under high salt conditions a histone octamer can be formed, then DNA can be added and while gradually decreasing the salt concentration nucleosomes will form.

To know the exact position of nucleosomes assembled *in vitro*, the Widom 601-nucleosome positioning sequence (Lowary and Widom, 1998) is commonly used. The Widom 601 sequence was found in a screen for DNA sequences with high affinity to the histone octamer. It displays strong nucleosome positioning and high yields in nucleosome reconstitution experiments which is why it is commonly used among chromatin researchers.

To date, many studies have uncovered an ever-increasing number of histone modifications and their influence on seemingly all DNA metabolic processes:

Chromatin is therefore critical to regulate the activity of the DNA molecule. This happens on the one hand by the formation of compartments known as euchromatin (open, active form of chromatin) or heterochromatin (dense and inaccessible form of chromatin), and on the other hand by additional epigenetic regulation. Epigenetics is a term summarizing a whole variety of modifications that regulate DNA transactions. In a nutshell, epigenetic modifications of DNA and histones regulate accessibility of genes, regulatory DNA elements and entire genomic regions (eu- and heterochromatin), helping to maintain a stable genome as well as expression of only the required subset of genes for the respective cell type (Bannister and Kouzarides, 2011; McGinty and Tan, 2015).

2. Nucleosome remodelers

Vital cellular processes like replication or transcription require polymerases to access the two strands of DNA apart from each other. However, the presence of nucleosomes poses a barrier for these crucial processes, so cells need to have the means to open up this condensed genetic information. For this, eukaryotes have enzymes called nucleosome remodelers (also known as chromatin remodelers): ATP-driven molecular machines that have the ability to dynamically shape chromatin structure.

Nucleosome remodelers belong to the superfamily 2 (SF2) of DNA translocases related to DNA helicases and as such undergo conformational changes when binding and hydrolyzing ATP while at the same time altering DNA-histone contacts (Becker and Workman, 2013; Clapier et al., 2017). In this way, remodelers can catalyze sliding, positioning and eviction of nucleosomes or edit nucleosomes by exchanging histones (Fig. 2). To catalyze specific remodeling reactions, like sliding nucleosomes or exchanging histones, additional interactions with DNA and histone proteins are necessary, for example at the nucleosome acidic patch (Clapier et al., 2017; Dao and Pham, 2022).

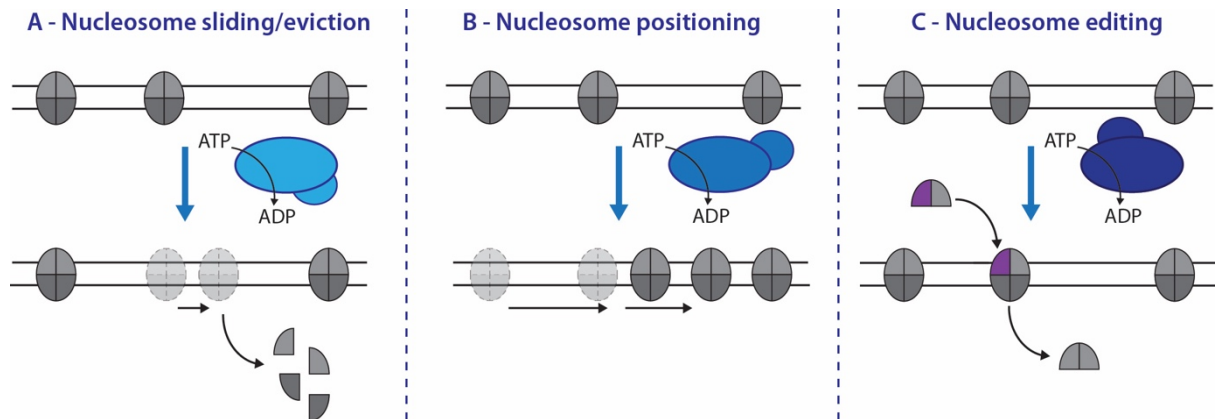


Figure 2: Activities of nucleosome remodelers (figure modified from Karl et al., 2022)

A: Nucleosome sliding/eviction: Nucleosomes (grey) are moved along DNA and/or evicted by a nucleosome remodeler (blue) in ATP-dependent manner. Color scheme continuous throughout the figure.

B: Nucleosome positioning: Nucleosomes are moved along DNA into a specific position, often to form a nucleosome array with regular spacing between nucleosomes, in ATP-dependent manner.

C: Nucleosome editing: Histone dimers in the nucleosome are exchanged with histone dimers that for example contain a histone variant (purple) in ATP-dependent manner.

Remodelers additionally require elements for specific recruitment and elements to regulate their activity in different chromatin regions. For this, many remodelers form large, multi-subunit complexes with subunits that are sometimes shared with other complexes.

Traditionally, they are sorted into one of four main families categorized based on the similarities and differences of the catalytic ATPase subunits, including chromodomain helicase DNA-binding (CHD1), INOsitol requiring 80 (INO80), imitation switch (ISWI) and switch/sucrose non-fermentable (SWI/SNF) (Clapier and Cairns, 2009). Phylogenetic analysis based on sequence conservation showed the existence of additional sub-families (Flaus et al., 2006), including the Ino80-related Fun30-SMARCAD1-ETL family, present in all eukaryotes, and some families not found throughout eukaryotes, like ALC1 or CHD7.

The current scientific consensus is that each family has specialized functions within the cell. SWI/SNF remodelers, for example SWI/SNF and RSC complexes, slide and eject nucleosomes thereby establishing nucleosome-depleted regions (Badis et al., 2008) and position the +1 nucleosome for transcription initiation (Angus-Hill et al., 2001). ISWI remodelers (Isw1a, Isw1b and Isw2 complexes), CHD1 and INO80-C position nucleosomes and create nucleosomal arrays with fixed distances (Lieleg et al., 2015). INO80 family chromatin remodelers, INO80 and SWR1, play a role in nucleosome editing by exchanging histone variants (Clapier and Cairns, 2009; Clapier et al., 2017). The remodeling mechanism of the Fun30-SMARCAD1-ETL sub-family is still elusive, but a key role of the enzymes in promoting long-range DNA end resection, a decisive step in repair pathway choice at DNA double-strand breaks, is conserved from yeast Fun30 to human SMARCAD1 (Chen et al., 2012; Costelloe et al., 2012; Eapen et al., 2012).

3. Role of chromatin in the cellular response to a DNA double-strand break

Genomic DNA is the most important biomolecule of the cell – all others – like RNA or proteins – are built from the information it contains, so it must be well-protected against damage and information loss. This is challenging since the DNA needs to be accessible for metabolic processes such as transcription and therefore is exposed from its protective chromatin packaging (Takata et al., 2013). Especially exposed DNA is vulnerable to DNA damage, which can cause mutagenesis and loss of genetic information, which can be correlated with ageing and disease (Kennedy et al., 2012; Lodato et al., 2018).

Persistent DNA damage can finally result in genomic instability, one of the established hallmarks of cancer (Hanahan, 2022; Hanahan and Weinberg, 2000; 2011).

Thus, fast and error-free DNA repair and maintenance of genome stability is crucial to ensure healthy survival. This is underlined by the connection between malfunctioning DNA repair systems and human diseases like Xeroderma pigmentosum or Fanconi anemia, which are characterized by premature ageing (progeria) and/or predisposition to cancer (O'Driscoll, 2012).

Out of different types of DNA lesions, the complete disruption of both phosphodiester-backbones of the DNA double helix – a double-strand break (DSB) – is seen as most severe form of damage. It can lead to loss of large amounts of genomic information – like entire chromosome arms – or dramatic genomic rearrangements (translocations, mis-guided recombination), in order to prevent the information loss (Pfeiffer, 1998).

DSBs can have exogenous and endogenous origins:

Exogenous origins of DNA breaks can be ionizing radiation, which can generate DNA breaks either directly or by producing free water radicals (Sonntag, 2006). Ultraviolet (UV) radiation can cause either nucleobase photo-products or DSBs at sites of clustered oxidative lesions (Greinert et al., 2012; Sinha and Häder, 2002).

Endogenous origins of damage can be caused by metabolic processes, for example by producing reactive oxygen species (Cadet and Wagner, 2013; Ohshima et al., 1999) or errors during DNA replication (Lindahl, 1993).

Some DSBs are also actively generated by endogenous enzymes, for example in mammalian B- or T-cells DSBs are induced as part of V(D)J recombination of antibody segments (Arya and Bassing, 2017) or in yeast cells a DSB at the MAT locus is critical for the switching of mating type cassettes (Haber, 2012).

No matter how these lesions arise, the genome is constantly checked for damage by a network of damage recognition and repair enzymes, called DNA damage response (DDR). In brief, DNA damage checkpoints operate throughout the cell cycle, detect lesions and act by locally assembling a signaling network, arresting cell cycle progression, upregulating DNA repair and, if the damage cannot be instantly repaired, they trigger apoptotic cell death (Zhou and Elledge, 2000).

Around the damage site, checkpoint kinases Mec1 and Tel1 (yeast homologs of ATR and ATM respectively) phosphorylate histone H2A at serine 129, then called γ H2A in yeast or γ H2A.X in mammals (Downs et al., 2000; Nakamura et al., 2004; Paull et al., 2000; Redon et al., 2002). In yeast, γ H2A spreads about 40

kb from the break site (Shroff et al., 2004). γ H2A then serves as recruitment platform on damaged chromatin for repair factors (Li et al., 2012; Ohouo et al., 2013).

4. Double-strand break repair pathways

Repair of DSBs mainly follows one of several repair pathways: Homologous recombination (HR) or canonical non-homologous end-joining (cNHEJ) are historically viewed to be the canonical pathways and evolutionary conserved (reviewed in Aylon and Kupiec, 2004; Scully et al., 2019). Since in this study the budding yeast *S. cerevisiae* is used as a model system, here the yeast terminology is used. The Ku complex (Yku70/80) recognizes the ends of a DSB and the MRX complex (Mre11, Rad50, Xrs2) is recruited for end processing. In NHEJ processed ends are ligated back together by Dnl4-Lif1, however through processing of DSB ends this process is rarely error-free and often deletions are observed. For this reason, when there is a homologous template, to copy any missing information and repair the damage in an error-free manner, repair by HR is preferred. Repair by HR is initiated by nucleolytic degradation of the 5' strands from the DSB ends to yield 3' single-stranded DNA (ssDNA), a process referred to as DNA end resection. Resection is initiated by the MRX complex together with Sae2 and more extensive resection is carried out either by the helicase complex Sgs1-Top3-Rmi1 (STR) together with nuclease Dna2 or by the 5'-3' exonuclease Exo1. Single stranded DNA is bound by Replication protein A (RPA) that protects the ssDNA and activates the DNA damage checkpoint via Mec1/Ddc2, checkpoint mediator Rad9 and effector kinase Rad53.

RPA is subsequently displaced by Rad51 to form a nucleoprotein filament that carries out homology search and strand invasion. The homologous sequence is then used as a template for DNA synthesis and finally the recombination structure is resolved, the newly synthesized DNA re-annealed and ligated, leading to error-free break repair. Notably, during the process of resection the substrate for repair by NHEJ is destroyed, making it a decisive step in pathway choice, that is therefore tightly controlled by the cell cycle, switching on resection only in cell cycle phases, in which the sister chromatid is present as repair template for HR (S, G2, M). In principle, in diploid cells the homologous chromosome can be used as template for HR, however this not favoured, since it could lead to loss of heterozygosity.

Both repair by NHEJ and HR have mutagenic potential: End-joining to a different DNA end, like an unprotected telomer or a different DSB leads to translocations. If nucleolytically processed ends are ligated back together that can cause deletions and frameshifts in the genetic code. While HR is less error-prone when a repair template is present, in absence of a template resected genetic material cannot be restored by recombination and is lost. Without donor sequence, also mis-targeted recombination events occur, that can cause global mutagenic events like translocations or gross chromosomal rearrangements, both typical features of cancer cells (Bunting and Nussenzweig, 2013).

5. DNA end resection

As decisive step in pathway choice, DNA end resection is tightly controlled and happens in consecutive steps (reviewed in Cejka and Symington, 2021): First MRX together with CDK-phosphorylated and thus cell-cycle regulated Sae2 nicks the 5' terminated strand in some distance from the break end. In the current model of bidirectional resection, resection starts in two directions from the nick: MRX mediates so-called short-range resection for hundreds of base pairs using its endonuclease activity to generate the initiating nick and its 3'-5'-exonuclease activity to resect towards the DSB. Long-range resection machineries

Exo1/STR-Dna2 resect for tens of thousands of base pairs into chromosomal DNA with 5'-3-exonuclease activity.

However, genomic DNA is densely packed chromatin, so for all processing and repair one needs to take into account that nucleosomes are present on the DNA.

Chromatin in resection

We summarized the current knowledge on influence of chromatin and nucleosome remodeling on the DNA DSB repair in a review article (Karl et al., 2022). Long-range resection nucleases are directly inhibited by the presence of nucleosomes on their substrate. Biochemical studies with a reconstituted resection system with yeast proteins showed that Exo1 is unable to resect a DNA substrate covered with nucleosomes. Interestingly, incorporation of histone H2A variant H2A.Z (Htz1) into nucleosomes results in decreased nucleosome stability (Abbott et al., 2001; Jin and Felsenfeld, 2007; Lewis et al., 2021; Watanabe et al., 2013; Zhang et al., 2005) which could be sufficient for nucleosome bypass by Exo1 since it seems to enhance Exo1-dependent resection both *in vitro* and *in vivo* (Adkins et al., 2013). Also the second long-range resection machinery, STR-Dna2, is inhibited by nucleosomes and requires a sufficient nucleosome-free DNA overhang of about 300 bp to resect through a nucleosomal substrate (Adkins et al., 2013). In addition to that, resection initiation by MRX nicking is predominantly found within nucleosome-free linker DNA, suggesting protection of nucleosomal DNA and/or substrate binding by MRX is influenced by nucleosomes (Mimitou et al., 2017; Wang et al., 2017).

This already shows a direct role of nucleosomes in regulating resection, but in chromatin also additional proteins can be recruited, for example through histone modifications, that stimulate or repress resection/repair. For example, checkpoint mediator protein Rad9, as well as its human homolog 53BP1, bind to modified histones after DNA damage and block resection.

In sum, nucleosomes are a barrier to the activity of resection nucleases and chromatin-bound factors influence resection, thus nucleosome remodelers are required to facilitate chromatin resection and regulate DSB repair.

6. Remodeling of DSBs

Consistent with the need for nucleosome remodeling, several remodelers have been localized to DSBs (Bantele et al., 2017; Bennett and Peterson, 2015; Chen et al., 2012; Downs et al., 2004; Lademann et al., 2017; Morrison et al., 2004; Shim et al., 2005; 2007; Tsukuda et al., 2005; van Attikum et al., 2004; 2007).

Early remodeling at DSBs

SWI/SNF and RSC are specifically recruited to DSBs (Bennett and Peterson, 2015; Bennett et al., 2013; Chai et al., 2005; Liang et al., 2007; Shim et al., 2005; 2007; Wiest et al., 2017) and interfering with their function causes a defect at the level of association of the MRX complex with DSBs (Shim et al., 2007; Wiest et al., 2017) indicating a role in the early stage of DSB remodeling.

RSC recruitment to DSBs happens within 10 minutes after break induction via a so far unknown signal and even precedes resection initiation (Chai et al., 2005). In contrast, SWI/SNF recruitment is slower and dependent on histone modification, especially acetylation, that is recognized by bromodomains in SWI/SNF remodelers (Bennett and Peterson, 2015; Cheng et al., 2021). Notably, it has recently been shown, that histone acetyltransferase NuA4 is specifically recruited to DSBs in MRX-dependent manner and that combined action of NuA4 and the SAGA complex, another histone acetyltransferase, is essential for DNA end resection (Cheng et al., 2021).

Interestingly however, resection was not fully abolished in these systems with deletion or conditional depletion of single subunits of either RSC or SWI/SNF. In contrast, resection is blocked in a double mutant suggesting redundancy of the two remodelers (Peritore et al., 2021). Of special note, in that system both resection and nucleosome eviction are blocked, indicating that nucleosome eviction and resection are intrinsically coupled.

Additionally, there is SWR1 recruitment to DSBs (Morillo-Huesca et al., 2010; van Attikum et al., 2007) as well as a transient H2A.Z increase in chromatin around the break site shortly after DSB induction (Kalocsay et al., 2009). This suggests the SWR1 complex incorporates histone variant H2A.Z containing dimers into nucleosomes around DSBs.

Late remodeling at DSBs

The block of the long-range resection nucleases by nucleosomes (Adkins et al., 2013) points toward long-range resection being dependent on nucleosome eviction. Consistent with this, also long-range resection appears to be stimulated by SWI/SNF (Wiest et al., 2017), however whether this stimulation depends on nucleosome eviction remains to be shown.

The INO80 complex is also recruited to DSBs (Downs et al., 2004; Morrison et al., 2004; van Attikum et al., 2004). It is thought to counteract H2A.Z incorporation by SWR1 by exchanging H2A.Z for H2A (Brahma et al., 2017; Papamichos-Chronakis et al., 2011). Additionally, INO80 is involved at a later step of HR promoting formation of the Rad51-nucleo-protein-filament after resection (Lademann et al., 2017).

Lastly, also the Fun30-SMARCAD1-ETL family of nucleosome remodelers plays a key role in regulating resection. Involvement of Fun30 in resection was found by screening for mutants deficient in resection-dependent repair of DSBs, in fact they behaved similar to mutants for the resection nucleases (Chen et al., 2012; Costelloe et al., 2012). If budding yeast cells lack Fun30, the kinetics of long-range resection of an induced, non-repairable DSB are decreased 2-3-fold compared to WT cells (Bantele et al., 2017; Eapen et al., 2012) and also the overall spreading of resection is reduced (Bantele et al., 2017).

7. The Fun30-SMARCAD1-ETL family of nucleosome remodelers

Best-studied members of the remodeler family are Fun30 (budding yeast), Fft3 (fission yeast), ETL1 (mouse) and SMARCAD1 (human), all to our knowledge single-subunit remodelers involved in diverse cellular functions (Bantele and Pfander, 2019; Karl et al., 2022). Two major functions appear to be evolutionarily conserved from yeast (budding yeast Fun30, fission yeast Fft3) to human (SMARCAD1).

First, these remodelers appear to function in the response to DNA damage. Both Fun30 and SMARCAD1 have been shown to promote DNA end resection of DNA double-strand breaks (DSBs) and repair by homologous recombination (Bantele et al., 2017; Chen et al., 2012; Costelloe et al., 2012; Eapen et al., 2012).

Fission yeast Fft3 is required for single-strand annealing based repair of an induced DSB and for resection of nascent strands at a stalled replication fork (Ait-Saada et al., 2019).

In case of budding yeast Fun30, our lab has previously identified a key regulatory mechanism. Fun30 is recruited to sites of DNA end resection depending on (S-)CDK-phosphorylation of two N-terminal serine

residues (S20, S28), the adapter-protein Dpb11 and the 9-1-1 complex, thus limiting Fun30 recruitment to cell cycle phases (S-M phase), where resection is activated (Bantele et al., 2017; Chen et al., 2016). A direct effect of Fun30 on Exo1-dependent long-range resection through chromatin could not be found *in vitro* (Adkins et al., 2013), indicating another factor might be missing from this reconstituted resection system. Supporting this, it has been found that *fun30* mutant phenotypes can be suppressed by additionally deleting resection inhibitor Rad9 (Bantele et al., 2017; Chen et al., 2012), pointing towards a functional antagonism between Fun30 and Rad9. Budding yeast cells lacking both Fun30 and Rad9 display fully functional resection (Peritore et al., 2021), suggesting that Fun30 is not required to overcome the general nucleosome barrier for resection nucleases. This could mean that for Fun30 promoting resection, Fun30 is not sliding, evicting or modifying just any nucleosome, but specifically Rad9-bound nucleosomes (Fig. 3). Human SMARCAD1 shows conservation of Fun30's cell-cycle regulation by CDK and its localization to DSBs via a scaffold protein (TOPBP1) (Bantele et al., 2017), as well as its role in promoting DNA end resection (Costelloe et al., 2012; Densham et al., 2016). Additionally, SMARCAD1 also shares the antagonistic relationship with an anti-resection and DNA damage checkpoint protein, called 53BP1 (Densham et al., 2016), underlining the conservation from yeast to human.

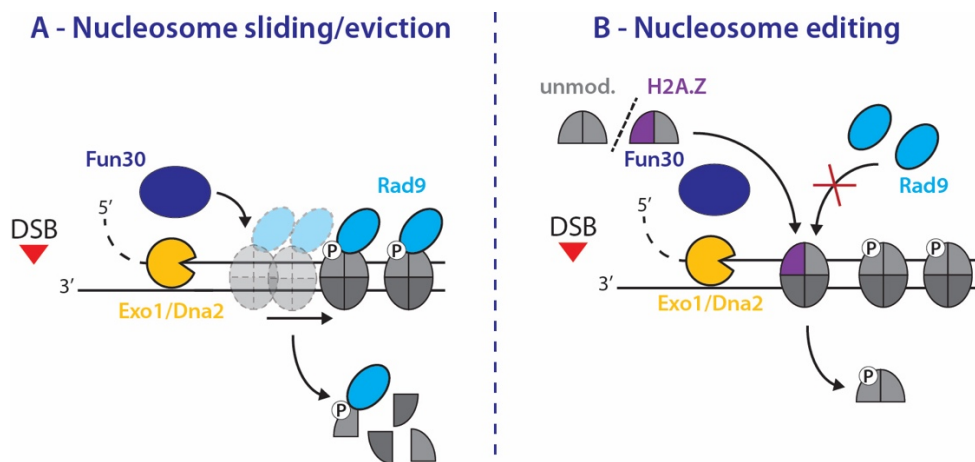


Figure 3: Potential remodeling of Rad9-bound nucleosomes by Fun30 (figure modified from Karl et al., 2022)
A: Nucleosome sliding/eviction of: Fun30 (dark blue) could slide Rad9-bound nucleosomes (grey) along DNA and/or evict them including resection inhibitor Rad9 (light blue) to facilitate resection by the resection nucleases Exo1 or STR-Dna2 (yellow). Color scheme continuous throughout the figure.
B: Nucleosome editing: Rad9 binds histone modifications, like phosphorylated S129 on H2A (γ H2A). Fun30 could edit nucleosomes by exchanging γ H2A with unmodified H2A or H2A.Z, preventing Rad9 association or maybe co-jecting Rad9 with γ H2A.

The second conserved function is in the maintenance of silent chromatin.

Again, Fun30, SMARCAD1 as well as fission yeast Fft3 have been shown to play a role in the upkeep of transcriptionally silent regions. In budding yeast, silencing is lost from telomeric and silent mating type loci upon deletion of *FUN30* (Durand-Dubief et al., 2012; Neves-Costa et al., 2009). Similarly, in fission yeast, transcriptional silencing and heterochromatin structure is lost from centromeres and sub-telomeres in the absence of Fft3 (Steglich et al., 2015; Strålfors et al., 2011).

Also in human, SMARCAD1 is required for heterochromatin maintenance, in this case specifically pericentric heterochromatin (Rowbotham et al., 2011).

Overall, this role appears to be linked to a function in chromatin maintenance during DNA replication (Rowbotham et al., 2011; Taneja and Grewal, 2017).

Lastly, the Fun30-SMARCAD1-ETL family may have additional functions in multiple biological processes, involving transcriptional regulation (Byeon et al., 2013; Lee et al., 2017), Exo1-dependent mismatch DNA repair of mis-incorporated or modified bases, another type of DNA lesion (Goellner et al., 2018; Terui et al., 2018) and mRNA splicing (Niu et al., 2020).

Notably, for most of these functions, it is only known that ATP hydrolysis by the enzyme is required, but the underlying remodeling mechanism is unknown.

In vitro studies of budding yeast Fun30 suggest activities in nucleosome sliding and histone dimer exchange as well as depositing entire octamers onto another DNA fragment (Awad et al., 2010). A recent study suggested also for SMARCAD1 to evict and assemble entire octamers and unlike other remodelers to dock to the nucleosome dyad (SHL 0) (Markert et al., 2021).

However, since they appear to act as single-subunit enzymes, indicating that all crucial functions for remodeling can be found in one of these proteins (Clapier et al., 2017), they make highly interesting targets to study the molecular mechanism of chromatin remodeling.

8. Studying single-subunit remodelers

Studying chromatin remodelers *in vivo* bears certain challenges: 1) Since the correct accessibility of the genetic material is essential, some nucleosome remodelers are essential and cannot easily be mutated or deleted for studying. 2) Since the chromatin remodeling is so important, several remodelers also have redundant functions and can at least partially cope for the loss of another one. 3) Several subunits are shared between different remodeling complexes, adding another layer of complexity and potentially making experimental data difficult to interpret.

Given the complexity of multi-subunit remodelers it can be promising to study single-subunit remodelers. This has the advantage of eliminating the shared subunit problem, but also by studying just one protein, one can find out about multiple elements of remodeler function. Studying single-subunit remodelers has the potential to lead to a conceptual understanding of a minimal set of functional elements for remodeler function. A single-subunit remodeler may also be easier to purify and perform mechanistic studies *in vitro*.

To date, there is no structure solved for any of the Fun30-SMARCAD1-ETL family members, except for parts of the conserved Fun30 ATPase domain (Liu and Jiang, 2017) and cryo-EM structure for SMARCAD1, which had however too low resolution to unambiguously build a structure (Markert et al., 2021).

The putative domain architecture of Fun30 (Fig. 4) shows the two-lobed ATPase domain with a relatively large insertion between the lobes, two important CDK-phosphorylation sites at the N-terminus and then a putative CUE-domain, however the ubiquitylated binding partner is unknown for Fun30 (Awad et al., 2010).



Figure 4: Domain architecture of Fun30 (yeast) shows the two-lobed SNF2-type ATPase domain in beige, a putative CUE-domain in rosy-brown and the CDK-phosphorylation sites (S20 and S28) important for cell-cycle dependent recruitment in brown.

Biochemical characterization of Fun30 has revealed that it is stimulated to hydrolyze ATP by DNA and nucleosomes (Awad et al., 2010) and even more efficiently by ssDNA and ssNucs (Adkins et al., 2017). Additionally, Fun30 is able to catalyze nucleosome sliding and histone dimer exchange *in vitro* (Awad et al., 2010; Byeon et al., 2013). However, besides ATP-dependence little is known about the remodeling mechanism of this important family of single-subunit remodelers. Hence, we set out to study the Fun30-SMARCAD1-ETL family, using the budding yeast member Fun30 as a model.

Objectives of the study

While in general our understanding of molecular mechanisms behind chromatin remodeling has increased substantially, especially through structural work on nucleosome remodelers bound to their substrate (Reyes et al., 2021), little is known for the Fun30-SMARCAD1-ETL family.

Nucleosome remodelers mostly have domains or subunits to mediate specific recruitment, to hold on to the nucleosome during DNA translocation and to regulate their activity. However, for most of these functions it is unknown, if they exist in a single subunit remodeler like Fun30, and if so, what the responsible domains are.

By investigating respective modules in Fun30, we can gain insights into multiple intriguing questions:

How is Fun30/SMARCAD1 regulated to act specifically where and when it is required?

What is the remodeling mechanism of this single-subunit remodeler family?

Can we deduce a minimal set of modules for a functional chromatin remodeler, by studying a single protein system capable of remodeling?

Is the same mechanism required for the two major functions in silencing and promoting DNA end resection?

We therefore aimed to find additional parts of Fun30 required for protein function, characterize them and understand how they are involved in remodeling.

For this we pursued two synergizing research approaches:

First, we systematically truncated previously uncharacterized parts of Fun30 and checked for phenotypes *in vivo*.

Second, we made multiple sequence alignments and structure prediction to find conserved regions and test respective mutants *in vivo* and *in vitro*.

Using this approach, we identified a new domain in Fun30-SMARCAD1-ETL remodelers, which we termed SAM-key. In the course of this thesis, we then characterized deletion and point mutants in the SAM-key and tested remodeling activities of purified proteins in reconstituted systems.

Thereby, our research provides new insights into molecular mechanisms of the Fun30-SMARCAD1-ETL family with implications in both chromatin remodeling and regulation of DNA end resection by focusing on Fun30. Moreover, structural comparison to other nucleosome remodelers suggests that elements of intramolecular regulation such as the SAM-key are a wide-spread means of control in nucleosome remodelers.

Results

1. Multiple sequence alignment shows high conservation of the SNF2-type, two-lobed ATPase domain and another central region of Fun30

To shed light on the minimal mechanistic modules for remodeling and potentially understand the mechanism by which Fun30 promotes DNA end resection and thereby repair by HR we first analyzed its sequence for conservation. The protein sequence of budding yeast Fun30 was compared with a set of orthologues ranging from closely related Saccharomycetales species over fission yeast (Fft3) to more distantly related model species worm, fly (Etl1), frog, mouse and human (SMARCAD1) using the ClustalWS algorithm (Troshin et al., 2011).

The multiple sequence alignment showed strong conservation for the C-terminal half of the protein harboring the conserved SNF2-type, two-lobed ATPase domain. Interestingly, there was another region of high conservation: N-terminal of the ATPase domain, the region around residues 250-400 showed high sequence conservation (Fig. 5). The sequences showed two conserved sequence blocks with an insertion between them that appeared to be Saccharomycetales-specific but not highly conserved. The first block (~275-320) showed mostly conserved hydrophobic residues and towards the end a highly conserved RPY/RPF motif. The second block (~350-390) was similarly conserved hydrophobic and harbors a highly conserved cysteine residue (C374).

Multiple sequence alignment of FUN30/SMARCAD1/ETL

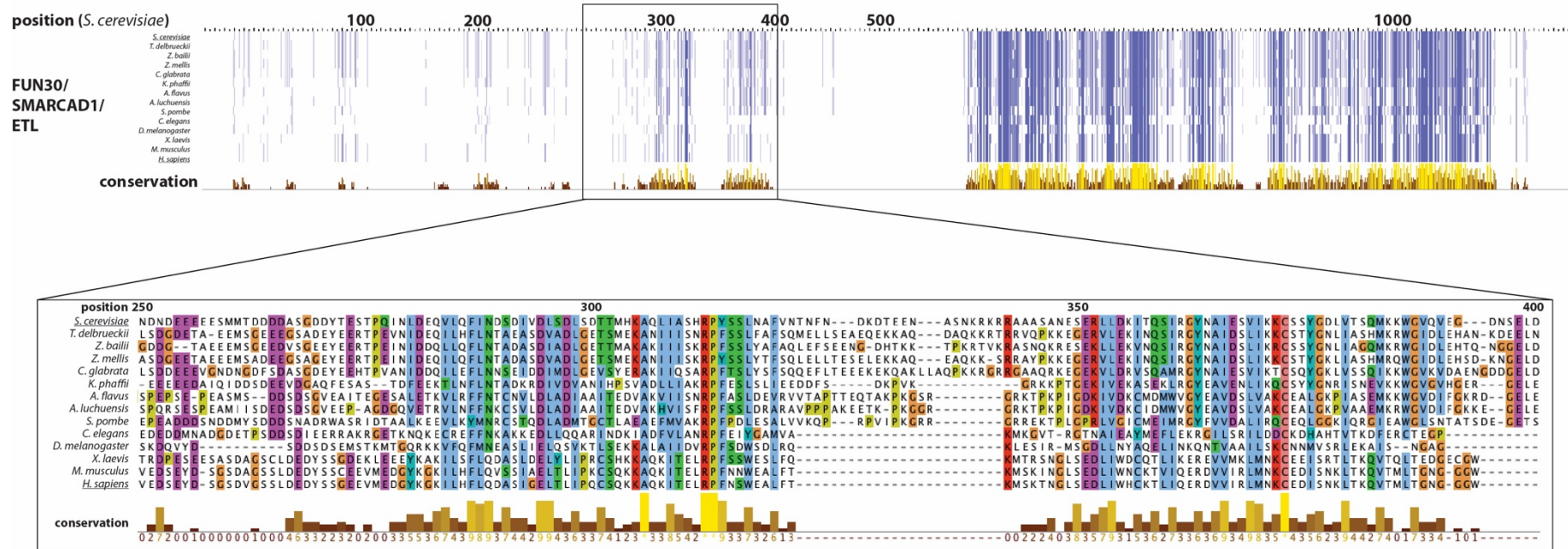


Figure 5: Multiple sequence alignment of Fun30/SMARCAD1/ETL

Multiple sequence alignment of budding yeast Fun30 and its orthologues Fft3/Etl1/SMARCAD1 from a diverse set of species. Protein sequences were retrieved by BLASTx search, specifically looking for commonly used model organisms. The sequences were aligned using the ClustalWS algorithm within the Jalview software (v2.11.0).

The upper panel shows alignment of the full protein sequences with conserved residues indicated by dark blue color. Highest conservation can be seen for the ATPase domain (C-terminal) but another region around residues 250-400 shows second highest conservation. The lower panel shows a zoom in on the sequence in this region with colors indicating the chemical properties of the amino acids. Light blue = hydrophobic, red = positively charged/basic, purple = negatively charged/acidic, green = polar uncharged, yellow = proline, orange = glycine.

2. Region between 247-389 is crucial for Fun30 function

To learn more about the conserved region and in how far it is required for Fun30 function in regulating DNA end resection we tested a series of N-terminal truncations of Fun30 in a Ddc1-Fun30-fusion-protein. The fusion forces recruitment to DSB sites and therefore allows to analyze defects in the context of functional recruitment of Fun30 to DSBs. This enables to distinguish between defects in recruitment and defects in protein function. Survival of yeast cells on plates with the genotoxic agent camptothecin (CPT) requires functional Fun30 protein. A yeast spotting on CPT-plates detected the region between amino acids 120-422 as crucial for Fun30 function (Fig. 6 A). Therefore, serine residues important for recruitment via CDK-phosphorylation (SS20, 28) were expendable in context of the fusion protein as was the CUE domain (Fig. 6 A). These results were confirmed by measuring the extent of resection by RPA-ChIP qPCR experiments: Cells with a truncated 422-C-construct and further truncations (501-C, 527-C) were resecting DNA poorly, and not as well as the FL constructs or truncations like 120-C, that included a bigger part of the N-terminus (Fig. 6 B). Another set of truncation mutants showed that the region between 338-389 was crucial for Fun30 function (Fig. 6 C). All changes were confirmed to not be due to changes in expression levels by Western blot (Fig. 6 D). As such we concluded, that the conserved region is highly important for Fun30 function in regulating DSB repair and thus likely to adapt a specific fold, forming a protein domain.

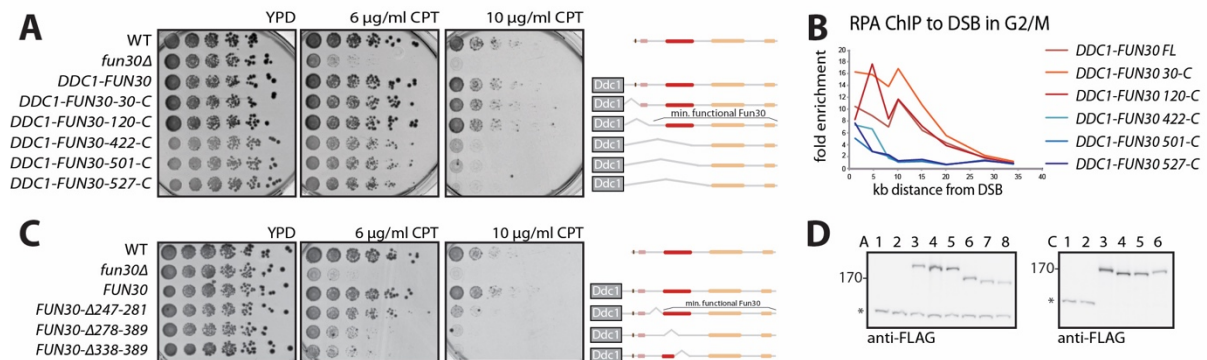


Figure 6: N-terminal truncations of nucleosome remodeler Fun30 reveals a previously uncharacterized, central (aa 247-389) region important for DNA damage repair function:

A: Sensitivity to genotoxic agent camptothecin (CPT) of N-terminal truncations of Fun30 as tested by a yeast spotting: Yeast strains carrying different truncated versions of a Ddc1-Fun30-fusion construct that forces recruitment to DSB sites were spotted in serial dilution onto plates with increasing concentrations of CPT. Truncations included or excluded respectively: The CDK-phosphorylation sites SS20,28 (brown), the CUE-domain (rosy brown), and differently sized fragments of the N-terminal part of the protein. All constructs contained the conserved SNF2-type two-lobed ATPase domain (beige). CPT sensitivity of yeast cells lacking Fun30 is demonstrated with a *fun30Δ* strain and the Ddc1-Fun30-fusion shows resistance to lower doses of CPT. The truncation construct starting at residue 422 (422-C) shows increased sensitivity similar to *fun30Δ*, as do the constructs 501-C and 527-C. n=3 biological replicates.

B: The pGal:HO system was used to induce a single DSB in G2/M phase at MAT locus in yeast strains carrying truncated Ddc1-Fun30-fusion constructs as in A. Spreading of resection as measured by RPA ChIP qPCR to the DSB shows the over-resection phenotype for Fun30 full-length and truncation constructs 30-C and 120-C (shades of red) while no long-range resection can be observed for 422-C, 501-C and 527-C (shades of blue).

C: Sensitivity to CPT as in A with a new set of truncations in context of Fun30-Ddc1-fusion. Truncations excluded differently sized fragments of the region 120-422 important for Fun30 function. The Δ247-281 construct shows increased sensitivity to CPT only at higher dose, while the region 278-389 also at the lower dose shows sensitivity comparable to *fun30Δ*. Interestingly, the region could be narrowed down even further, since Δ338-389 is also highly sensitive, indicating that a crucial part for Fun30 function is within this fragment. Representative plate of n=3.

D: Western blot (representative blot of n=2) against the FLAG-tag shows similar expression levels for full-length and truncated Fun30 constructs used in the experiments Fig. 2 A-C (equal amounts of log-phase cell extract).

Left blot shows strains used in Fig. 6 A+B: A1=WT (untagged), A2=*fun30Δ*, A3=*fun30Δ* + *DDC1-FUN30*, A4=*fun30Δ* + *DDC1-FUN30-30-C*, A5=*fun30Δ* + *DDC1-FUN30-120-C*, A6=*fun30Δ* + *DDC1-FUN30-422-C*, A7=*fun30Δ* + *DDC1-FUN30-501-C*, A8=*fun30Δ* + *DDC1-FUN30-527-C*. Right blot shows strains used in Fig. 6 C: C1=WT (untagged), C2=*fun30Δ*, C3=*fun30Δ* + *FUN30*, C4=*fun30Δ* + *FUN30-247-281Δ*, C5=*fun30Δ* + *FUN30-278-389Δ*, C6=*fun30Δ* + *FUN30-338-389Δ*.

3. Structure prediction shows SAM-like helix bundle with elongated protruding alpha helix – termed SAM-key domain

No domain was assigned by to the region 270-400 by UniProt’s automatic annotation pipeline, actually parts 242-273 and 327-350 are automatically annotated as disordered. BLASTing the protein sequence (Altschul et al., 1990) yielded only Fun30 and orthologues. With only part of the Fun30 ATPase domain (809-1120) solved as crystal structure (Liu and Jiang, 2017), we lacked a structure of Fun30 or its orthologues to analyze this region further, so we turned to structure prediction algorithms.

We used Phyre2 (Kelley et al., 2015) as well as AlphaFold2 (Jumper et al., 2021; Varadi et al., 2022) to predict the structure of the conserved region. The Phyre2 model was very similar to SAM-like domains (sterile alpha motif), a small bundle of short alpha helices (Fig. 7 A). AlphaFold2 gave a largely similar model, but additionally showing a long alpha helix without interruption for residues 343-388 of the putative SAM-like domain (Fig. 7 B). The overall confidence of both predicted models was high. For the AlphaFold2-model the average pLDDT was 81.97. For the Phyre2-model the overall confidence was <70%, but the residues predicted to form the SAM-like fold were modeled with >90% confidence. We did not find a structural analog using the AlphaFold2 model on the Dali server for comparing protein structures in 3D (Holm, 2022).

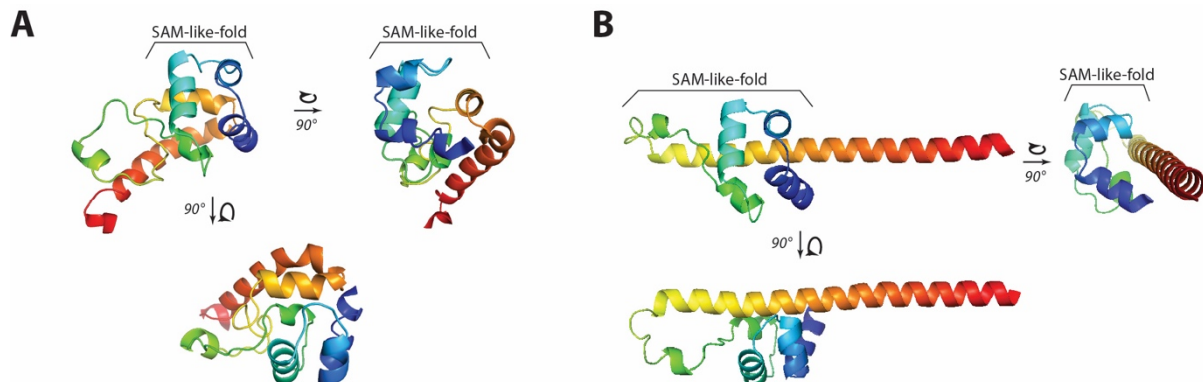


Figure 7: Structural models of the conserved region of Fun30 276-388 in rainbow coloring from N- (blue) to C-terminus (red).

A: Predicted model generated by intensive modeling by the Phyre2 algorithm (Kelley et al., 2015). 42% of residues were modelled at >90% confidence, but the overall confidence in the model is below 70%. 4 among the 6 templates used to generate this model harbor a sterile alpha motif (SAM)-like fold.

B: Predicted model generated by AlphaFold2 (Jumper et al., 2021). The overall confidence in this model (pLDDT-score) is 81.97. The N-terminal helices are very similar in both predictions and to the SAM domain. However, one major difference between the models is the C-terminus (K340-K387): While in the Phyre2-model at S360 a short loop is predicted, making the C-terminus a helix-turn-helix and the entire fold more globular, in AlphaFold2 the region K340-K387 is predicted to form a single, long, protruding alpha helix, giving the overall shape of a key.

SAM domains form a cluster of about five short alpha helices, however the relative position of the helices towards each other is rather diverse, as seen in several solved structures of SAM domains (Fig. 8 A-B). The fold is commonly relevant for homo- and hetero-protein-protein interactions (Kim and Bowie, 2003). Due

to the resemblance to a SAM-like fold yet also the distinguishing feature of the long protrusion from the main bundle, we termed this structure “SAM-key”, because the entire structure resembles that of a key (Fig. 8 C). Notably, the previously mentioned two conserved blocks correspond well to i) the predicted SAM-like fold and ii) the predicted long, protruding helix, which is basically identical with the region crucial for Fun30 function (338-389) (Fig. 6 C), indicating an important role for the protrusion.

Additionally, we compared the structure predictions for the SAM-key region of Fun30 and its orthologues and characteristically found each model being highly similar to the model for the Fun30 SAM-key. Of specific interest was the human orthologue SMARCAD1. As aforementioned it lacks the fungi-specific insert between SAM-like fold and long helix but is predicted to form an almost identical structure (Fig. 8 D), only the long helix is tilted relative to the SAM-like fold when comparing with Fun30 (Fig. 8 C). Given the fact that we predict a conserved function of the SAM-key module, highly important for remodeling, this met our expectations.

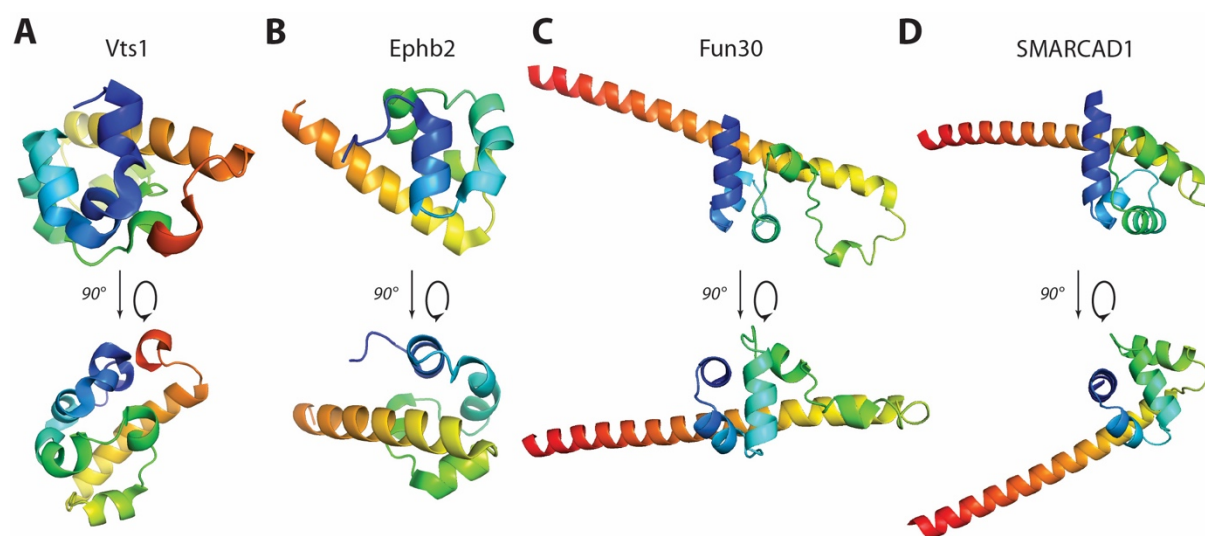


Figure 8: Comparison of solved SAM-domain structures and SAM-key models

All structures are shown in rainbow coloring from N- (blue) to C-terminus (red) for comparison, aligned according to first N-terminal alpha helix (blue).

A: Crystal structure of SAM-domain from yeast Vts1 (PDB: 2d3d). The short alpha helices are arranged to form a compact bundle. The second helix (light blue) projects towards the left.

B: Crystal structure of SAM-domain from human EphB2 (PDB: 1f0m). The short alpha helices are arranged to form a compact bundle with different orientations between the helices: compared to Vts1. The second helix projects towards the right (light blue).

C: AlphaFold2 prediction of SAM-key in Fun30 shows N-terminal bundle of short helices which then connects to one long, protruding helix via a loop (green).

D: AlphaFold2 predicts a very similar fold to Fun30 in the human orthologue SMARCAD1 with high confidence (pLDDT of 94.53).

4. Fun30 Δ SAM mutant (Fun30 Δ 275-436) generates a defect in resection and resistance to camptothecin

To investigate the predicted SAM-key domain and its role in Fun30 function we used a deletion mutant construct Fun30 Δ 275-436, referred to as Fun30 Δ SAM, that fully lacks the predicted domain and flanking residues. We therefore tested the phenotype of a *fun30* Δ SAM strain in CPT spottings and RPA ChIP qPCR experiments. Notably, the Fun30 Δ SAM was not able to rescue the sensitivity to CPT of a *fun30* Δ strain and phenocopied the deletion (Fig. 9 A). Similarly, after inducing a single DSB in G2/M phase with the

pGAL:HO-system, RPA ChIP experiments showed two effects: (I) RPA enrichment and therefore ssDNA as a proxy of resection was spreading further away from the DSB to up to 20 kb after 4 hours post induction for the wildtype and only about 7 kb for *fun30Δ* and *fun30ΔSAM*. (II) RPA enrichment was following different kinetics. When comparing the 2h-timepoints, in WT RPA enrichment could already be observed up to about 7 kb from the break site while for the mutants it did not spread to 5 kb (Fig. 9 B). This demonstrates Fun30ΔSAM is deficient in long range resection as is a *fun30Δ* strain. Again, the differences should not be due to a change in expression levels as shown by Western blot (Fig. 9 C).

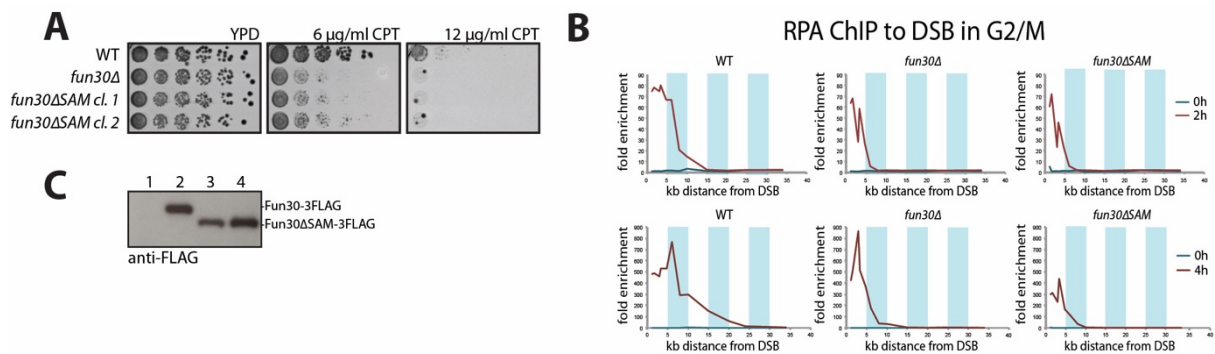


Figure 9: Domain deletion mutant Fun30ΔSAM (Δ275-436) is not able to rescue *fun30Δ* phenotypes in CPT resistance and spreading of resection.

A: Sensitivity to different dosages of CPT of WT, *fun30Δ* and *fun30ΔSAM* (275-436) budding yeast cells in growth assay. *fun30Δ* cells and *fun30ΔSAM* cells are sensitive to 6 μg/mL CPT, which the wildtype can tolerate. Representative plate of n=3.

B: Spreading of resection as measured by RPA ChIP qPCR to a single DSB at the MAT locus at different timepoints (0, 2 and 4 hours) after induction with the pGAL:HO system in nocodazole-arrested cells (G2/M phase). Strains with Fun30 wildtype (WT), Fun30ΔSAM (*fun30ΔSAM*) or lacking Fun30 (*fun30Δ*) are compared side by side. *fun30Δ* and *fun30ΔSAM* strains show reduction of resection spreading and slower kinetics compared to WT. Upper panels show 0h and 2h timepoints, lower panels show 4h. Blue bars indicate 5 kb.

C: Western blot (representative of n=2) against FLAG-tag shows similar expression levels for wildtype and ΔSAM mutants. 1 = untagged; 2 = Fun30-3xFLAG; 3 = Fun30ΔSAM-3xFLAG clone 1; 3 = Fun30ΔSAM-3xFLAG clone 2.

5. The SAM-key domain is required for Fun30's function in silencing

Fun30 is also involved in generating heterochromatin-like genomic regions in which transcription is silenced. To test if Fun30ΔSAM is still functional in context of silencing we used a silencing assay (Fig. 10 A). In this assay, a functional *URA3* was integrated into a silenced genomic region in strains in which the endogenous *URA3* gene is mutated. Functional silencing represses *URA3* and the strain depends on uracil in the growth medium and is resistant to counter-selection by 5'-FOA. When a defect in silencing is induced, cells can synthesize uracil and thrive on medium lacking uracil, yet become sensitive to the counter-selective drug 5'-FOA.

We tested two different silent genomic loci – the telomer of chromosome VII and the silent mating type locus *HMR*. *fun30Δ* showed no requirement for uracil but sensitivity for 5'-FOA, hence a silencing defect, while the wildtype showed the opposite. The *fun30Δ* phenotype could be rescued by giving back Fun30 but not Fun30ΔSAM (Fig. 10 B). We also compared Fun30ΔSAM to the previously described Fun30-SS20,28AA (Fun30-SSAA) mutant and Walker-A-mutant Fun30-K603R. Fun30-SSAA has been shown to be specific for the function in resection but not affecting the silencing function of Fun30 (Bantele et al., 2017). This result was confirmed (Fig. 10 C) but Fun30ΔSAM fails to rescue a *fun30Δ* strain same as the ATP-binding-deficient Fun30 K603R (Fig. 10 D). Thus, we concluded that the SAM-key is required not

only for the function in DSB repair, but also for the function in silencing or to put it differently in both major functions of Fun30.

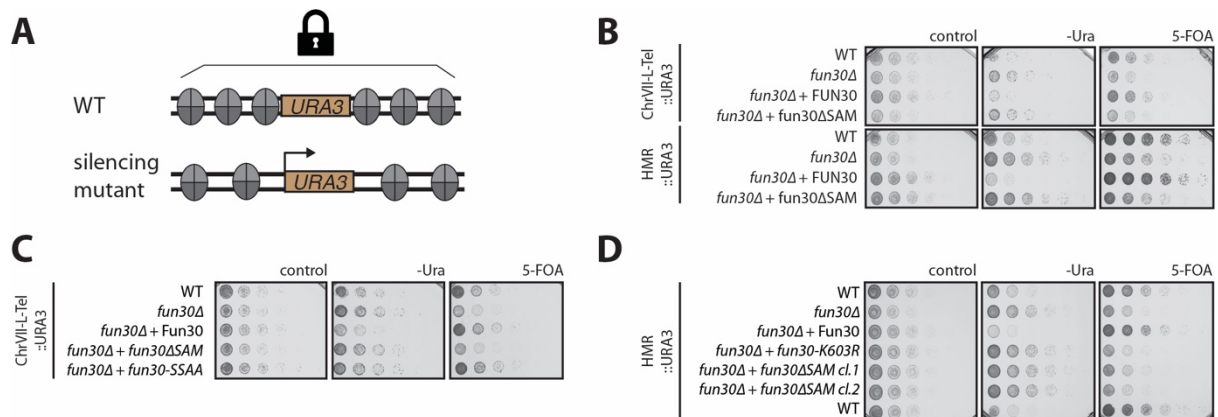


Figure 10: Fun30 function in silencing requires the SAM-key domain.

A: Schematic for gene silencing assay: The auxotrophic marker *URA3* is integrated into a transcriptionally silenced region of the yeast genome. In a wildtype (WT) strain these regions are transcriptionally repressed, upon loss of silencing however, *URA3* is expressed allowing growth on SC-Ura medium, but not on 5'-FOA.

B: Two sets of strains carry the *URA3* at different silenced loci: Set 1 in the telomer on the left arm of chromosome VII (ChrVII-L-Tel, upper panel) and set 2 in the silent mating type locus *HMR* (lower panel). The strain with Fun30 WT cannot grow on medium lacking uracil, but survives upon counter-selection by 5'-FOA. For *fun30Δ* the situation is inverted: Cells can grow on SC-Ura plates but cannot grow on the 5'-FOA plate. A *fun30Δ* silencing defect is rescued by expression of Fun30 WT, but not Fun30ΔSAM protein. n=3 biological replicates.

C: Unlike the previously described Fun30-SSAA mutant that specifically blocks recruitment to DSBs but not the silencing function of Fun30 (Bantele et al., 2017), Fun30ΔSAM is not able to rescue *fun30Δ*. n=3 biological replicates.

D: Walker-A-mutant Fun30-K603R cannot rescue *fun30Δ* in the silencing assay. Fun30ΔSAM phenocopies the K603R-mutant. n=3 biological replicates.

6. Establishment of a purification strategy for Fun30 from bacteria

With the previous results we could conclude that Fun30 is unable to perform its function without the SAM-key. To be able to understand what is the crucial function of the SAM-key, we wanted to characterize Fun30 and the Fun30ΔSAM mutant *in vitro*, so we expressed and purified the proteins from both *S. cerevisiae* and *E. coli*. For yeast, we used galactose-induced overexpression of an integrated Fun30-3xFLAG-CBP construct and a two-step purification strategy: First an anti-FLAG IP, followed by elution with 3xFLAG peptide and an ion exchange chromatography (Fig. 11 A). For bacteria we used IPTG-induced overexpression of a 6xHis-GST-3C-Fun30 construct and a three-step purification strategy: First an IMAC, followed by elution with imidazole, then affinity purification (AP) with glutathione sepharose, elution by tag cleavage using 3C protease and finally gelfiltration (Fig. 11 B). Both strategies yielded comparable amounts for Fun30 and Fun30ΔSAM (Fig. 11 A+B), however the yield of the yeast expression system was lower by a factor of 5. Both strategies resulted in active Fun30 protein as determined by DNA stimulated ATPase assay and nucleosome remodeling and eviction assays. The assays showed a similar stimulation of ATP hydrolysis when stimulated with 100 ng/μL herring sperm DNA, leading to a $k_{cat} \sim 1.5$ molecules ATP hydrolyzed per second per remodeler (Fig. 11 C). As for nucleosome remodeling, both preparations exhibited similar activity in sliding as well as eviction (Fig. 11 C). With comparable activity for both strategies but the procedure from bacteria being more efficient, Fun30 constructs purified from bacteria were used throughout this study.

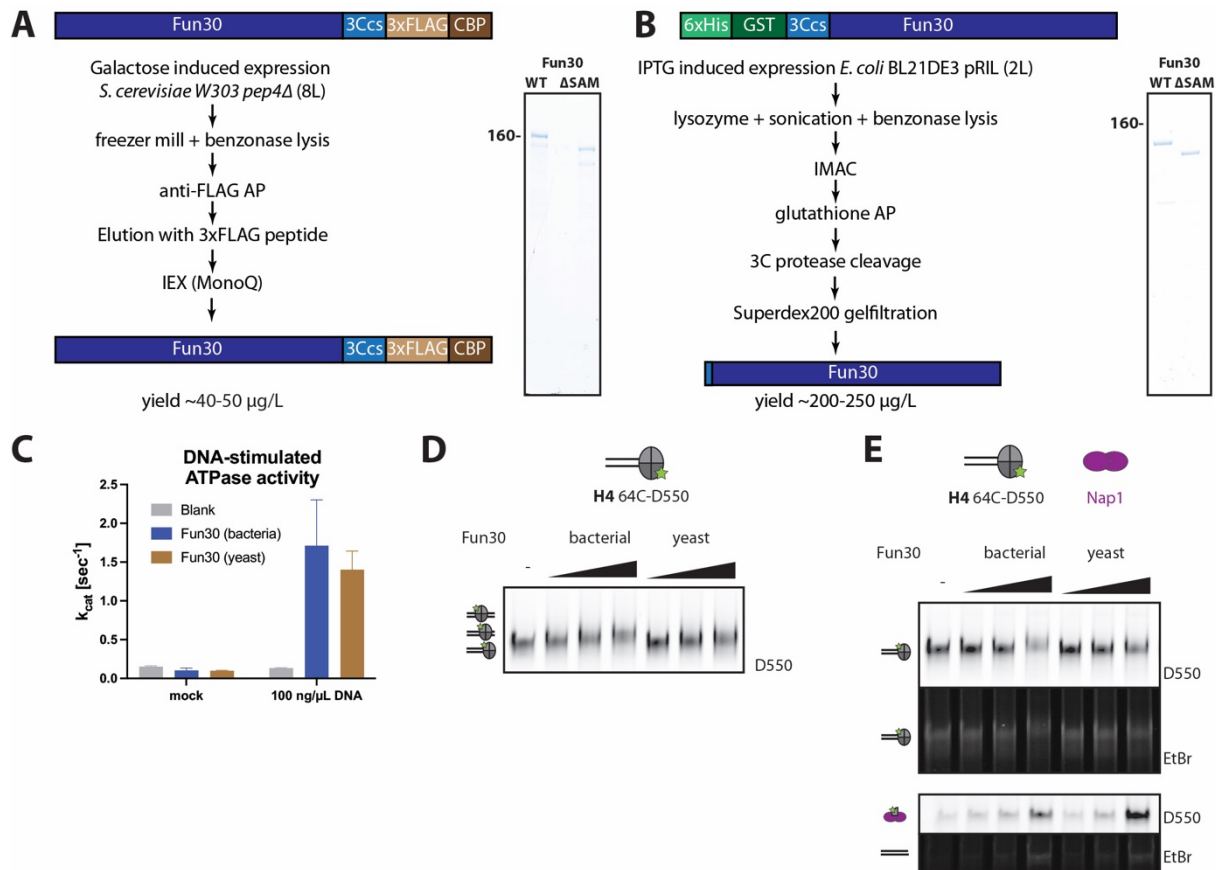


Figure 11: Functional Fun30 can be purified from both yeast and bacteria.

A: Schematic of expression and purification strategy from *S. cerevisiae*. Gal-promoter controlled Fun30 with C-terminal 3xFLAG-CBP-tag and a 3C-protease (PreScission) cleavage site was expressed in *S. cerevisiae* W303 *pep4Δ* by addition of galactose. Purification was achieved by cell lysis with cryo-mill, clearing the lysate with benzonase, 1st anti-FLAG affinity chromatography, 2nd IEX (MonoQ). The final yield was 40-50 µg/L for both Fun30 WT and Fun30ΔSAM (representative gel, n=3).

B: Schematic of expression and purification strategy from *E. coli*. Lac-operon controlled Fun30 with N-terminal 6xHis-GST-tag and a 3C-protease (PreScission) cut site was expressed in *E. coli* BL21 DE3 with pRIL (for rare tRNAs) by addition of IPTG. Purification was achieved by cell lysis, clearing the lysate with benzonase, 1st IMAC, 2nd glutathione affinity purification (AP), followed by tag cleavage and gel filtration (Superdex200). The final yield was 200-250 µg/L for both Fun30 WT and Fun30ΔSAM (representative Coomassie gel, n=4).

C: Absorbance-based (A340) ATPase assay using Fun30 purified from bacteria (dark blue) and Fun30 purified from yeast (brown), ATP and DNA stimulus (herring sperm DNA, 100 ng/µL). n=2 biological replicates, each in technical duplicates. Shown is mean k_{cat}, error-bars depict standard deviation.

D: Sliding of nucleosomes with labeled H4 (64 C-D550, 100 nM) assembled on a 100W0 fragment (247 nt fragment with end-positioned Widom 601-positioning-sequence) as seen by upshift in gel. Shown is a titration (5, 25, 100 nM) of Fun30 purified from either yeast or bacteria. Both allow sliding and show comparable activity. Representative gel of n=2 biological replicates.

E: Eviction of nucleosomes with labeled H4 (64 C-D550, 100 nM). Eviction is seen by (i) decrease of labeled nucleosome (top), (ii) decrease of nucleosome signal in ethidiumbromide stain (2nd from top), (iii) increased Nap1-bound labelled histone (3rd from top), (iv) increase of “free” DNA in ethidiumbromide stain (bottom). Shown is a titration of Fun30 purified from either yeast or bacteria. Both evict nucleosomes with comparable activity. Representative gel of n=2 biological replicates.

7. Characterization of Fun30ΔSAM mutant showed normal folding and stability

To ensure that Fun30ΔSAM was stable and properly folded and to exclude that the inactivity of mutants *in vivo* was rooting in unstable and degraded mutant protein, we compared the mutant to the wildtype protein with several biophysical and biochemical methods.

Limited proteolysis was used to show changes in protein folding by different accessibility of protease cleavage sites. A limited proteolysis experiment with a set of five different proteases did not display major changes in the pattern of degradation products observed by silver staining (Fig. 12 A). This underlines normal accessibility of cleavage sites, thus normal folding and additionally shows that Fun30 Δ SAM is as stable in solution as the wildtype. Interestingly, during gelfiltration Fun30 Δ SAM exhibited a slightly different elution profile compared to Fun30 WT. The elution was spanning more and earlier fractions and the UV-spectrum showed an additional elution peak, earlier than the main peak observed for Fun30 and Fun30-K603R, indicating some level of stabilization of a higher order oligomer (Fig. 12 B).

Mass photometry enables the accurate mass measurement of single molecules in solution without the need for labels. When checking the molecular mass of Fun30 and Fun30 Δ SAM we could observe indeed that a proportion of molecules was of higher mass than Fun30 monomer with about 130 kDa (Fun30 WT) or 110 kDa (Fun30 Δ SAM), but corresponding to a dimer with about 240 kDa. We observed this for both WT and for Fun30 Δ SAM in the earlier fraction 18 with almost equal amounts of dimer and monomer, but only for a fraction of the protein in the main peak fraction 21 (Fig. 12 C). The higher order species seemed to dissociate within hours after gelfiltration, as measurements later or after freeze-thawing with the same fractions did not have substantial dimer content any more (data not shown). This reversibility of the oligomerization after gelfiltration and the fact, that only a fraction of the protein was in oligomeric state, speaks for a dynamic and transient oligomerization of Fun30 that may be slightly stabilized in Fun30 Δ SAM. Nano differential scanning fluorimetry (nanoDSF) is a label-free method to analyze protein stability using the intrinsic tryptophan fluorescence. When the protein unfolds tryptophan residues that are usually folded towards the inside in a hydrophobic environment get exposed to hydrophilic environment at the outside. While in hydrophobic environment the fluorescence peaks at 330 nm, in hydrophilic environment the fluorescence shifts towards red (350 nm) and increases. Thermal unfolding for Fun30 and Fun30 Δ SAM showed for both one main unfolding event, starting at -55°C with the inflection point almost identical with 61.7°C (Fun30) and 61.3°C (Fun30 Δ SAM) (Fig. 12 D). Another unfolding event which is more clearly visible for Fun30 WT was observed at $\sim 40^{\circ}\text{C}$. For Fun30 Δ SAM there was also a minor increase in the 350/330 ratio at this temperature, albeit less prominent and masked by the initial decrease of the ratio from 20°C - 40°C . Considering Fun30 Δ SAM is predicted to lack the folded the SAM-key domain and the truncation removes one tryptophane residue from in total only 6 in Fun30 the unfolding of the two proteins could be considered similar with slight expected differences.

In vitro CoIP of Fun30-3xFLAG-CBP with either Fun30 or Fun30 Δ SAM confirmed that both proteins are able to form homo-oligomeric species (Fig. 12 E). It has been shown before that Fun30 is able to self-interact by others (Awad et al., 2010). This result underlined that Fun30 Δ SAM is not deficient in homo-oligomerization, maybe even forms a slightly more stable oligomer (Fig. 12 B+C).

Also crosslinking mass spectrometry (XL-MS) with lysine-specific crosslinker BS3 showed similar crosslinking pattern for Fun30 and Fun30 Δ SAM, indicating comparable folding of the two (Fig. 12 F).

Overall, we concluded that Fun30 Δ SAM is folded comparable to wildtype and any defects observed should not be due to gross misfolding or instability of the mutant.

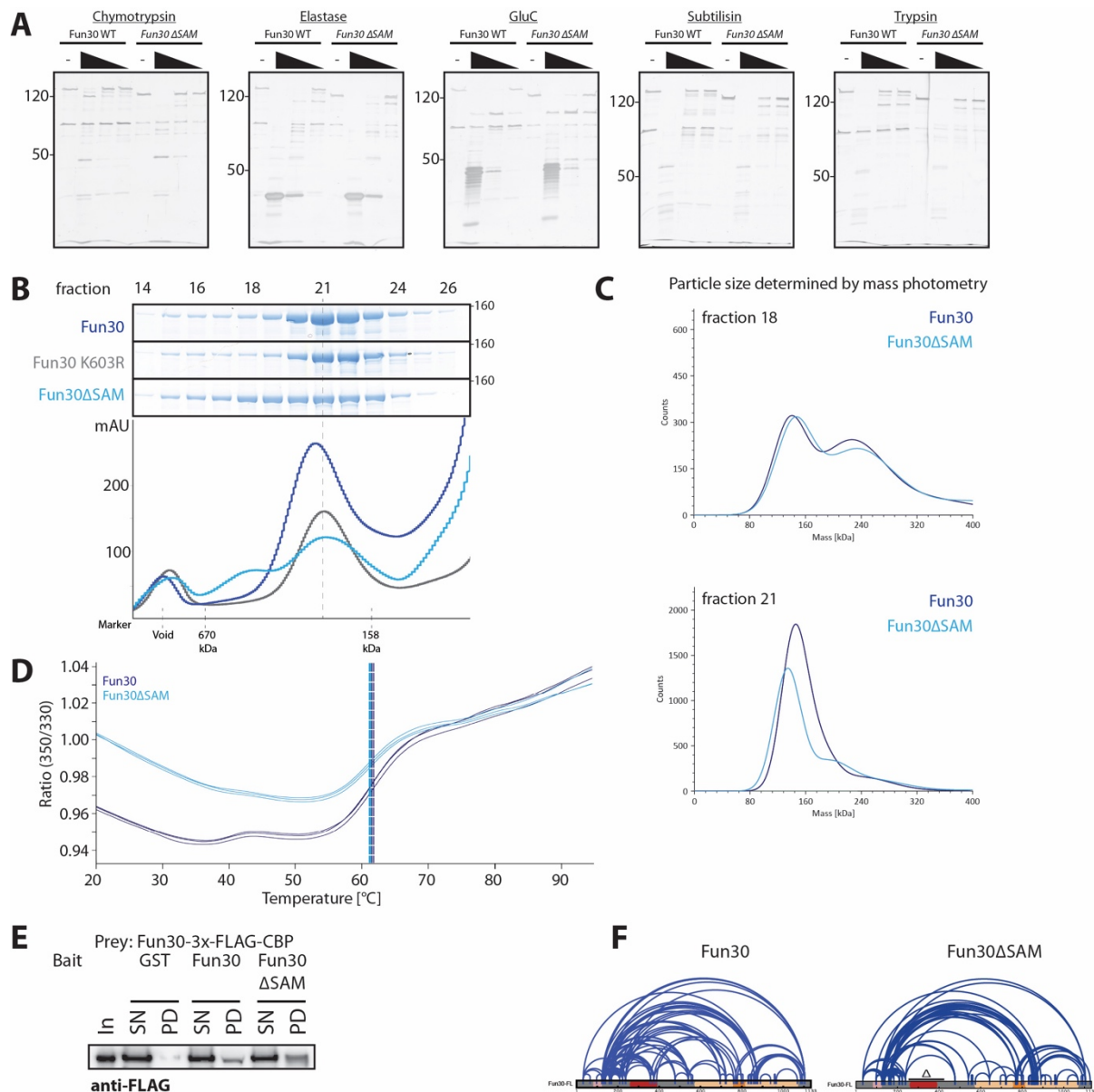


Figure 12: Lack of the SAM-key does not induce gross misfolding of Fun30 or abrogate DNA or nucleosome binding. **A:** Limited proteolysis of Fun30 WT and Fun30 Δ SAM displays highly similar degradation profiles, demonstrating similar folding and stability. Titration of different proteases (chymotrypsin, elastase, GluC, subtilisin and trypsin) revealed similar stable proteolytic fragments of Fun30 and Fun30 Δ SAM. Due to the lower molecular weight of Fun30 Δ SAM some proteolytic fragments also show a lower weight respectively. Representative silver-stained gel, n=2. **B:** Representative elution profiles and chromatograms of gel filtration (Superdex200, n=4 replicates): Fun30 WT (dark blue) and Walker A mutant K603R (grey) peak around fraction 21. Fun30 Δ SAM (light blue) however has a more spread elution profile with a second peak visible in the chromatogram that is eluting earlier, around fraction 18. Fractions are 0.5 mL, fraction 14 corresponds to void. X-axis indicates elution peaks of marker proteins. **C:** Mass photometry with Fun30 (dark blue), and Fun30 Δ SAM (light blue) after gel filtration shows differences for early (18) and peak (21) fractions. For fraction 18 two peaks are visible, one around the molecular weight of the monomer (~130 kDa), the other one almost equally high of a dimer (~240 kDa), suggesting approximately 1:1 ratio of monomer and dimer. For fraction 21 mainly the monomer for both Fun30 and Fun30 Δ SAM is detected. A shoulder peak, likely corresponding to the size of a dimer, making up approximately 30% for Fun30 Δ SAM and about 10% for Fun30. Particle counts of 50 nM in 20 μ L buffer on measurement of 60 seconds, representative histograms, n=2.

D: NanoDSF of Fun30 and Fun30 Δ SAM shows similar thermal unfolding (20-90°C gradient at a rate of +1°C/min) between Fun30 WT and Fun30 Δ SAM. Main inflection points are almost identical with 61.7°C (WT) and 61.3°C (Δ SAM) (measured in triplicates).

E: CoIP of Fun30-3xFLAG-CBP with His-GST-Fun30 WT or His-GST-Fun30 Δ SAM and a tag-only construct (GST-pulldown). Anti-FLAG-tag Western blot shows both Fun30 and Fun30 Δ SAM display similar low binding capacity to Fun30-3xFLAG-CBP. Representative blot, n=2.

F: XL-MS with BS3 crosslinking (100x molar excess) of both Fun30 and Fun30 Δ SAM show a comparable number of crosslinks (n=135 for Fun30 and n=143 for Fun30 Δ SAM) and a similar pattern (shown in 2D, both crosslinking data sets were mapped on the full-length sequence for comparison, deleted sequence in Fun30 Δ SAM indicated with “ Δ ”).

8. Fun30 Δ SAM is proficient in DNA and nucleosome binding

Next, we tested whether the SAM-key may influence the binding of Fun30 to DNA or nucleosomes and a mutant may have altered interaction with the substrate and thus be defective. We performed gel-shift analysis after native PAGE to test Fun30 binding to double-stranded (ds) DNA carrying an end-positioned Widom-601-positioning sequence (100W0; 247 bp).

Fun30 displays moderate DNA binding at high nanomolar concentrations, but binding was not influenced by the deletion of the SAM-key (Fig. 13 A+E).

Next, we tested binding to end-positioned mono-nucleosomes that were assembled on the same dsDNA with a 100 bp overhang (100W0) and labelled on histone H2A with the fluorophore Dylight 550 maleimide (Safaric et al., 2022). A large proportion of these nucleosomes were bound by Fun30 in the nanomolar concentration regime, but binding was independent of the SAM-key domain (Fig. 13 B+E). SAM-key independent binding of Fun30 to nucleosomes was also confirmed by *in vitro* coIPs of nucleosomes using the His-GST-tagged versions of Fun30 and Fun30 Δ SAM (Fig. 13 C). Nucleosome binding was reversible by addition of excess herring sperm DNA (Fig. 13 D). In all, Fun30 binding to its nucleosome substrate is largely intact in the absence of the SAM-key.

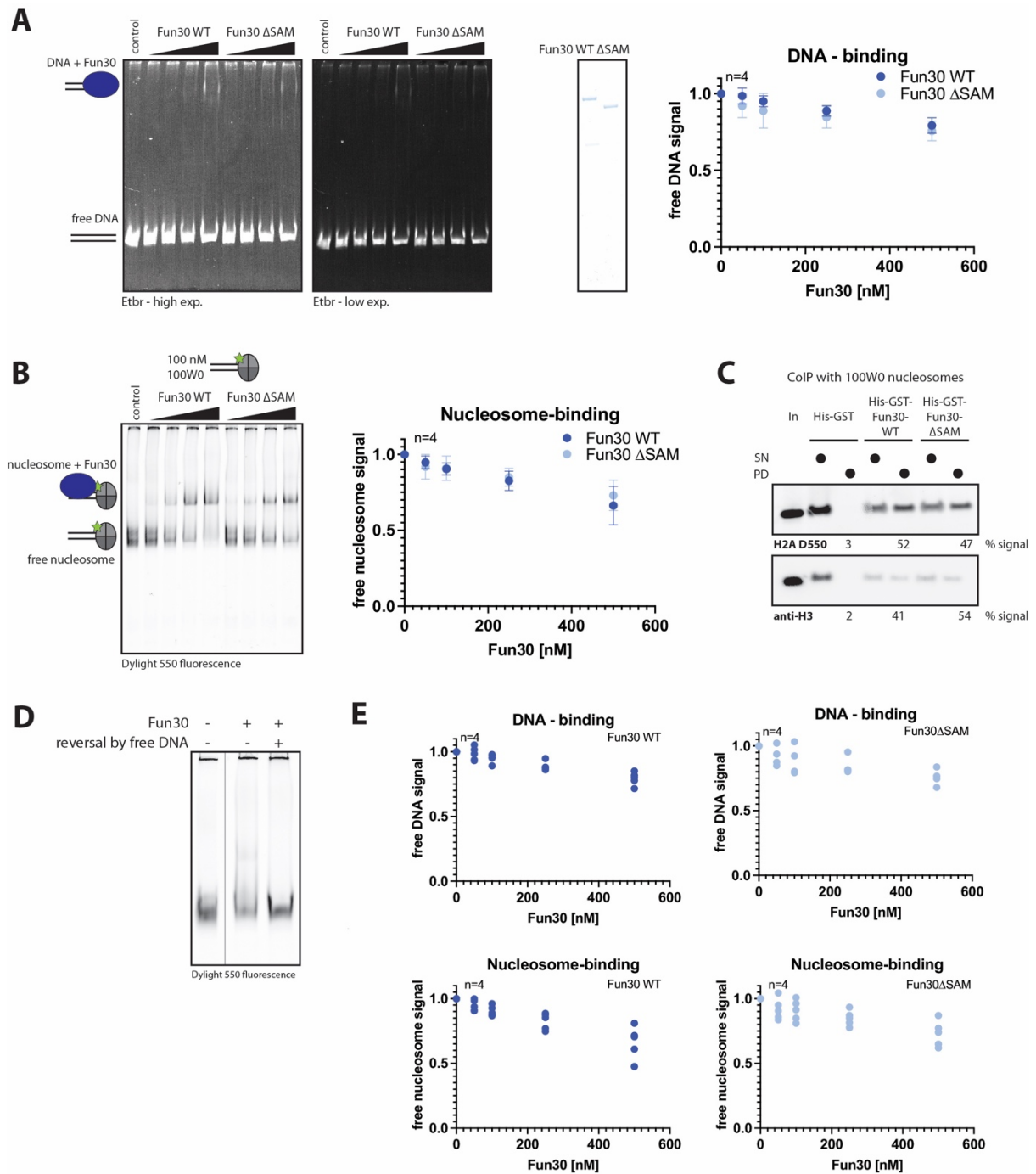


Figure 13: The SAM-key domain is not required for Fun30 binding to DNA or nucleosomes.

A: SAM-key is not required for DNA binding.

Left: Representative gel picture ($n=4$ biological replicates) showing binding of purified Fun30 and Fun30 Δ SAM in gel-shift with a 247bp dsDNA construct (100 nM), carrying an end-positioned Widom 601 nucleosome positioning sequence (100W0) stained by ethidiumbromide. Protein titration: 50, 100, 250, 500 nM. High exposure (left) and lower exposure (right) are shown to visualize shifted species. Coomassie gel (middle) shows equal amounts of input protein (same for Fig. 13 B, DNA and nucleosome binding experiment was performed side-by-side). Right: Quantification of free DNA in presence of Fun30 WT (dark blue) and Fun30 Δ SAM (light blue) normalized to control lane (without remodeler). $n=4$ replicates, shown is mean, error-bars depict standard deviation. Individual datapoints of replicates are shown in Fig. 13 E.

B-C: SAM-key is not required for nucleosome binding.

B: Gel-shift assay as in A, but with end-positioned yeast nucleosome on the 100W0 DNA. Histone H2A was labeled with Dylight550 maleimide (ThermoFisher) at cysteine 46 (H2A 46-C-D550). $n=4$ replicates, shown is mean, error-bars depict standard deviation. Individual datapoints of replicates are shown in Fig. 13 E.

C: Nucleosome pulldown with His-GST-Fun30 WT or His-GST-Fun30 Δ SAM and a tag-only construct (IP for GST) and reconstituted yeast nucleosomes. Western blot for histone H3 and fluorescence imaging of labeled H2A (H2A 46-C-D550) shows both Fun30 proteins bind comparably to nucleosomes. Percentage numbers below indicate quantification of the signal in the pulldown band relative to total signal.

D: Nucleosome binding by Fun30 is reversible by addition of herring sperm DNA (1 μ g), as shown for the highest titration value (500 nM). Histone H4 was labeled with Dylight550 maleimide (ThermoFisher) at cysteine 64 (H4 64-C-D550), n=2 replicates.

E: Single replicate values for quantification from Fig. 13 A and B.

9. DDC1-Fun30 Δ SAM does not make cells hyper-resective

To see if the apparently intact substrate recruitment of Fun30 Δ SAM may be an *in vitro* artifact, we tested the mutant *in vivo* in a *DDC1-FUN30 Δ SAM*-fusion construct that forces recruitment to DSB sites. We measured resection by RPA ChIP qPCR to a single, induced DSB. The force-recruitment of the protein to a DSB lead to a hyper-resection phenotype with resection spreading up to 20 kb after 2h, compared to about 10 kb with non-fusion Fun30 (Fig. 14 A). The *DDC1-FUN30 Δ SAM*-fusion failed to achieve this hyper-resective phenotype, resection spreading similar to the non-fusion Fun30 (Fig. 14 A). To verify this, we also tested resistance to CPT with the *DDC1-FUN30 Δ SAM*-fusion. At lower dosage (6 μ g/mL CPT) a slightly better growth compared to *fun30 Δ* could be observed, but at higher dosage (10 μ g/mL) no difference to *fun30 Δ* could be observed (Fig. 14 B). This consolidates that the deficiency of the Fun30 Δ SAM mutant does not seem to be recruitment to breaks, DNA or nucleosomes.

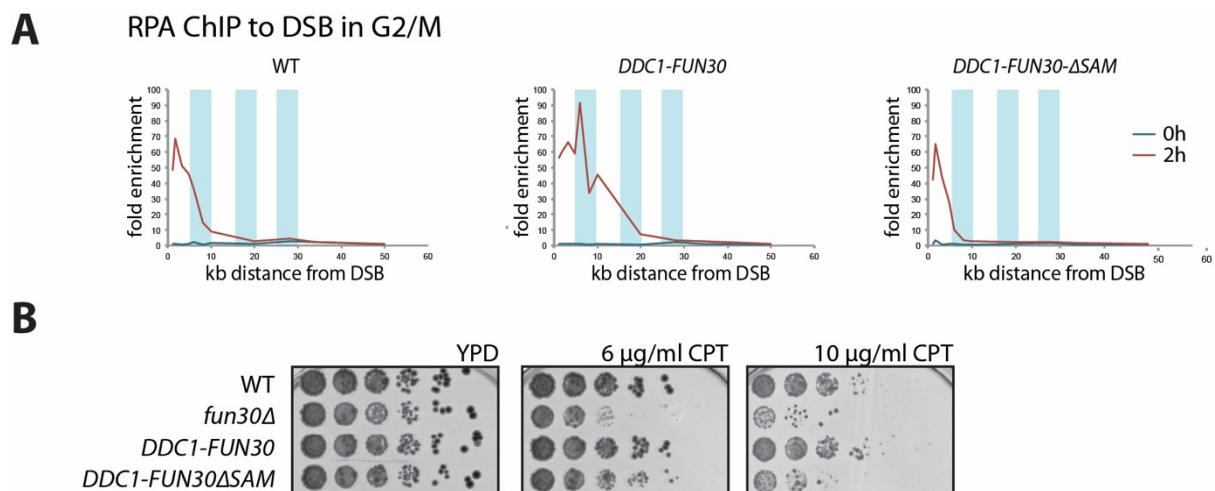


Figure 14: Ddc1-Fun30 Δ SAM-fusion does not cause over-resection phenotype.

A: Spreading of resection as measured by RPA ChIP qPCR to a single, induced DSB (MAT locus) in G2/M phase shows the over-resection phenotype for Ddc1-Fun30 full-length while no over-resection can be observed for Ddc1-Fun30 Δ SAM.

B: CPT sensitivity of a *fun30 Δ* strain. Ddc1-Fun30-fusion is able to rescue *fun30 Δ* while Ddc1-Fun30 Δ SAM is not. Representative plate of n=3.

10. Fun30 Δ SAM is inactive

Given that deletion of the SAM-key resulted in a loss-of-function phenotype *in vivo*, we tested for Fun30 catalytic activity *in vitro*. Previous work had shown that purified Fun30 is able to slide end-positioned nucleosomes on dsDNA to a more central position (Awad et al., 2010; Byeon et al., 2013) in an ATP-dependent reaction (Fig. 15 A). Similarly, we observed that also in our hands, Fun30 is able to slide nucleosomes off an end-positioned Widom-601-sequence (100W0) in a reaction that required ATP

hydrolysis (Fig. 15 B, seen for differentially H4- and H2A-labelled nucleosomes). Titrating Fun30 concentration, we observed that Fun30 was able to catalyze sliding, but neither the catalytic inactive Fun30-K603R mutant nor Fun30 Δ SAM were able to support this reaction (Fig. 15 C).

It has been argued that histone dimer or octamer eviction was a key enzymatic activity of Fun30-SMARCAD1-Etl remodelers (Awad et al., 2010; Markert et al., 2021). To measure histone eviction, we employed the histone chaperone Nap1, which is known to bind H2A-H2B dimers as well as H3-H4 tetramers (McBryant et al., 2003; Park et al., 2005). When added to sliding reactions, Nap1 functions as acceptor for evicted histones and we can therefore follow H2A-H2B eviction with fluorescently labelled H2A (Fig. 15 D). Furthermore, we can detect eviction not only by loss of original nucleosome signal but also by appearance of a labeled H2A-H2B in complex with Nap1 as well as re-appearance of free DNA (Fig. 15 E-G). Specifically, we observed that eviction is dependent on Fun30 in an ATP-hydrolysis- as well as concentration-dependent manner (Fig. 15 E). Moreover, H2A-H2B eviction was abolished in Fun30 Δ SAM and Fun30-K603R mutant proteins, showing that also in this context, the SAM-key was required for remodeling activity (Fig. 15 F-G).

While Fun30 was shown to have H2A-H2B dimer exchange activity, the occurrence of nucleosome-free DNA suggests that in the context of our assay nucleosomes are entirely removed from DNA and complete removal of the histone octamer from DNA has been a suggested mechanism for SMARCAD1 (Markert et al., 2021). Therefore, we measured eviction of H3-H4 tetramers using labelled histone H4 (Fig. 15 H). Also in this case, we observed eviction with wildtype Fun30, but not with Fun30 Δ SAM protein.

As a third, quantifiable read-out of Fun30 activity, we measured ATP hydrolysis. To this end, we used a NADH-oxidation-coupled, absorbance-based (A₃₄₀) assay to measure ATP hydrolysis rates at steady state (Forné et al., 2012). This assay showed very low ATP hydrolysis by isolated Fun30, but different constructs of single-stranded and double-stranded DNA stimulated ATP hydrolysis by Fun30 up to k_{cat} of 3 s⁻¹ (Fig. 15 I-J). Interestingly, the stimulus that seemed to be best for Fun30 appeared to be ssDNA, likely with some secondary structures as a ssDNA oligonucleotide (120 nt) and denatured and sheared herring sperm DNA were stimulating higher ATP hydrolysis with lower concentrations (Fig. 15 J).

Notably, when we compared Fun30 Δ SAM to the full-length protein with herring sperm DNA stimulus titration (Fig. 15 K) or using 100 ng/ μ L herring sperm DNA as standard concentration (Fig. 15 L), we found that the SAM-key was required for DNA-stimulated ATP hydrolysis.

We concluded that the SAM-key is either intrinsically required for ATP hydrolysis or that it is critical for allosteric activation of the ATPase.

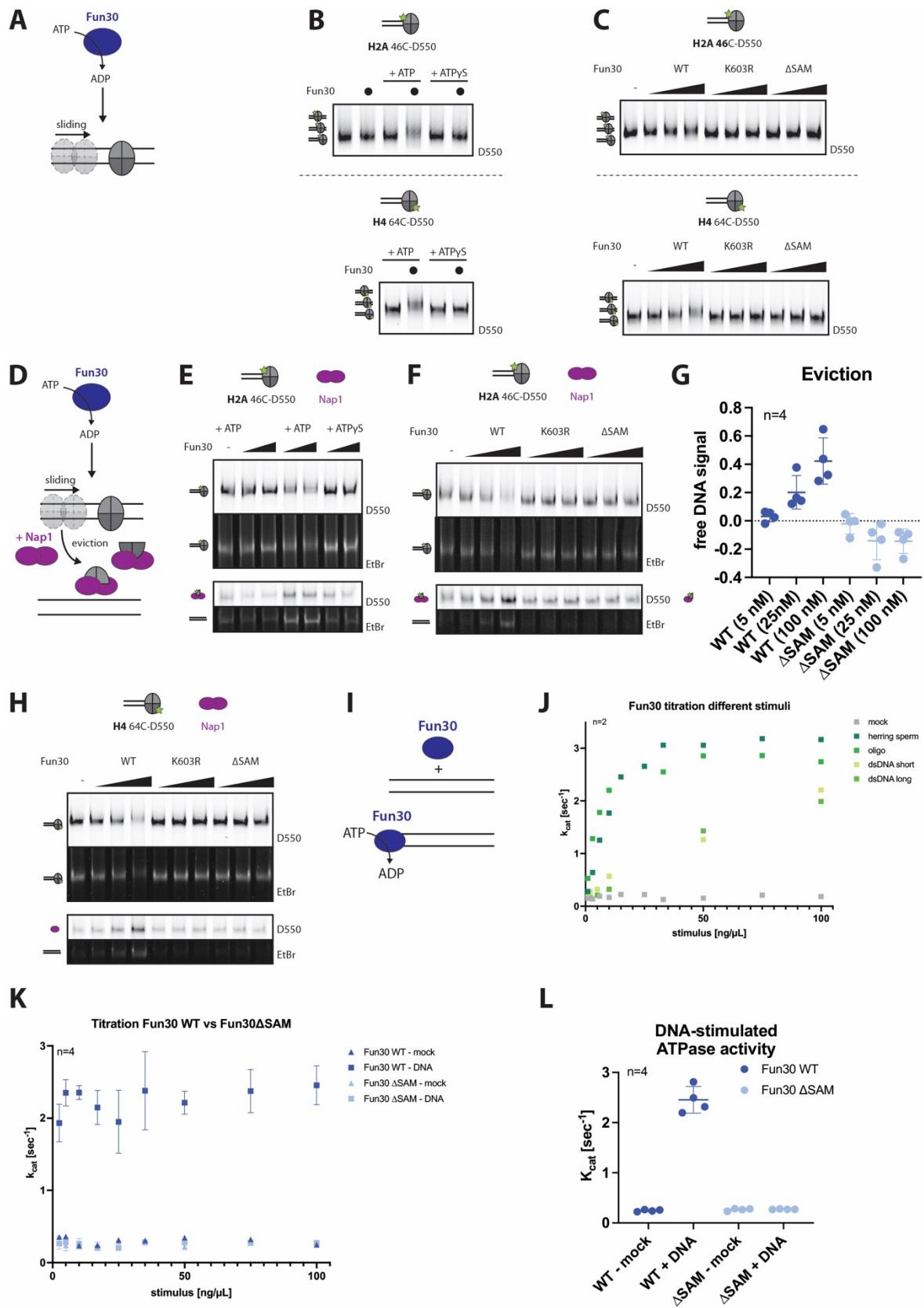


Figure 15: The SAM-key is required for Fun30 nucleosome remodeling.

A-C: The SAM-key is required for nucleosome sliding.

A: Schematic of nucleosome sliding assay: An end-positioned nucleosome is mobilized towards the center of a DNA fragment catalyzed by remodeler in ATP-dependent fashion.

B: Sliding of nucleosomes with labeled H2A (46 C-D550, top) or labeled H4 (64 C-D550, bottom) assembled on a 100W0 fragment (247 nt fragment with end-positioned Widom 601-positioning-sequence) as seen by upshift in gel. Shown is ATP-dependence as addition of ATP, but not ATP γ S allows sliding. Representative gel of n=4 biological replicates.

C: Sliding assay as in B, but Fun30 WT, Fun30 K603R (Walker A mutant) and Fun30 Δ SAM mutant. Representative gel of n=4 biological replicates.

D-G: The SAM-key is required for nucleosome eviction.

D: Schematic of nucleosome eviction assay: Addition of remodeler, ATP and histone chaperone Nap1, which acts as acceptor for nucleosomes, leads to eviction. Nap1 binds the free H2A-H2B dimers and H3-H4 tetramers. Additionally, since end-positioned nucleosomes are used, also sliding can be observed. The nucleosome is mobilized towards the center of a DNA fragment by Fun30 under consumption of ATP and in the presence of histone chaperone Nap1 the nucleosome is evicted from the DNA.

E: Eviction of nucleosomes with labeled H2A (46 C-D550, top). Eviction is seen is by (i) decrease of labeled nucleosome (top), (ii) decrease of nucleosome signal in ethidium bromide stain (2nd from top), (iii) increased Nap1-bound labelled histone (3rd from top), (iv) increase of “free” DNA in ethidiumbromide stain (bottom). ATP- and remodeler-dependent eviction is shown by addition of ATP, ATP γ S and Fun30. Representative gel of n=3 biological replicates.

F: Eviction assay as in E, but with Fun30 WT, Fun30 K603R (Walker A mutant) and Fun30 Δ SAM mutant and with labeled H2A (46 C-D550). Representative gel of each n=4 biological replicates.

G: Quantification of nucleosome eviction of Fun30 WT (dark blue) or Fun30 Δ SAM (light blue) by free DNA signal (H4-label as representative), shown is intensity of free DNA peak normalized to control without remodeler. n=4 replicates shown is mean, error-bars depict standard deviation.

H: Eviction assay as in F, but with labeled H4 (64 C-D550). Representative gel of n=4 biological replicates.

I: Schematic of DNA stimulated ATPase activity: Nucleosome remodeler can be stimulated to hydrolyze ATP when in the presence of DNA or nucleosomes as stimulus.

J: Titration of different DNA constructs to stimulate ATPase activity of Fun30 wildtype: Herring sperm DNA (denatured) and a short 120 nt ssDNA oligo give the best stimulation up to a k_{cat} of about 3.0. DsDNA fragments required higher amounts to stimulate a similar amount of ATP hydrolysis. Without stimulus background was a k_{cat} of about 0.2. DsDNA short was 147 bp, long was 5 kb, n=2, shown is mean.

K: Titration herring sperm DNA constructs to stimulate ATPase activity of Fun30 (dark blue) or Fun30 Δ SAM (light blue): herring sperm DNA (square) would stimulate a k_{cat} of about 2.5 in Fun30 from as low as 10 ng/ μ L. Fun30 Δ SAM did reach a k_{cat} of about 0.2, comparable to background/unstimulated WT-rate (triangle), n=4 replicates shown is mean, error-bars depict standard deviation.

L: Absorbance-based (A340) ATPase assay using Fun30 (dark blue), Fun30 Δ SAM (light blue), ATP and DNA stimulus (herring sperm DNA, 100 ng/ μ L). n=4 replicates shown is mean, error-bars depict standard deviation.

11. SAM-key *in trans* complementation is possible

We therefore wondered whether the SAM-key could only function *in cis* as part of the same protein or whether *in trans* addition of the isolated SAM domain could restore catalytic activity of Fun30 Δ SAM. High amounts of the SAM-key (aa 275-436, yield ~1 mg/L culture) could be expressed and purified in *E. coli* (Fig. 16 A), further confirming its nature as protein domain. Addition of excess SAM-key could rescue the ATPase defect of Fun30 Δ SAM (Fig. 16 B) and also the nucleosome sliding defect (Fig. 16 C).

We therefore concluded that at sufficiently high concentrations the isolated SAM-key can bind to Fun30 Δ SAM and restore its function.

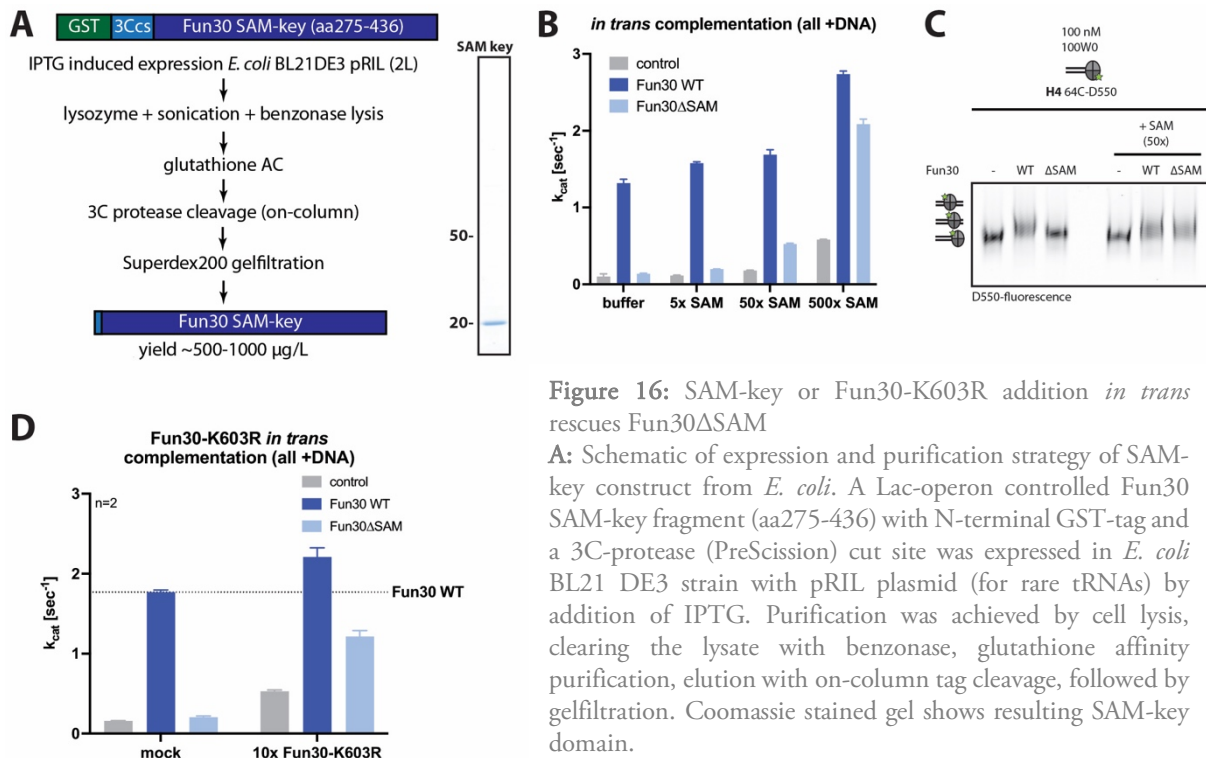


Figure 16: SAM-key or Fun30-K603R addition *in trans* rescues Fun30 Δ SAM

A: Schematic of expression and purification strategy of SAM-key construct from *E. coli*. A Lac-operon controlled Fun30 SAM-key fragment (aa275-436) with N-terminal GST-tag and a 3C-protease (PreScission) cut site was expressed in *E. coli* BL21 DE3 strain with pRIL plasmid (for rare tRNAs) by addition of IPTG. Purification was achieved by cell lysis, clearing the lysate with benzonase, glutathione affinity purification, elution with on-column tag cleavage, followed by gel filtration. Coomassie stained gel shows resulting SAM-key domain.

C: Sliding of nucleosomes with labeled H4 (64C-D550) assembled on a 100W0 DNA as seen by upshift in gel. Shown is dependence on the SAM-key domain as the Fun30 Δ SAM cannot slide but addition of a SAM-key construct (50x molar excess) *in trans* allows sliding. Representative gel of n=3 biological replicates.

D: Absorption-based (A340) ATPase assay Fun30 (dark blue), Fun30 Δ SAM (light blue) or control reactions (grey). All reactions included ATP and DNA stimulus (herring sperm DNA 100ng/ μ L), titrating Fun30-K603R as *in trans* addition of different molar excess. With both Fun30 Δ SAM and excess (10x) of Fun30-K603R a k_{cat} of ~ 1.2 can be observed. n=2 biological replicates, shown is mean, error-bars depict standard deviation.

Since it has been previously suggested that the dimeric form of Fun30 is the active remodeler, we also tested if the SAM-key present in the Fun30-K603R mutant could rescue the defect of the Fun30 Δ SAM mutant. Addition of excess Fun30-K603R could restore the ATPase defect of Fun30 Δ SAM to a certain degree (Fig. 16 D). Due to limiting protein amount we did not test as high excess of Fun30K603R over Fun30 Δ SAM as with the SAM-key construct. This suggests that a hetero-dimer of Fun30-K603R and Fun30 Δ SAM was able to perform DNA-stimulated ATP hydrolysis, while the respective monomers or homodimers could not. The lower activity/the requirement for excess of Fun30-K603R could be explained by the fact that most likely only a fraction of the molecules will be engaged as heterodimer at any time, especially considering the previously mentioned slightly higher stability of Fun30 Δ SAM oligomers observed during gel filtration (Fig. 12 B) and the fact that only a fraction of purified protein is in oligomeric form (Fig. 12 C) that additionally decreased over time.

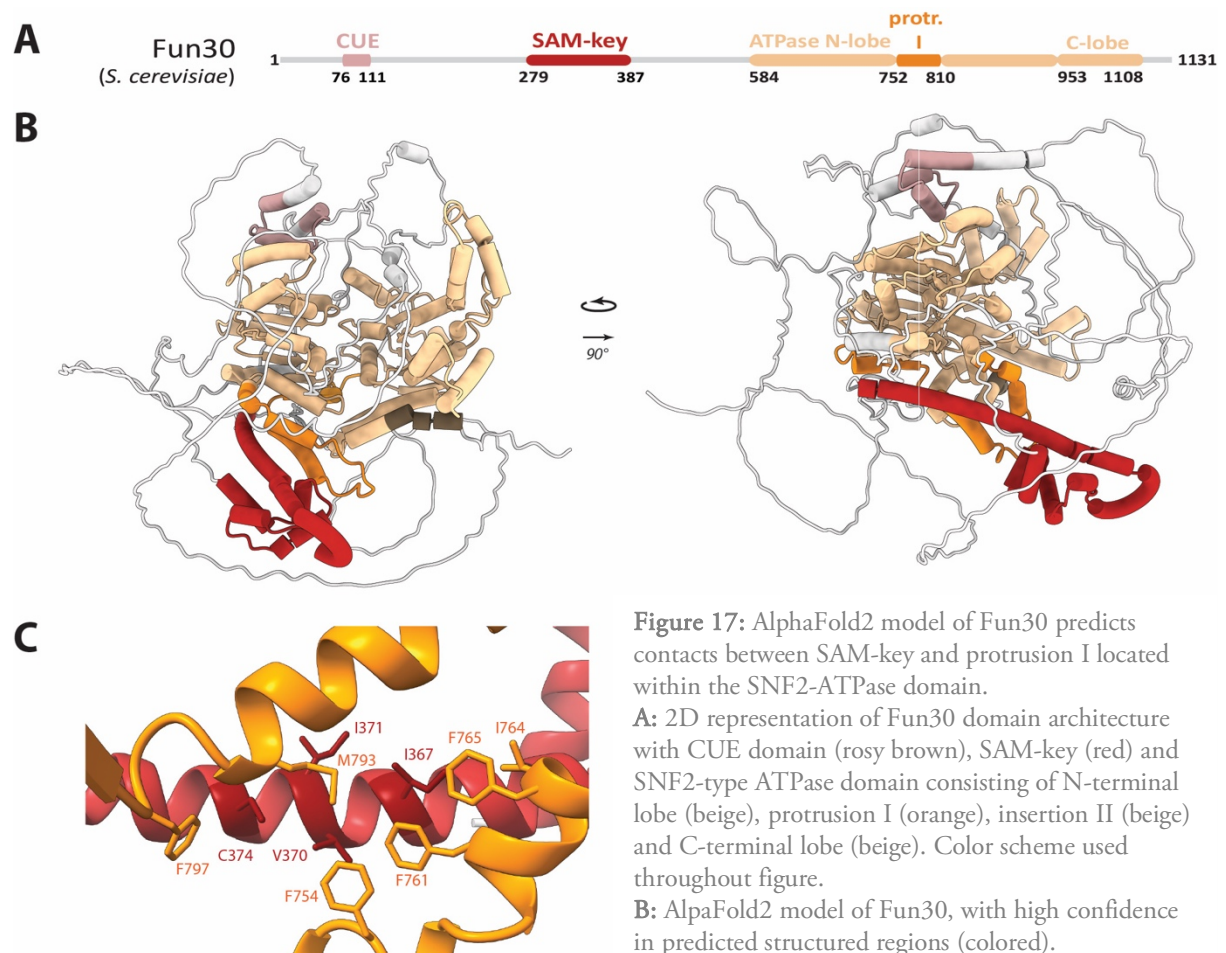
Still, in case a heterodimer forms, we conclude that the SAM-key of Fun30-K603R can bind to Fun30 Δ SAM and restore its function. With the K603R mutant being unable to bind ATP we can also exclude that this ATP hydrolysis is performed by the K603R molecule. Compared to the SAM-key alone, in the context of Fun30 there are likely additional areas that drive binding to Fun30, therefore stabilizing the interaction and thus lowering the requirement for excess SAM-key to activate the protein.

12. AlphaFold2 modeling of Fun30 predicts hydrophobic interaction of SAM-key with ATPase domain – specifically with protrusion I

Without any Fun30 structure larger than part of the ATPase domain (Liu and Jiang, 2016) and in order to identify the mechanism by which the SAM-key affects nucleosome remodeling by Fun30-SMARCAD1-ETL remodelers we turned to a structural model for the full-length protein obtained using AlphaFold2 (Jumper et al., 2021; Varadi et al., 2022). The AlphaFold2 model of Fun30 shows the structure of the two-lobed ATPase domain (Fig. 17 A+B, beige), including the insertion between the two lobes (beige) harboring protrusion I (orange) (Fig. 17 A+B). The model predicts the N-terminal half of the protein as largely unstructured with the exception of CUE (rosy brown) and SAM-key (red) domains (Fig. 17 B). Notably, the model shows an interaction surface between SAM-key and protrusion I (Fig. 17 B+C).

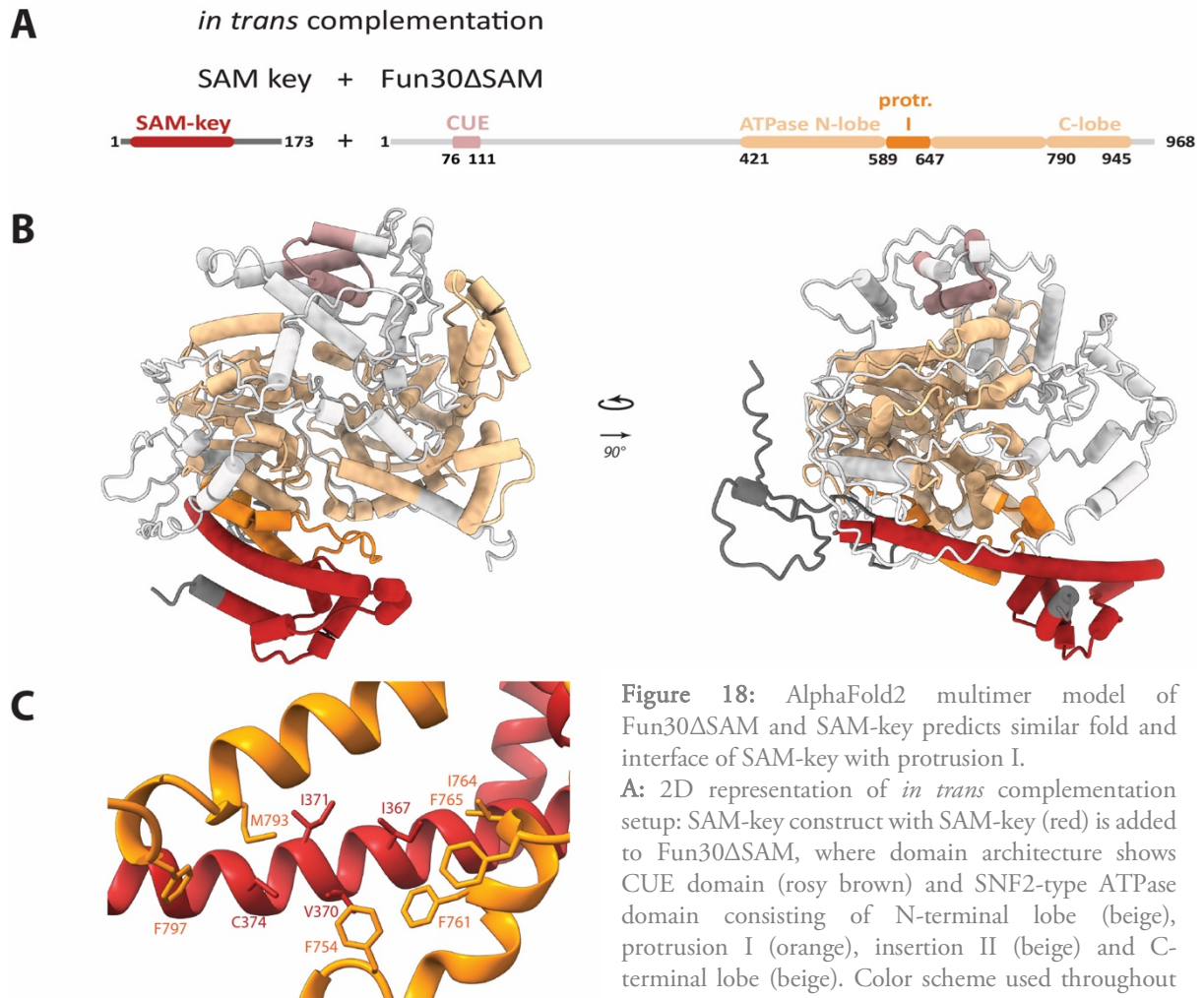
Specifically, this interaction surface involves the long SAM-key helix (345-388) and helices 1 (761-769) and 2 (781-799) of protrusion I.

The interaction appears to be mediated by hydrophobic interactions by several residues: I367, V370, I371 and C374 -all highly conserved, C374 being one of the most conserved residues (Fig. 5)- of SAM-key (Fig. 17 C, red) and F754, F761, I764, F765, M793 and F797 of protrusion I (Fig. 17 C, orange).



C: Zoom in of SAM-key (red) with predicted interaction to the protrusion I (orange). Amino acids likely contributing to hydrophobic interaction surface are highlighted: I367, V370, I371 and C374 of SAM-key (red) – F754, F761, I764, F765, M793, F797 of protrusion I (orange).

Notably, AlphaFold2 multimer (Jumper et al., 2021) modelled the same interaction surface when SAM-key and Fun30 Δ SAM were provided as separate polypeptide chains, as is the case in the *in-trans*-complementation scenario (Fig. 18 A-C). Overall, the model strongly suggests a hydrophobic interaction of SAM-key with protrusion I of the ATPase domain, potentially important for function of the ATPase domain.



B: AlphaFold2 multimer model of Fun30 Δ SAM and SAM-key shows interaction surface between SAM-key and protrusion I as in the full-length protein. Model shows high confidence in predicted structured regions (colored).

C: Zoom in of SAM-key (red) with predicted interaction to the protrusion I (orange). Amino acids contributing to hydrophobic Interaction surface are highlighted: I367, V370, I371, C374 of SAM-key (red) and F754, F761, I764, F765, M793 and F797 of protrusion I (orange).

13. XL-MS data confirm AlphaFold2 model of Fun30 and position of the SAM-key close to protrusion I

To verify the AlphaFold2 models, we conducted crosslinking mass-spectrometry (XL-MS) using the lysine-selective crosslinker BS3. We tested full-length Fun30 in the absence or presence of ATP, as well as using the *in-trans*-complementation conditions with SAM-key added to Fun30 Δ SAM (Fig. 18). All conditions gave a similar number of crosslinks ranging from 135-153, with the exception of the *in trans*

complementation setup with >200 (Fig. 19+20 A). Also the overall pattern of crosslinks was similar for Fun30 without and with addition of ATP (Fig. 19 B) as well as for Fun30 and Fun30 Δ SAM (Fig. 20 B). To use the XL-MS datasets to ascertain the AlphaFold2 model of Fun30, we filtered for crosslinks between two amino acids that were located in structured parts of the model +/- 2 amino acids (Fig. 20 A) and tested whether those crosslinks would satisfy a 35 Å distance threshold (Fig. 19 C-D). We found n=7 (Fun30-ATP) or n=4 (Fun30+ATP) crosslinks connecting the CUE domain to other parts of the protein that did not satisfy the distance constraint, suggesting wrong relative position of CUE domain in the model and/or a flexible location within the overall Fun30 structure (Fig. 19 C).

In contrast, the remaining crosslinks (n=40 for -ATP / n=31 for +ATP) were matched to the structural model and connected different parts of the ATPase domain and the SAM-key (Fig. 19 C). Notably, this included n=4 crosslinks that confirm close proximity of the predicted interaction surface of protrusion I and SAM-key (Fig. 19 D).

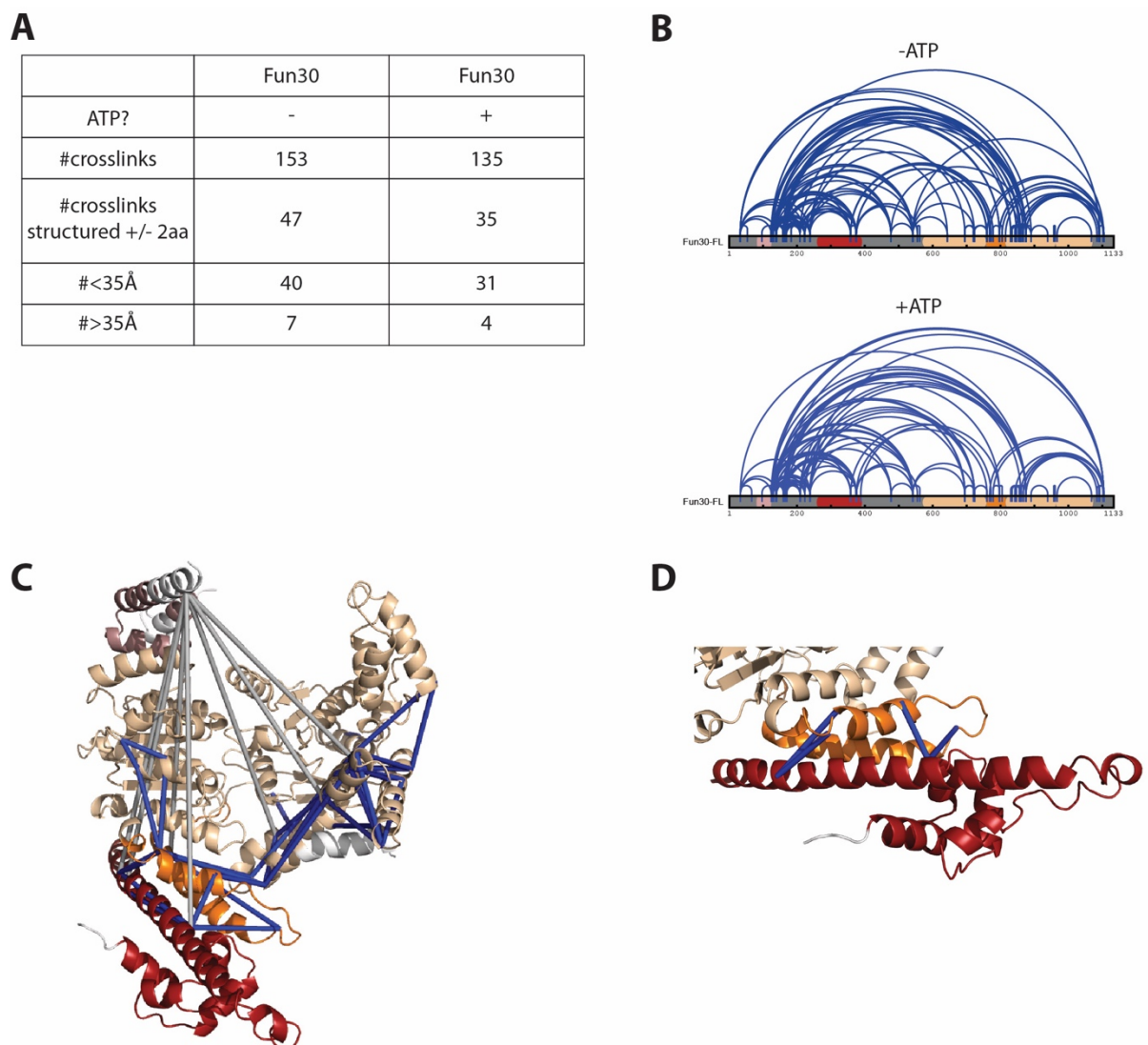


Figure 19: XL-MS with BS3 crosslinking verifies the AlphaFold2 model.

A: Table showing XL-MS results for Fun30 with or without ATP. Shown are number of crosslinks before and after filtering crosslinks according to position in a predicted structured region (+/- 2 aa) in the AlphaFold2 model and calculated length with a threshold for BS3 of 35 Å.

B: 2D-representation of crosslinks in blue on Fun30 with or without ATP (unfiltered). To get an overview of the general crosslinking pattern all measured crosslinks were considered. No major changes were detected between the sample crosslinked in absence of ATP (n=153, top) compared to the sample with ATP (n=135, bottom).

C: 3D-mapping of crosslinks on AlphaFold2 model. Crosslinks shown as connectors for Fun30 without ATP. Crosslinks in low confidence, unstructured regions were removed, only crosslinks within predicted structured regions +/- two additional aa residues were considered. Blue crosslinks (n=40) match the model with a length restriction for BS-3 of 35 Å. Grey crosslinks (n=7) violate the threshold (>35 Å) and all involved the CUE domain (rosy brown).
D: SAM-key showed 4 crosslinks, all matching 35 Å distance constraint and confirming the position in close proximity to protrusion I.

Overall similar results were obtained when SAM-key was crosslinked to Fun30ΔSAM (Fig. 20 A-D) and comparing it to the AlphaFold2 multimer prediction. The multimer model was strikingly similar to the model of the wildtype with the exception of the CUE domain (rosy brown) being in similar position but in a different angle relative to the rest of the protein compared to the model for Fun30 WT. This could be another indication that CUE domain is in a wrong relative position in the model and/or that its location is flexible. We found again - as for Fun30 WT - several crosslinks (n=6) connecting the CUE domain to other parts of the protein that do not satisfy the distance constraint (CUE and crosslinks not depicted). We also found two other crosslinks that did not match the threshold, connecting the two ends of the long helix of the SAM-key, K338 with K372 or K373 respectively (Fig. 20 C). This could indicate that towards the N-terminal part the helix does not stretch as far as predicted and this region is more flexible. Another explanation could be that under SAM-key excess conditions we cannot exclude confounding inter-protein crosslinks between different SAM-key molecules.

In contrast, the other n=56 crosslinks were matched to the structural model and connected different parts of the ATPase domain and the SAM-key (Fig. 20 C). Notably, also in this case that included n=3 crosslinks that confirm close proximity of the predicted interaction surface of protrusion I and SAM-key (Fig. 20 D).

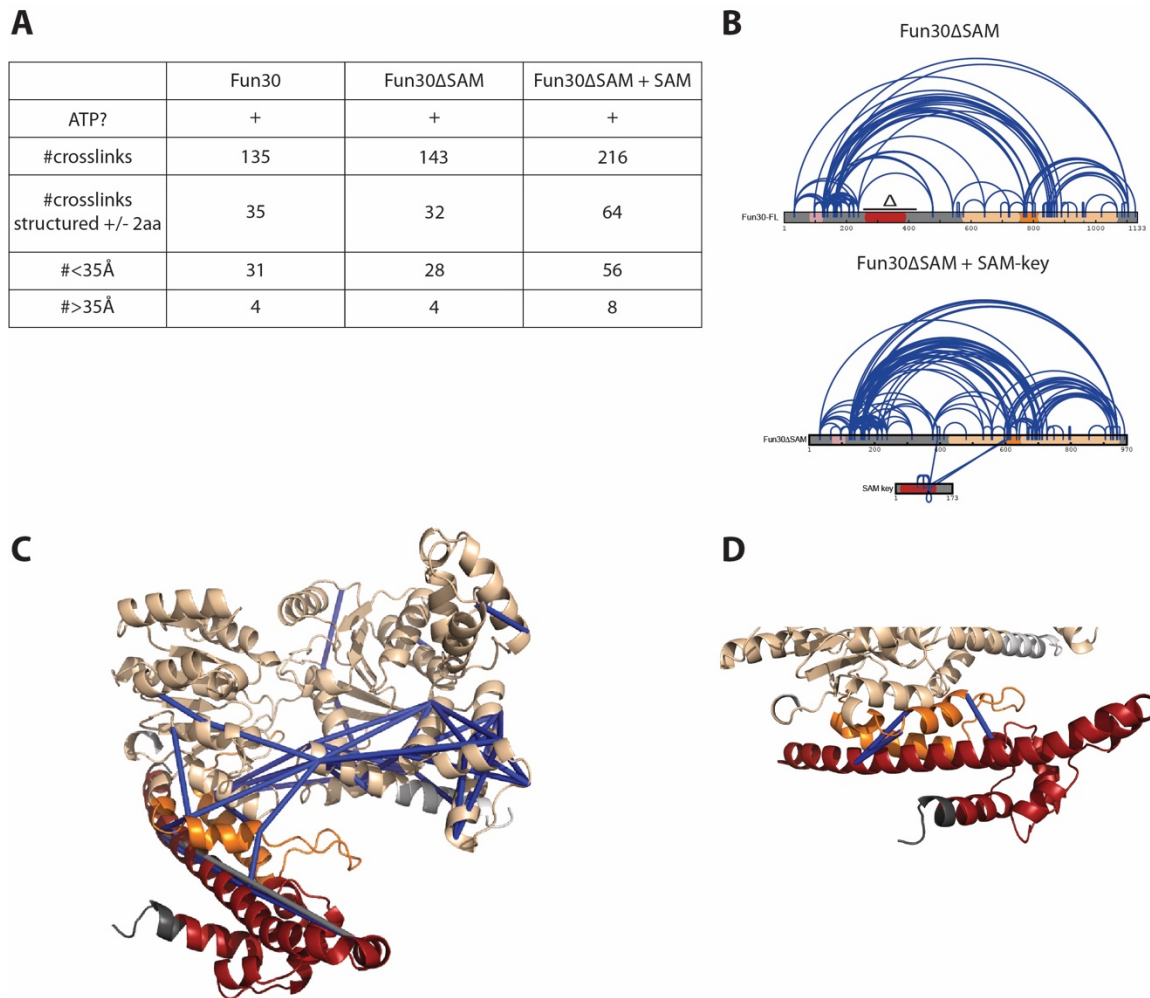


Figure 20: XL-MS verifies AlphaFold2 multimer model of Fun30 Δ SAM and SAM-key domain added *in trans*.
A: Table showing XL-MS results for Fun30 WT, Fun30 Δ SAM and the *in trans* complementation Fun30 Δ SAM + SAM (25x molar excess), all in presence of ATP, before and after filtering crosslinks according to position in a predicted structured region (+/- 2 aa) in the AlphaFold2 model and calculated length with a threshold for BS3 of 35 Å.
B: 2D-representation of crosslinks in blue on Fun30 with or without ATP (unfiltered). Crosslinks shown as connectors on 2D-projection of the wildtype Fun30 molecule for Fun30 Δ SAM and on the truncated sequence for the *in trans* complementation scenario. To get an overview of the general crosslinking pattern all measured crosslinks were considered. Excluding SAM-key crosslinks, no major changes were detected between the crosslinking pattern for Fun30 Δ SAM in absence of SAM-key (n=143, top) compared to the sample with SAM-key (n=216, bottom).
C: 3D-mapping of crosslinks on AlphaFold2 multimer model. Crosslinks shown as connectors for Fun30 Δ SAM + SAM. Crosslinks in low confidence, unstructured regions were removed, only crosslinks within predicted structured regions +/- two additional aa residues were considered. Blue crosslinks (n=56) match the model with a length restriction for BS3 of 35 Å. 2 crosslinks (grey) connect the two sides of the long helix of SAM-key with a distance >35 Å. The CUE domain and 6 other crosslinks >35 Å are not shown.
D: SAM-key showed 3 intermolecular crosslinks to Fun30 Δ SAM, all matching 35 Å distance constraint and confirming the position in close proximity to protrusion I.

We concluded that *in silico* structural modelling of Fun30 followed by experimental verification points toward the SAM-key contacting protrusion I, a part of the ATPase domain that is known to facilitate regulation of catalytic activity in nucleosome remodelers (Clapier et al., 2016; 2020; Szerlong et al., 2008).

14. Model comparison with other remodeler structures mostly lacks a structural analog for the SAM-key

To ascertain whether the SAM-key had any structural analogy to elements in other nucleosome remodelers, we made overlay of known remodeler structures with the AlphaFold2 model of Fun30 (Fig. 21 A). Of particular interest we thought were comparisons with other single-subunit remodelers like ALC1 from human or Chd1 from budding yeast. But we did overlays also for multi-subunit complexes like RSC or INO80 to see, if the SAM-key had an analogous function to one of the subunits there.

When we super-imposed the Fun30 model with structures of other remodelers and more specific their catalytic subunits, we saw a good fit of the highly conserved ATPase domain for all (Fig. 21 B-H). For ALC1 (Fig. 21 B) and Chd1 (Fig. 21 D), as well as Swr1 (Fig. 21 C) no structure at a similar position as the SAM-key could be seen. However, in case of Swr1 also a large part of the N-terminus of the protein is not resolved.

For Snf2, one helix from 671-689 could be in a similar position as the Fun30 SAM-key (Fig. 21 E, arrow), however also here a large part of the N-terminus of the protein is not resolved. For Isw1 (Fig. 21 F) some helices (103-143, Fig. 21 F, arrow) seem to be in similar position as the SAM-key. Yet again the structure is not fully resolved at this part, so it is difficult to judge analogous positioning. For Sth1 (RSC) again one helix from 393-407 could be in a similar position as the Fun30 SAM-key (Fig. 21 G, arrow), here the sequences both N- and C-terminal of this helix are not resolved. Also, the long helix of the HSA could be reminiscent of the long helix of the SAM-key, only turned by about 90° (Fig. 21 G).

Finally and most strikingly, we compared the Fun30 model to the composite model of cryo-EM plus crystal structure of the Arp-module (Kunert et al., *in press*) of Ino80 and found an almost perfect overlay of the long helix of the SAM-key with the very long helix consisting of post-HSA and HSA domain in Ino80 (Fig. 21 H, arrow).

Notably, the post-HSA/HSA domain in SWI/SNF and SWR1/INO80 remodelers bind to and assemble the so-called A-module involved in sensing extra-nucleosomal DNA and regulating activity of the remodeler (more details in chapter “Discussion”).

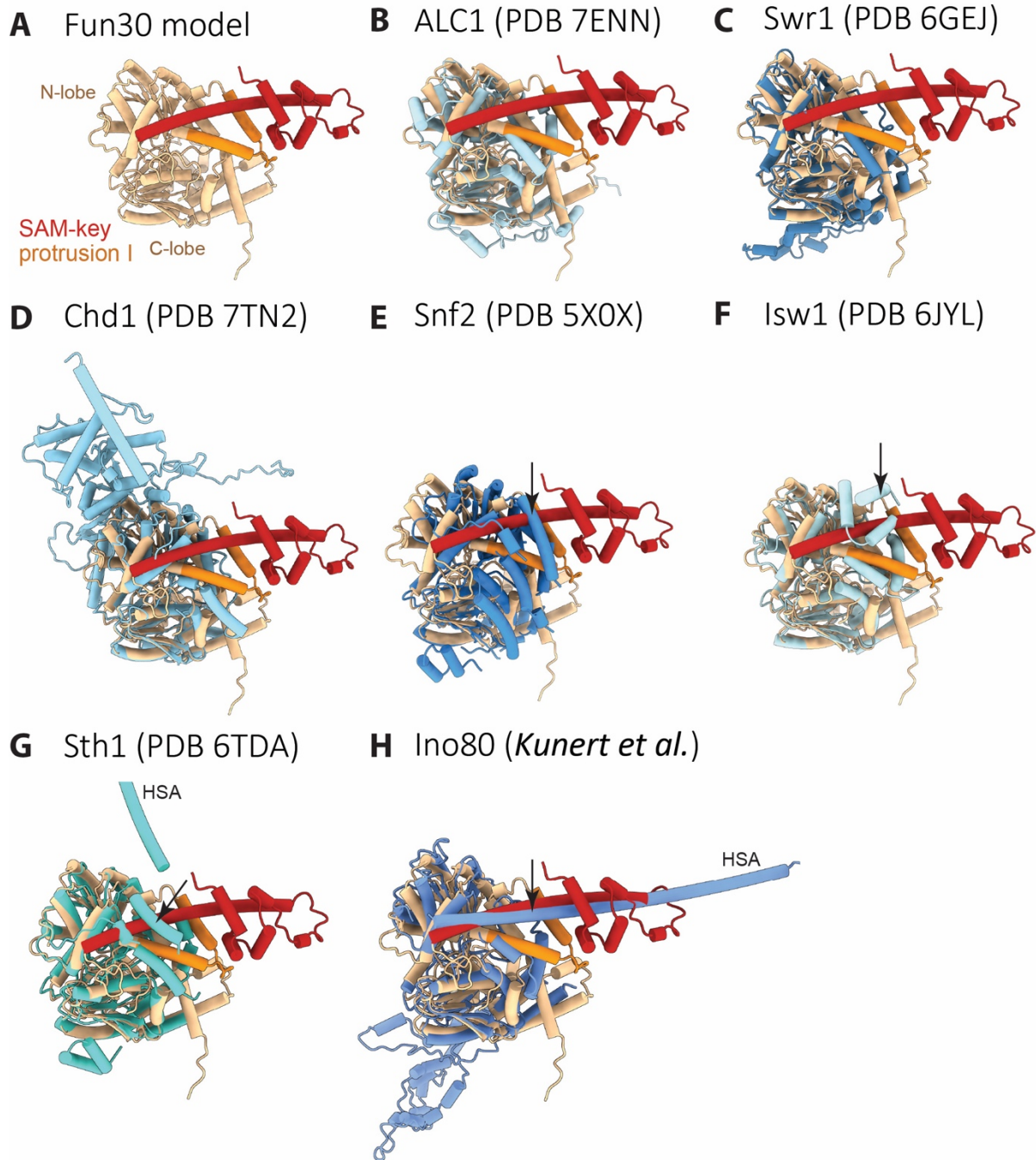


Figure 21: Overlays of Fun30 model with solved structures of other remodelers shows high conservation of the ATPase domain, and propose post-HSA/HSA as structural analog for the SAM-key.

A: Fun30 model showing only Fun30 SAM-key (red) and the ATPase domain (beige) with protrusion I (orange). Catalytic subunits of other remodelers (different shades of blue) were aligned to this model. Color scheme used throughout figure.

B: Overlay of Fun30 model with ALC1 (*H. sapiens*) (PDB: 7ENN)

C: Overlay of Fun30 model with Swr1 (SWR1 complex) (*S. cerevisiae*) (PDB: 6GEJ)

D: Overlay of Fun30 model with Chd1 (*S. cerevisiae*) (PDB: 7TN2)

E: Overlay of Fun30 model with Snf2 (SWI/SNF) (*S. cerevisiae*) (PDB: 5X0X); arrow indicates helix 671-689 in similar position as SAM-key.

F: Overlay of Fun30 model with Isw1 (ISWI) (*S. cerevisiae*) (PDB: 6JYL); arrow indicates helices 103-143 in similar position as SAM-key.

G: Overlay of Fun30 model with Sth1 (RSC complex) (*S. cerevisiae*) (PDB: 6JYL); arrow indicates helix 393-407 in similar position as SAM-key.

H: Overlay of Fun30 model with Ino80 (INO80 complex) (*C. thermophilum*) (Kunert et al., *in press*); arrow indicates post-helicase-SANT-associated/ helicase-SANT-associated (post-HSA/HSA) helix contacting the ATPase domain in highly similar manner to the Fun30 SAM-key.

15. Docking of the model to nucleosomes suggest SAM-key could be a functional and structural analog to post-HSA domain

To understand the function of nucleosome remodeler Fun30 one needs to consider how it may engage a nucleosome and how the SAM-key is positioned with relation to nucleosomal DNA and histones. So we aligned the Fun30 model with remodeler-nucleosome co-structures, engaging the nucleosome at SHL+2 or SHL-6. We also docked the Fun30 model to the dyad as observed in cryo-EM for SMARCAD1 (Markert et al., 2021), using the typical Swi2/Snf2 ATPase-DNA interactions at SHL+2 as guide.

Alignment with the Ino80 ATPase at SHL-6 (Fig. 22 B+C) reveals that the long helix of the SAM-key projects along DNA in a manner similar to the INO80 post-HSA/HSA domain (Fig. 22, B-C). Alignment at SHL+2 like Chd1 or RSC (Fig. 22 B) could indicate the SAM-key projects the loop at the N-terminus of the long helix towards nucleosomal DNA at the dyad (Fig. 22 C). Docking at SHL 0 (dyad) indicated that at this location, the SAM-key may contact exit DNA (Fig. 22 C).

The apparent similarity to HSA/post-HSA domains of Ino80 and Sth1 (Fig. 21 G+H) suggests that the SAM-key helix may be (at least in part) a structural and functional analog. In these multi-subunit remodelers, the HSA domain is the base for the assembly of the so-called A-module, which is involved in sensing of extranucleosomal DNA (Eustermann et al., 2018; Knoll et al., 2018; Kunert et al., *in press*). This module is also interacting with protrusion I and regulating remodeler activity (Szerlong et al., 2008). While no assembly of an additional module is expected in single-subunit remodeler Fun30, binding entry DNA to regulate remodeling accordingly seems plausible.

We also observed a group of basic amino-acids (KRRRR 338-342) that AlphaFold2 localizes with moderate confidence to a loop connecting the SAM-like fold with the N-terminus of the long helix. This basic loop might therefore be poised for interaction with DNA (Fig. 22 C), even though these residues do not appear to be strongly conserved in Fun30-SMARCAD1-ETL remodelers (Fig. 5).

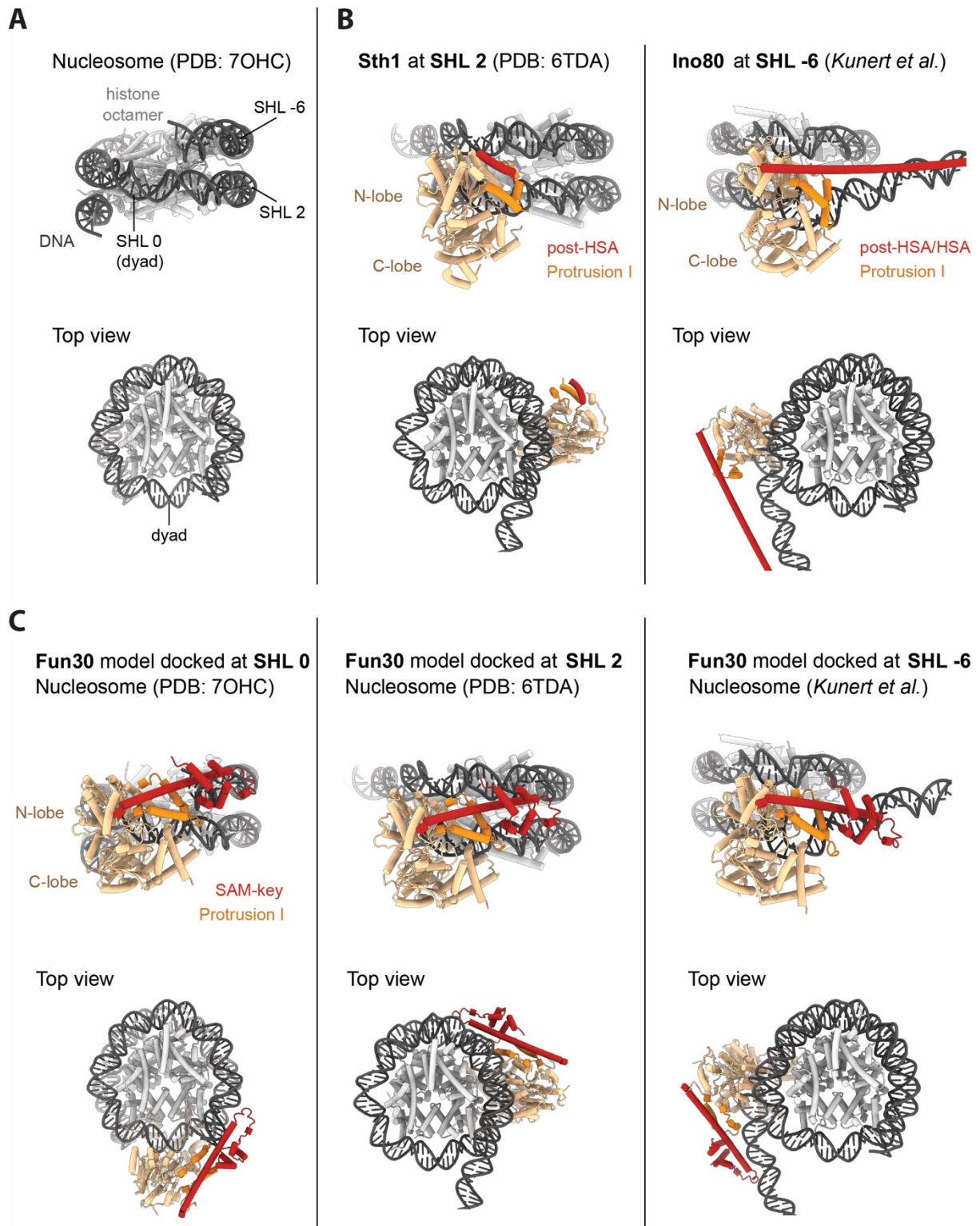


Figure 22: Docking the Fun30 model onto a nucleosome in different superhelical positions suggests analogy to post-HSA/HSA modules in RSC and INO80 remodelers.

A: Nucleosome structure (PDB: 7OHC) in side and top view. Histone octamer (grey) and superhelical positions SHL0 (dyad), SHL2 and SHL-6 are indicated.

B: Structures of catalytic subunits Sth1 (RSC) and Ino80 (INO80) bound to the nucleosome in side and top view. Left: Sth1 ATPase domain (beige) with protrusion I (orange) and part of the post-HSA domain (red) bound to the nucleosome in SHL2 (PDB: 6TDA).

Right: Ino80 ATPase domain (beige) with protrusion I (orange) and post-HSA/HSA domain (red) bound to the nucleosome in SHL-6 (Kunert et al., *in press*).

C: AlphaFold2 model of Fun30 docked to the nucleosome at dyad, SHL2, SHL-6 in side and top view.

Left: Fun30 ATPase domain (beige) with protrusion I (orange) and SAM-key (red) bound to the nucleosome at the dyad, as suggested for SMARCAD1 (Markert et al., 2021), but adjusted in the angle of binding to allow the conserved ATPase domain to interact with DNA analogous to known structures. Color scheme used throughout Fig. 22 C. A positively charged loop on the Fun30 SAM-key (top in top view) is poised for interaction with entry DNA.

Center: Fun30 bound to the nucleosome at SHL2, analogous to Sth1 (PDB: 6TDA). A positively charged loop on the Fun30 SAM-key (left in top view) is poised for interaction with nucleosomal DNA.

Right: Fun30 bound to the nucleosome at SHL-6, analogous to Ino80 (Kunert et al., *in press*). A positive loop on the Fun30 SAM-key (bottom in top view) is poised for interaction with entry DNA.

In all, our comparison to other remodelers therefore suggests similarities of how SAM-key and post-HSA helices interact with protrusion I, suggesting a common control mechanism of enzymatic activity.

16. The protrusion I-SAM-key interface is required for Fun30 remodeling activity

Protrusion I is an extension of the N-terminal lobe of the ATPase domain, which in INO80/SWR1 and SWI/SNF remodelers, connects to the post-HSA domain (Jungblut et al., 2020). Pioneering work on the RSC complex has shown that a key function of the protrusion I-post-HSA interaction is to promote coupling of ATP hydrolysis and DNA translocation (Clapier et al., 2016). This work highlights the importance of protrusion I and its binding to other parts of the enzyme and suggests a key regulatory role, even though the precise function of protrusion I may differ between remodelers. Of note, to our knowledge SAM-keys are absent from other remodelers.

Structural modelling suggested two sets of key residues: Set 1 consisting of residues involved in the interaction of SAM-key and protrusion I and set 2 consisting of a basic, positively charged patch, exposed N-terminally of the long helix making it a putative interaction point of SAM-key and DNA (Fig. 17 C + 22 C).

To ascertain the functional importance of such interactions, we mutated those residues and tested mutant proteins in functional assays.

To test the basic residues that could be involved in DNA binding, we deleted the positively charged amino acids (Δ KRKRR 338-342). However, the Fun30 Δ KRKRR protein retained DNA-stimulated ATPase and remodeling activities (Fig. 23 A-D). These data indicate that the basic amino acids of the tip of the SAM-key are either not involved in DNA binding, that this protein-DNA interaction is not important for Fun30 functions tested here or that other parts of the protein function redundantly.

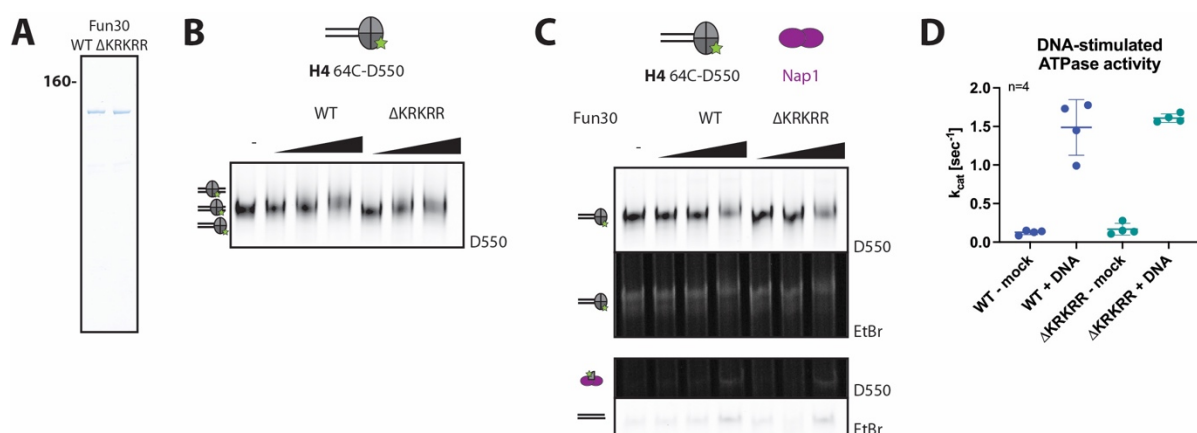


Figure 23: The Fun30 basic patch deletion mutant (Δ KRKRR) does not affect sliding, eviction and ATPase activity. **A:** Coomassie gel showing Fun30 WT and Δ KRKRR mutant side by side (representative, n=2).

B: Nucleosome sliding assay (with 100W0 end-positioned nucleosomes and labelled H4 as in Fig. 15 B-C) shows nucleosome sliding for both Fun30 and Fun30 Δ KRKRR. Representative gel of n=3 replicates.
C: Eviction assay (with labelled H4 as in Fig. 15, H) shows nucleosome eviction for both Fun30 and Fun30 Δ KRKRR. Representative gel of n=3 replicates.
D: Absorption-based (A340) ATPase assay using Fun30 (dark blue), Fun30 Δ KRKRR (turquoise), ATP and DNA stimulus (herring sperm DNA 100 ng/ μ L). Both Fun30 and Fun30 Δ KRKRR exhibit comparable levels of ATP hydrolysis ($k_{cat} \sim 1.5$). n=4 replicates, shown is mean, error-bars depict standard deviation.

Next, to test the importance of the interaction surface between SAM-key and protrusion I, we mutated two hydrophobic amino acids (I367, C374) to charged, bulky arginines (Fun30-ICRR) to weaken or abolish this inter-domain interaction. Purified Fun30-ICRR showed similar folding and stability in limited proteolysis (Fig. 24 J) and was still able to bind to DNA and nucleosomes similarly as the WT protein (Fig. 24 A-C, G), suggesting the protrusion I-SAM-key interaction is expectedly not involved in nucleosome binding. When we tested nucleosome remodeling, however, we found that even at high concentrations, Fun30-ICRR was neither able to slide nor evict nucleosomes (Fig. 24 D-E). These data further strengthen the structural model (Fig. 17), and we conclude that nucleosome remodeling activity by Fun30 was abrogated by the disruption of SAM-key binding to protrusion I.

Given the known role of protrusion I in regulating ATPase activity of remodelers, we also tested whether Fun30-ICRR was ATPase active upon DNA stimulation. Here we observed that Fun30-ICRR showed a strong defect in DNA-stimulated ATPase activity, similar to Fun30 Δ SAM (Fig. 24 F). This defect could, however, be complemented by the addition of the isolated SAM-key, again similar to Fun30 Δ SAM (Fig. 24 I) as could the defect in nucleosome sliding (Fig. 24 H), suggesting that extrinsically added SAM-key can interact with protrusion I within the context of the Fun30-ICRR protein and restore function.

We therefore conclude that protrusion I is a key element of control. In Fun30, protrusion I is contacted by the SAM-key in an interaction mediated by hydrophobic residues, which facilitates allosteric activation of the remodeler.

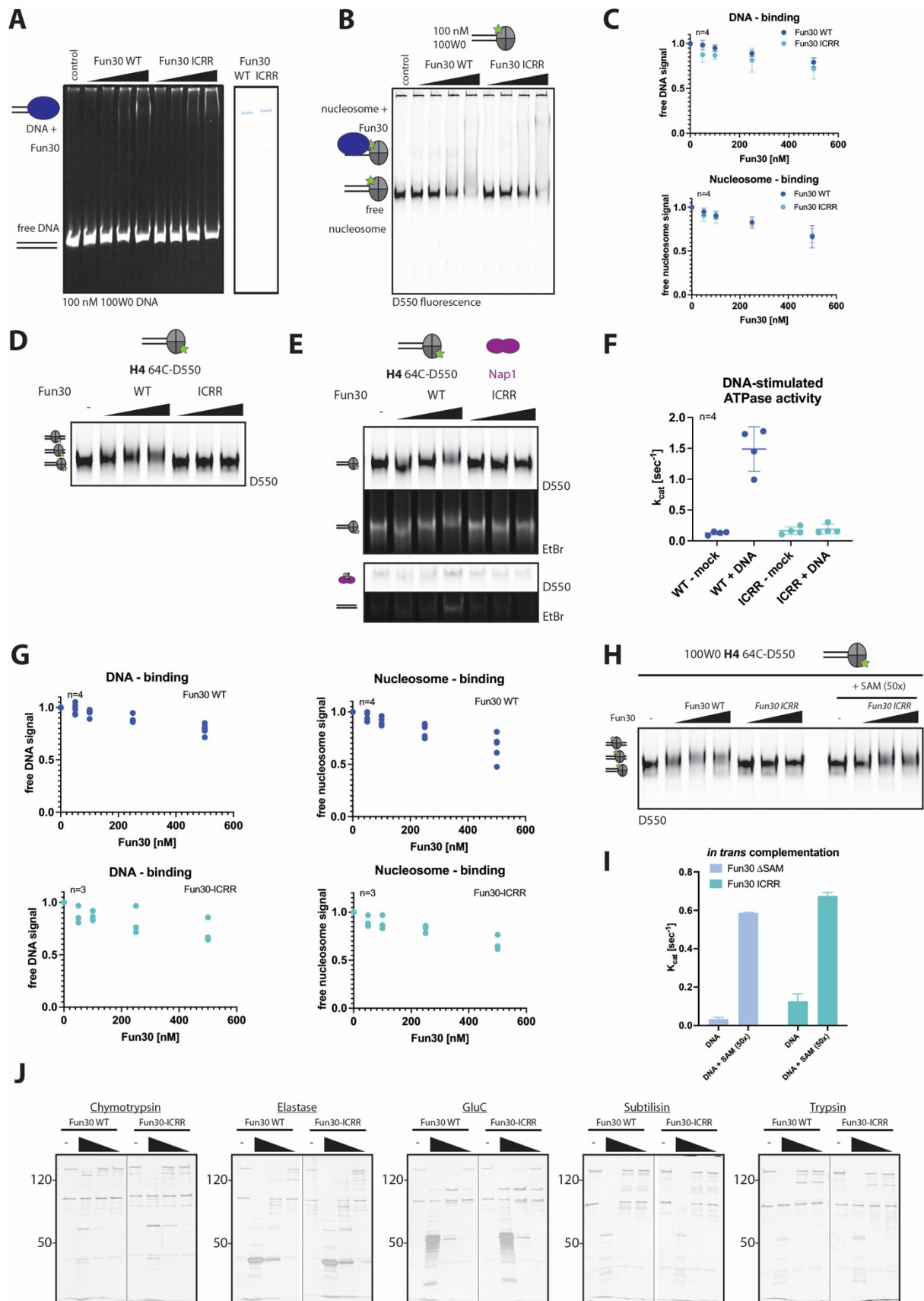


Figure 24: The Fun30 interface mutant I367R, C374R (Fun30-ICRR) phenocopies Fun30 Δ SAM in binding, nucleosome sliding, eviction and ATPase activity.
A-C: Similar to Fun30 Δ SAM, the mutant Fun30-ICRR with a defect in the SAM-key-protrusion I interface binds normally to DNA and nucleosome.

A: DNA binding to 247bp dsDNA construct. Left: Gel shift in native gel with Fun30 WT and Fun30-ICRR and DNA stained with ethidium bromide. Representative gel of n=4 biological replicates. Right: Coomassie staining shows equal amounts of WT and mutant protein were used in both DNA (Fig. 24 A) and nucleosome binding experiments (Fig. 24 B) (quantified from band intensity).

B: Binding to 100W0 nucleosomes of Fun30 WT and Fun30-ICRR, native gel stained with ethidiumbromide. Representative gel of n=4 biological replicates.

C: Top: Quantification of DNA binding as in Fig. 13 A. n=4 replicates, shown is mean, error-bars depict standard deviation. Bottom: Quantification of nucleosome binding as in Fig. 13 B. n=4 replicates, shown is mean, error-bars depict standard deviation.

D-F: Fun30 nucleosome remodeling requires SAM-key interaction with protrusion I of the ATPase catalytic domain.

D: Nucleosome sliding assay (with 100W0 end-positioned nucleosomes and labelled H4 as in Fig. 15 B) shows nucleosome sliding defect of Fun30-ICRR. Representative gel of n=2 biological replicates and n=4 technical replicates.

E: Eviction assay (with labelled H4 as in Fig. 15 H) shows nucleosome eviction defect of Fun30-ICRR. Representative gel of n=2 biological replicates and n=4 technical replicates.

F: DNA-stimulated ATPase assay as in Fig. 15 with Fun30-ICRR. Unlike Fun30 WT that reaches a k_{cat} of 1.5 sec^{-1} , Fun30 ICRR only reaches a k_{cat} of 0.2 sec^{-1} comparable to Fun30 Δ SAM. n=4 replicates, shown is mean, error-bars depict standard deviation.

G: Left: Quantification of DNA binding by Fun30 WT (blue) and Fun30-ICRR (sea green) as in Fig. 24 C. n=4 replicates, shown are single replicate values. Right: Quantification of nucleosome binding by Fun30 WT (blue) and Fun30-ICRR (sea green) as in Fig. 24 C. n=4 replicates, shown are single replicate values.

H: Sliding of nucleosomes with labeled H4 (64C-D550) assembled on a 100W0 fragment (247 nt fragment with end-positioned Widom 601-positioning-sequence) as seen by upshift in gel. Shown is dependence on the SAM-key domain as the Fun30-ICRR alone cannot slide but addition of a SAM-key construct (50x molar excess) *in trans* allows sliding. Representative gel of n=3 biological replicates.

I: ATPase assay using Fun30 Δ SAM (light blue), Fun30-ICRR (sea green), ATP and DNA stimulus (herring sperm DNA 100ng/ μ L) with or without SAM-key as *in trans* addition (50x molar excess). With both Fun30 Δ SAM and Fun30-ICRR only in presence of SAM-key ATP hydrolysis higher than background level can be observed ($k_{cat} \sim 0.6$). n=2 biological replicates, shown is mean, error-bars depict standard deviation.

J: Limited proteolysis of Fun30 WT and Fun30-ICRR as in Fig. 12 A displays highly similar degradation profiles, demonstrating similar overall folding and stability. Representative silver-stained gel, n=2.

Discussion

Mechanistic understanding of chromatin remodeling

Chromatin remodelers utilize the energy provided by ATP hydrolysis to weaken DNA-histone contacts and use the gained flexibility to remodel nucleosomes in different ways: Sliding an intact histone octamer, evicting the histone octamer, exchanging histone variants, and altering nucleosome conformation. For some remodelers, studies have provided mechanistic insights on how accessory domains and subunits regulate remodeling activity of the conserved RecA-like ATPase domain, while for others we still lack a better understanding on the mechanistic level. For the sub-family Fun30-SMARCAD1-ETL1, a family of single-subunit remodelers with a conserved role in DNA repair, to date we lack deeper mechanistic understanding (Bantele and Pfander, 2019). Both the importance for DNA repair as well as our current lack of knowledge make this family particularly interesting to study. No other remodeler can act redundantly with Fun30 in promoting long-range resection through chromatin (Peritore et al., 2021), suggesting a unique underlying mechanism. Studying this mechanism and comparing it to known mechanistic details from other nucleosome remodeling machines could advance our understanding of what is essential for remodeling. Investigating how this family of remodelers works and is regulated may not only lead to developing tools to manipulate the Fun30-SMARCAD1-ETL family specifically, but also provide insights that could be applicable to other remodeler mechanisms, like a set of common minimal modules to look for in any remodeling machine.

Identification of the SAM-key as novel domain important for Fun30 function

So far, Fun30 functions could not be linked to a specific remodeling mechanism.

To find regions of Fun30 required for its function, we applied two strategies: First, a multiple sequence alignment to identify conserved parts of the protein (Fig. 5) and second, testing function of Fun30 truncations in a Ddc1-Fun30-fusion, with forced recruitment to sites of resection (Fig. 6). We find that the Fun30 region 270-400 is highly conserved and required for Fun30 function and concluded the existence of a previously uncharacterized domain important for Fun30 function. Based on the observation that the presumed function was independent of recruitment to chromatin, we hypothesized the domain to be involved in the ATP-dependent remodeling function of Fun30 (Bantele et al., 2017; Eapen et al., 2012).

Structure prediction algorithms use the amino acid sequence of a protein to predict its 3D structure, making use of alignments to proteins with solved structures and machine learning. Using two different prediction tools, Phyre2 (Kelley et al., 2015) and AlphaFold2 (Jumper et al., 2021), we obtained two highly similar models of a SAM-like domain, both with high confidence (Fig. 7).

The main difference between the models was the C-terminal helix being long and continuous for AlphaFold2 or split into a helix-turn-helix motif for Phyre2. However, for the Phyre2 model, this region was outside the region of highest confidence and no direct alignment with a known structure was present. The AlphaFold2 model on the other hand had calculated a confidence similar to the rest of the fold, so we based our further analysis of the domain on the AlphaFold model. The overall structure of the domain resembled a key and given that it contained a SAM-like fold we termed it SAM-key. Of note, also for human SMARCAD1 a SAM-key was predicted with high confidence.

We deleted the SAM-key from Fun30 and found defects in both major functions of Fun30 -gene silencing and DSB repair - while expression levels of Fun30 Δ SAM were similar to Fun30 WT (Fig. 9+10). In contrast, the Fun30-SS20,28AA mutant, that destroyed serine residues important for phosphorylation-dependent recruitment to DSBs, separated Fun30 functions and was defective in DSB resection, but proficient in silencing (Fig. 10 C, Bantele et al., 2017).

SAM-like domain functions

We consulted the literature about SAM-like domains, to potentially find hints on the function of the putative domain in Fun30.

The sterile alpha motif (SAM) was first identified by Ponting, as conserved domain of about 70 residues in several proteins required for sexual differentiation (Ponting, 1995). The short 5-helical domain was found to be related to similar domains identified in other protein families and Schultz and colleagues grouped all of them together and referred to them as SAM domains with protein interaction function (Schultz et al., 1997). Over 1000 proteins throughout eukaryotes and bacteria are predicted to have SAM-like domains (Kim and Bowie, 2003), making it a highly abundant protein domain.

However, SAM-like domains display great functional diversity (Kim and Bowie, 2003): They are involved in many different biological processes, exist in all subcellular locations, can have propensity to homo- or hetero-oligomerize in different stoichiometries, bind a variety of proteins, but also RNA (Green et al., 2003) and lipids (Barrera et al., 2003). The fold of the helix bundle is also showing some variability with regards to relative position of the helices to each other (see Fig. 8). This indicates that the SAM-like fold is merely a scaffold, presenting the required interaction surface in a certain position.

Of note, SAM domains have already been implicated to be involved in chromatin regulation: Ets-2, a transcriptional activator that carries a SAM domain, works together with mammalian Brg-1 (catalytic subunit of mammalian SWI/SNF) to transcriptionally repress the *BRCAl*-promoter (Baker et al., 2003). The function of the well-known Polycomb repressive complex (PRC1) depends even on multiple SAM domain interactions: Sfmbt (PhoRC subunit) associated to a Polycomb response element in the genome nucleates PRC1 recruitment by direct interactions of Sfmbt-SAM and Scm-SAM (PRC1 subunit). Consequently, Scm-SAM and Ph-SAM (another PRC1 subunit) mediate polymerization resulting in the formation of PRC1-compacted chromatin (Frey et al., 2016). More recently, SAMD1, a protein named after the SAM domain, has been identified as repressive chromatin regulator (Stielow et al., 2021). However, its interaction with unmethylated CpG islands is performed by another domain and the SAM domain is required for interaction with L3MBTL3, which in turn interacts with a histone demethylase complex to control transcriptional repression.

In all of these cases, the mechanism mediated by SAM domains was the interaction with another protein. However, since Fun30 is established to be a single-subunit remodeler and showed activity in our *in vitro* assays without additional binding partner, this option seems rather unlikely or at least it may not be the only function of Fun30's SAM-key domain.

Fun30 dimerization

Since some SAM-like domains are involved in hetero-oligomerization, we tested whether the SAM-key in Fun30 may mediate dimerization. So far, dimerization of Fun30 has been observed by others in different contexts: As purification product of tagged Fun30 and with Co-IP experiments of differently tagged Fun30

proteins from *S. cerevisiae* (Awad et al., 2010). We detected Fun30 oligomerization and self-interaction as well (Fig. 12).

However, the mutant Fun30 Δ SAM not only did not show a defect in oligomerization, it even appeared to have a slightly stabilizing effect on the oligomeric state, as seen by an early eluting side-peak in gel filtration and increased percentage of dimeric molecules in mass photometry (~25% for Fun30 Δ SAM and ~10% for Fun30 WT).

In order to find the potential dimerization interface, we tried to obtain an AlphaFold2 multimer prediction of a Fun30 dimer to identify a potential dimer interface. However, the prediction failed to give a high confidence model (not shown).

We could speculate that the Fun30 dimer would be inactive, while the monomer is the active form of the enzyme and a stabilized dimer of Fun30 Δ SAM thus locks it in an inactive form. Two pieces of evidence speak against that: First, our observation that the dimerization is dynamic and transient and the majority of molecules in solution at the concentrations used in the assays should be monomeric. Second, we showed that Fun30 Δ SAM can be re-activated, either by addition of a free SAM-key or the Fun30-K603R Walker A mutant (Fig. 16). Since Fun30-K603R cannot bind ATP, it cannot be the cause of the observed ATP hydrolysis. In these assays a background ATPase activity could be observed for SAM-key and Fun30-K603R with high amounts of protein. We think this could be due to a minor ATPase contamination in the preparation, which cannot explain the similar to wildtype levels of ATP hydrolysis achieved by combining them with Fun30 Δ SAM (Fig. 16).

These experiments indicate that dimeric or oligomeric forms of the remodeler are the active species. However, without a mutant that specifically disrupts dimerization in Fun30 the question whether its active form is a monomer or dimer cannot be definitely answered.

Characterization of the Fun30 Δ SAM mutant

1. Folding and stability

Since the putative SAM-key domain is essential for Fun30 function *in vivo*, we decided to continue studying it *in vitro*.

In vitro systems have advantages for mechanistic studies, since the experimental conditions can be clearly controlled and manipulated, without the complication common to *in vivo* studies of nucleosome remodelers, that several remodelers have redundant functions.

To characterize the SAM-key and its role in Fun30 function *in vitro* we established purification protocols for Fun30 overexpressed either in budding yeast cells (Fig. 11 A) or in *E. coli* (Fig. 11 B). Since both strategies yielded active protein (Fig. 11 C), we used the higher-yielding bacterial expression and purification strategy for further mutants and experiments.

With the *in vivo* experiments we ensured similar expression levels of Fun30 and Fun30 Δ SAM, but protein activity also depends on correct folding and stability. We characterized the purified proteins and showed with several approaches that a similar overall folding for Fun30 Δ SAM and wildtype is highly likely: Limited proteolysis showed similar degradation patterns (Fig. 12 A), crosslinking-MS with BS3 showed a similar crosslinking pattern for Fun30 WT and Δ SAM (Fig. 12 F) and nanoDSF showed similar thermal unfolding curves for both Fun30 WT and Δ SAM (Fig. 12 D), all underlining that stability and overall folding of the two proteins is similar.

Protein activity may also be regulated by post translational modifications (PTMs) or activation by additional (co)factors.

Since the Fun30 protein was obtained from *E. coli*, it does not contain eukaryotic PTMs. While we therefore cannot exclude that we lack insights into activities that depend on PTMs, the activities tested by us do not depend on PTMs (Fig. 11 C). In the same vein, we cannot exclude that *in vivo* additional (co)factors are important for Fun30 function, but for Fun30 activity in our *in vitro* experiments they are not required, as can be seen by the results of Fun30 WT.

2. DNA and nucleosome binding

After testing for self-interaction and folding, we tested whether Fun30 Δ SAM could still interact with its putative substrate DNA and/or nucleosomes. We found neither binding to DNA nor binding to mono-nucleosomes required the SAM-key (Fig. 13).

Notably, in our hands Fun30 showed enhanced binding to nucleosomes compared to naked 100W0 DNA. Awad and colleagues showed that 0W0 DNA is bound by Fun30 preferably over 0W0 nucleosomes, but 0W0 DNA is bound with similar affinity as are 0W47 nucleosomes (Awad et al., 2010). Our results demonstrate Fun30's preference for the nucleosome over free DNA when there is a sufficiently long flanking DNA.

Awad and colleagues had speculated that one nucleosome is bound by two molecules of Fun30 and that this binding mode is stabilized by flanking free DNA. The comparison of our data with previously published data may be seen in support of this hypothesis, but binding studies where different DNA/nucleosome substrates are compared side-by-side will be needed to affirm this. Another study analyzed Fun30 binding to nucleosomes and ssNucs, histone octamers assembled on ssDNA, and showed preference of Fun30 for ssNucs over nucleosomes (Adkins et al., 2017). We did not control for this as results from our lab had previously shown that at sites of resection no nucleosomes remain on ssDNA (Peritore et al., 2021), making ssNucs a likely artificial binding partner.

In future, it will be interesting to test Fun30 Δ SAM binding to different nucleosome substrates of biological relevance, for example nucleosome arrays in close proximity to a ss-ds-DNA junction, mimicking sites of resection, or Rad9-bound nucleosomes.

Since some SAM-like domains have been shown to interact with other SAM-like domains, one could also envision interaction of the Fun30 SAM-key with another SAM-like domain containing protein bound to DNA or nucleosomes *in vivo*, maybe enhancing interaction or retention on the substrate. However, to date no such interaction has been shown, but with improvement in techniques and technology, also weaker or transient interactions may be possible to detect.

Importantly, in the context of our *in vitro* experiments Fun30 binding to DNA and nucleosomes is intact without contribution of the SAM-key.

3. Catalytic activity

Fun30 has been shown to exhibit several enzymatic activities *in vitro*: First, Fun30 is able to slide nucleosomes towards a central position on a DNA fragment (Awad et al., 2010; Byeon et al., 2013), even though less efficient than RSC (Awad et al., 2010). Second, Fun30 can displace an H2A-H2B dimer from a nucleosome and transfer it onto an acceptor tetrasome – a Widom-601-DNA fragment with H3-H4-tetramer assembled (Awad et al., 2010). Third, Fun30 can catalyze the transfer of an entire histone octamer from chromatin onto a different DNA fragment, thereby catalyzing both nucleosome eviction and

deposition (Awad et al., 2010). Notably, this was suggested recently also as mechanism for SMARCAD1, Fun30's human orthologue (Markert et al., 2021).

To study involvement of the SAM-key in Fun30 activities, we established our own *in vitro* assays and adapted them to existing strategies: For nucleosome sliding we use end-positioned labelled histone octamers with sufficient DNA overhang to visualize changes in running behavior in native PAGE. As nucleosome eviction assay, we use the same nucleosome substrate, but add the histone chaperone Nap1 to function as sink for histone dimers and tetramers. To test for ATPase activity, we use a NADH oxidation-coupled assay with different substrates for stimulation.

3.1. The Fun30 SAM-key in nucleosome sliding and eviction

In our nucleosome sliding assays, Fun30 slid the end-positioned nucleosome towards the center of the DNA construct in an ATP-dependent manner, consistent with the previous findings. This sliding however is dependent on the presence of the SAM-key, as Fun30 Δ SAM was not active in this assay (Fig. 15). Fun30 Δ SAM could however be reactivated, if the SAM-key was provided *in trans* using either a domain-only construct or the Walker A mutant Fun30-K603R (Fig. 16).

This shows that Fun30 sliding activity is dependent on the SAM-key, however not on its presence within the same molecule.

We applied a Nap1-assisted eviction strategy, since we did not detect nucleosome eviction without a histone acceptor in the assay. We could not observe octamer transfer to a free DNA fragment as reported for HeLa nucleosomes (Awad et al., 2010) and assembly of histone H3-H4 tetramers on DNA was inefficient and difficult to control for. As Nap1 is able to bind all histones (McBryant et al., 2003) and Fun30 had been suggested to evict H2A-H2B dimers as well as entire octamers, we used it in excess as acceptor that should be able to capture any evicted constellation of histones.

As expected, we could observe ATP-dependent nucleosome eviction by Fun30. Fun30 displaces all histones from nucleosomes, since we observed both labelled H2A and H4 bound by Nap1 (Fig. 15) and under physiological salt conditions H2A forms a stable dimer with H2B, as H4 forms a stable dimer with H3 (reviewed in Andrews and Luger, 2011).

Additionally, the re-appearance of a band of free DNA is evidence for full eviction of histones from DNA, however only a fraction of the nucleosomes is evicted (Fig. 15). This suggests, that under the tested conditions, Fun30 is more potent in nucleosome sliding than eviction.

However, eviction activity of Fun30 is also dependent on the presence of the SAM-key, as Fun30 Δ SAM was not active in this assay (Fig. 15). Reactivation experiments by providing the SAM-key *in trans* were inconclusive, since addition of the SAM-key in presence of Nap1 caused strong background signal at the height of Nap1-bound labelled histones, even without Fun30 WT or Fun30 Δ SAM (data not shown).

Together this shows that Fun30 eviction activity is dependent on the SAM-key and on a histone acceptor.

Instead of Nap1, we also tried to use the histone chaperone complex FACT, purified from yeast, that is able to bind both H2A/H2B and H3/H4 as alternative histone acceptor (Kemble et al., 2013; 2015). However, with FACT we did not see eviction or sliding by Fun30 (data not shown). This brings up the question, whether this is due to FACT binding to the nucleosomes and protecting them from remodeling by Fun30, or whether it is for some reason incompatible with nucleosome eviction by Fun30.

On the other hand, Fun30 might specifically work with Nap1, as has been suggested for RSC: High concentrations of Nap1 have been suggested to act in concert with RSC to fully disassemble mononucleosomes *in vitro* (Lorch et al., 2006), while other data suggested that during remodeling of mononucleosomes by RSC Nap1 evicts one H2A-H2B dimer (Kuryan et al., 2012). Another study found Nap1 involved in disassembly of dinucleosomes by RSC and showed that neither replacement of RSC by SWI/SNF nor replacement of Nap1 by Vps75 lead to the same result (Prasad et al., 2016). So far, no specific connection between Nap1 and Fun30 has been shown, but this may be an interesting line of research to follow up on, for example with epistasis studies of *fun30Δ* and *nap1Δ* strains.

Our results for nucleosome sliding and eviction by Fun30 are consistent with the idea of Fun30 helping resection nucleases overcome the nucleosome barrier. Fun30 is not directly evicting nucleosomes for resection nucleases in an *in vitro* reconstituted resection system (Adkins et al., 2013). However, Nap1 was absent from this reconstituted system, and should be considered when re-visiting reconstitution of resection. Still, *in vivo* data show that eviction at sites of resection is mainly performed by RSC and SWI/SNF, even in presence of Nap1 (Peritore et al., 2021).

In sum, Fun30 is able to slide nucleosomes and together with Nap1 to eject all histones from DNA, but both activities are dependent on the SAM-key domain and it remains to be determined whether this is part of its function *in vivo*.

3.2. The Fun30 SAM-key in DNA-stimulated ATP hydrolysis

ATP hydrolysis by other remodelers was shown to be strongly stimulated by nucleosomes and often more poorly or to similar extent by DNA, suggesting stimulation by the substrate (Hauk et al., 2010; Mueller-Planitz et al., 2013). Fun30 in contrast can be stimulated very efficiently by DNA alone, similar to RSC (Awad et al., 2010; Boyer et al., 2000; Saha et al., 2002), and ssDNA has been shown to be a better stimulus for Fun30 than dsDNA (Adkins et al., 2017).

Our ATPase assay showed very low ATP hydrolysis by isolated Fun30 (k_{cat} below 0.3 s^{-1}), but this could be stimulated up to a k_{cat} of 3 s^{-1} by different constructs of single-stranded and double-stranded DNA (Fig. 15 J). Our data confirm that ssDNA or ssDNA containing stimuli, such as sheared herring sperm DNA, stimulate the ATPase activity of Fun30 better than dsDNA.

Overall, it is still unclear what structure exactly is the stimulus for Fun30, but our work suggests that stimuli that contain likely both ssDNA and ss-ds-junctions are better stimuli in our assay than dsDNA (Fig. 15 J) or nucleosomes (data not shown). RPA did not stimulate Fun30 and when added together with ssDNA stimuli it abolished the stimulation (data not shown). Whether by covering ssDNA or by preventing secondary structures we cannot say. Short oligonucleotides (<60 nt) were not efficient in stimulation, indicating that either extended ssDNA or secondary structures are required to stimulate Fun30.

Considering that the role of Fun30 is to promote DNA end resection at DSBs and that previous work localized Fun30 to ss-ds-DNA junctions where it is recruited by the 9-1-1 complex (Bantele et al., 2017; 2019), one can speculate that some DNA structure present at sites of DNA end resection, likely ss-ds-DNA junctions or single-stranded DNA, is bound by Fun30 and stimulates the remodeler. This stimulation could involve the SAM-key and result in stimulation of ATP hydrolysis.

A single-stranded oligonucleotide (120 nt) and sheared herring sperm DNA are both efficient stimuli of Fun30 (Fig. 15 J). Of note, the shearing process of herring sperm DNA may generate ssDNA or ssDNA-

overhangs at dsDNA fragments and the used ssDNA construct may form secondary structures, generating ss-dsDNA junctions.

Notably, when we compared Fun30 Δ SAM to Fun30 WT, we found that the SAM-key was required for DNA-stimulated ATP hydrolysis (Fig. 15 K+L). Without the energy provided by ATP hydrolysis the enzyme cannot catalyze reactions and thus this would explain a phenotype *in vivo* similar to *fun30 Δ* or *fun30-K603R*. We conclude from this result together with the requirement for nucleosome sliding and eviction, that the SAM-key is either intrinsically required for ATP hydrolysis by the ATPase domain or that it is critical to allosterically activate the ATPase domain.

Considering allosteric activation, we wondered whether *in trans* addition of the isolated SAM-key domain could restore DNA-stimulated ATPase activity of Fun30 Δ SAM.

In line with an allosteric mechanism, an AlphaFold2 model of full-length Fun30 predicted the SAM-key to make intramolecular contact with the ATPase domain at protrusion I (Fig. 17), a part of the ATPase domain that has been found to regulate ATPase activity and coupling of ATP hydrolysis and remodeling in other remodelers (Clapier et al., 2016; 2020), see in more detail below). This contact to protrusion I was also predicted when providing SAM-key and Fun30 Δ SAM as separate polypeptides (Fig. 18).

Notably, addition of excess SAM-key alone or within the Fun30-K603R mutant rescued the ATPase defect of Fun30 Δ SAM and restored WT levels of ATP hydrolysis (Fig. 16), however only in presence of DNA stimulus (data not shown). We therefore conclude that the SAM-key together with a DNA stimulus allosterically activates ATP hydrolysis by Fun30. Together with the results for nucleosome sliding we conclude that at sufficiently high concentrations the isolated SAM-key can bind to Fun30 Δ SAM and restore its function.

We need to be aware of the limitations of our *in vitro* assay. To mimic the *in vivo* scenario, a reconstitution of damaged chromatin including the ssDNA-binding protein RPA, nucleosomes, the 9-1-1-complex and Dpb11, which recruit Fun30 to damaged chromatin would be required, at best also including Rad9 bound to nucleosomes methylated at H3 K79 and phosphorylated at H2A S129 (γ H2A) nucleosomes. Such a system may be ultimately required to determine the resection-promoting mechanism of Fun30, via including, excluding or mutating single factors.

Structural analysis based on Fun30 AlphaFold2 model

1. Structural analogy of the SAM-key with post-HSA domains in other remodelers

Structure prediction puts the SAM-key in contact with the ATPase domain at protrusion I (Fig. 17), so we were wondering if we could find a similar module in other remodelers.

Structural overlay of the Fun30 model with structures of other chromatin remodelers showed structural analogy of the SAM-key domain to post-HSA domains in Snf2, Sth1 and Ino80 and the related post-post-HSA (ppHSA) domain in ISWI (Fig. 21).

For Ino80, the analogy is striking with the post-HSA/HSA aligning very well with the key helix of the Fun30 SAM-key. Additionally, Ino80 post-HSA interacts protrusion I, again highly similar to Fun30 SAM-key.

With Isw1, Snf2 and Sth1 the similarity is less pronounced, which could partly be due to the fact, that the respective structures lack parts of the post-HSA domain (or post-post-HSA domain) and adjacent sequence.

It could be, that the interaction site at the ATPase domain (protrusion I) is common, but the module that makes contact and with it and the precise interaction site evolutionarily diverged to transmit different regulatory input to the ATPase core.

This seems to be the case for ISWI, where the ppHSA domain was found to be largely expendable for ATP hydrolysis and nucleosome sliding. Crosslinking in a slightly different position to ATPase lobe 2 (Ludwigsen et al., 2017), it was suggested to mainly participate in docking the regulatory elements AutoN and AcidicN to ATPase lobe 2.

For RSC the HSA domain in Sth1 binds Arp7 and Arp9. The adjacent post-HSA and protrusion I are required for protein function *in vivo*, but not for Arp association (Szerlong et al., 2008). Interestingly, mutations in protrusion I or post-HSA domain are able to suppress *arpΔ* phenotypes (Szerlong et al., 2008). Also, the post-HSA of Sth1 has been shown to downregulate the ATPase activity and subsequent remodeling activities of the enzyme *in vitro* (Clapier et al., 2016). Protrusion I therefore has been suggested to detect the conformation of the ARP-module and post-HSA domain, serving as an “integrator” that communicates to the ATPase domain appropriate ATPase and coupling levels, thus regulating sliding and ejection by RSC (Clapier et al., 2016). The post-HSA-protrusion I-interface has been verified by cryoEM structures (Baker et al., 2021; Wagner et al., 2020).

For SWI/SNF the post-HSA of Snf2 also contacts the ATPase at the end of lobe 1, where protrusion I, here also called SuppH, is located (Xia et al., 2016). Upon nucleosome binding the post-HSA and protrusion I undergo coordinated movement, without being directly involved in substrate recognition or ATPase lobe1–lobe2 communication (Liu et al., 2017), suggesting that SWI/SNF activity is regulated by protrusion I. Of note, in the nucleosome-bound structure two C-terminal brace helices were spanning the interconnection of the ATPase lobes and interacting with protrusion I (SuppH) and this interaction was important for coupling ATP hydrolysis to remodeling (Liu et al., 2017). In the AlphaFold model of Fun30 a similar element can be seen with two C-terminal (1079-1123) helices also protruding from lobe2 and spanning towards the interconnection of the two lobes. Interestingly, we find this region crosslinking to protrusion I and the insertion between the lobes (Fig. 19 B), indicating a similar position and suggesting another conserved element that may regulate Fun30 activity.

Lastly, for Ino80, the post-HSA domain in Ino80 continues as the long helical HSA domain, that makes contact to entry DNA. The HSA, together with actin, Arp4 and Arp8 form a stable sub-module of the Ino80 complex that regulates the catalytic activity of Ino80 (Shen et al., 2003; Szerlong et al., 2008).

In sum, structural overlays show striking structural analogy of the Fun30 SAM-key to post-HSA/HSA modules, that are involved in regulating ATPase activity in RSC, SWI/SNF and Ino80.

2. A common structural regulatory hub in the catalytic subunits of chromatin remodelers

Recently, Clapier and colleagues analyzed mutations in human cancers affecting BAF/PBAF, the orthologue of budding yeast RSC complex (Clapier et al., 2020). Taking these mutations together with structural data and mutations found in yeast, they postulate an integrative structural regulatory hub at the interconnection of the ATPase lobes, consisting of post-HSA domain, protrusion I, which they divide in N-terminal and C-terminal section (SuppH), and the brace domain. They show conservation of this structural hub in other remodeler-nucleosome complexes and that the protrusion I (SuppH) is in central position (Baker et al.,

2021; Han et al., 2020; He et al., 2020; Liu et al., 2017; Wagner et al., 2020; Ye et al., 2019). Changes in the domains forming this regulatory hub induced by cancer-associated mutations would lead to hyper- or hypoactivation of the remodeler.

Interestingly, they tested the effect of mutations in the RSC complex on chromatin organization *in vivo* by ATAC-seq. The result showed moderate increase in open chromatin for viable gain of function mutations and major genome-wide increase in open chromatin for non-viable lethal mutations, suggesting that these mutations could deregulate gene expression on a genome-wide level in tumors and therefore act as cancer-driver mutation.

Since the Fun30 SAM-key domain appears to be a structural analog to the post-HSA domain, the regulatory hub of protrusion I appears to be conserved also in the Fun30-SMARCAD1-ETL family of remodelers. Only instead of the post-HSA/HSA with Arp-module in Fun30 the SAM-key acts like an allosteric regulator for ATP hydrolysis.

3. XL-MS confirms Fun30 model and suggests SAM-key interacts with protrusion I

Our results and structural overlays suggest that the SAM-key is required for activation of the ATPase domain, so we compared the Fun30 AlphaFold2 model with XL-MS data to verify the model. We analyzed the model especially with regards to the SAM-key, especially looking for its relative position to other domains, potential interactions and exposed residues.

XL-MS data confirm the 3D-model with almost all crosslinks in structured regions fitting a 35 Å threshold (Fig. 19+20). We have chosen a threshold that is higher compared to the length of BS3 linkers (30 Å), given that AlphaFold2 models may reflect a mixture of apo- or nucleotide-bound state of the enzyme (Jumper et al., 2021).

The software mapping the crosslinks to the 3D-model cannot accommodate flexibility for unstructured regions, but takes the coordinates in the model as fixed position and therefore without filtering for structured parts most crosslinks violate the threshold. By only considering crosslinks within structured parts of the model we find most crosslinks satisfy the threshold, with exception of the crosslinks involving the CUE domain. This indicates that the position of CUE in the model is wrong, which goes in line with the predicted aligned error (PAE) calculated by AlphaFold that gives a low probability for the relative position of CUE to other parts of Fun30 (Varadi et al., 2022). The position of the CUE domain could also be flexible, since multiple crosslinks from CUE go to very different regions of the protein (Fig. 19 B). Complementation of Fun30 Δ SAM with SAM-key showed >35 Å crosslinks also for the SAM-key. In this scenario, we cannot exclude that these are actually intermolecular crosslinks, because of the excess SAM-key used in the experiment. In all, the XL-MS data therefore verifies the structural model and the interaction of the SAM-key with the ATPase domain of the remodeler (Fig. 19 B).

No major difference in crosslinking pattern could be detected for Fun30 when ATP was added or omitted (Fig. 19 B). Subtle conformational changes of Fun30 upon nucleotide binding can however not be excluded, especially since they may become more pronounced upon substrate-binding. To shed light on this, XL-MS with nucleosome substrate or DNA stimulus bound to Fun30 and the state of the enzyme trapped with a non-hydrolysable ATP analogue like ATP γ S would be a promising direction.

Crosslinks of the SAM-key helix to the C-terminus of the CUE domain and residues C-terminal of the suggested domain. In the 3D model these additional residues are predicted structured and are likely still

part of the CUE domain (Fig. 19 C). This indicates proximity of the two domains in at least one conformation of Fun30.

The crosslinks connecting SAM-key with protrusion I fulfill the distance threshold and verify the close proximity and interaction predicted in the model (Fig. 19). Protrusion I crosslinks to the C-terminus of Fun30, more specifically with the region that forms the two brace helices in the prediction (1079-1123) (Fig. 19 B+C). This goes in line with the suggested conserved structural hub involving protrusion I and brace helices to regulate the ATPase domain (Clapier et al., 2020). Of particular interest are the hydrophobic interactions of the SAM-key helix with ATPase domain protrusion I helices (Fig. 17). Notably, this interface was predicted almost identical using AlphaFold multimer prediction and SAM-key and Fun30 Δ SAM as separate polypeptides (Fig. 18) and in both cases XL-MS confirmed close proximity between SAM-key and protrusion I (Fig. 20).

4. Mutation of the SAM-key-protrusion I interface phenocopies Fun30 Δ SAM

As summarized above, protrusion I has been postulated as common regulatory element for this type of ATPase domain (Clapier et al., 2016; 2020; Szerlong et al., 2008). Matching the SAM-key - protrusion I interface with the multiple sequence alignment, the hydrophobic residues involved in the interaction are highly conserved (Fig. 5).

We disturbed the predicted hydrophobic interface with I367R, C374R mutations (Fun30-ICRR). Notably, these mutations phenocopied Fun30 Δ SAM and the mutant was inactive in DNA-stimulated ATP hydrolysis as well as nucleosome sliding and eviction (Fig. 24). Additionally, Fun30-ICRR activity could be restored by addition of a wildtype SAM-key *in trans*, same as Fun30 Δ SAM (Fig. 24). This provides additional evidence for the predicted interface and for the interaction being required for Fun30 activation. Importantly, while the mutated residues I367 and C374 are both highly conserved (Fig. 5), we ruled out misfolding of the mutated protein by limited proteolysis (Fig. 24). Very high conservation like for C374 could also indicate a role in catalysis or forming a crucial cystine-bridge. However, another mutant - Fun30KC(373,374)AA - showed wildtype levels of DNA-stimulated ATP hydrolysis (data not shown), speaking against the specific requirement of a cysteine but in line with a hydrophobic interaction interface that should not be disturbed by alanine.

This provides additional evidence for the interaction of SAM-key and protrusion I being mediated by this hydrophobic interface.

As additional control one could try to introduce the complementary mutations in the protrusion I interaction surface. By mutating for example M793 and/or F797 to arginine, one could disturb the hydrophobic interface from the C-terminal helix of protrusion I (SuppH). By mutating F761 and/or I764 to arginine, one could disturb the interface from the N-terminal helix of protrusion I, or one could combine the mutants, similar to Fun30-ICRR with two mutants on different sides of the interface. In line with our data and the model, we predict this to abrogate the hydrophobic SAM-key contact site and phenocopy the Fun30-ICRR mutant, underlining the importance of this interaction for ATPase activity. We also predict, that this mutant could not be rescued by extrinsically adding SAM-key domain.

One could further underline this by demonstrating *in trans* activation of Fun30 Δ SAM function by SAM-key *in vivo*. For this, overexpression of the SAM-key in *fun30\Delta SAM* cells and checking for rescue in CPT spottings and silencing assays would be a promising approach.

5. Fun30 docking to the nucleosome according to nucleosome-remodeler co-structures

To learn more about how Fun30 may engage a nucleosome and how the SAM-key would be placed in relation to nucleosome and DNA, we wanted to investigate Fun30 bound to a nucleosome. Since no structure of Fun30 bound to a nucleosome is available, we docked the Fun30 AlphaFold model in three likely binding positions. For this, we used remodeler-nucleosome co-structures of Ino80, SMARCAD1 and RSC as templates with DNA binding of the ATPase lobes at SHL-6, SHL0 and SHL2 respectively. All three dockings were plausible without substantial clashes, if we consider some structural flexibility of the ATPase lobes (Fig. 22).

SHL-6 is where Ino80 binds the nucleosome. Among the remodelers, Ino80 and Fun30 are most closely related (Flaus et al., 2006) and overlay of Fun30 model with the Ino80 structure showed the clearest analogy of the long helix from Fun30 SAM-key and the long helical post-HSA/HSA domain of Ino80, protruding along entry DNA.

Binding of a nucleosome remodeler at the dyad (SHL0) has recently been reported for a cryo-EM structure of SMARCAD1, the human orthologue of Fun30 (Markert et al., 2021). In this position Fun30 would be very close to the C-terminal tail of histone H2A and serine 129, which is phosphorylated during the DNA damage response (γ H2A). It has been shown, that Fun30 prefers to bind to nucleosomes with this residue unphosphorylated (Eapen et al., 2012), while its antagonist Rad9 binds phosphorylated H2A. So, phosphorylation on H2A could regulate Fun30 association to SHL0 or its remodeling activity, however as the histone tails are flexible, this cannot exclude Fun30 binding to other superhelical positions.

At SHL2 a majority of chromatin remodelers binds the nucleosome with reported cryo-EM structures for ISWI, SWI/SNF, RSC and CHD1 (reviewed in (Morgan et al., 2021)). SWI/SNF is bound at SHL2 and shows interaction between the histone H4 tail and catalytic subunit Snf2, that stimulates remodeling activity *in vitro* (Liu et al., 2017). Notably, SMARCAD1 binds to H3 and H4 tails and especially the interaction with the H4 tail is important for ATPase activity (Markert et al., 2021). However, the histone tails are flexible and could also be bound if Fun30 bound to other superhelical locations.

In a nucleosome-bound Snf2 structure, the authors identify a secondary DNA binding motif that, while the primary interaction is with one DNA gyre at SHL2, would make contact with the other nucleosomal DNA gyre at SHL-6 and prevent rotation of the enzyme (Liu et al., 2017). Similar additional contacts at SHL-6 have been observed for RSC (Wagner et al., 2020). The interacting motif consists of several basic residues clustering on the surface of ATPase lobe 1. Looking at the model of Fun30, there is a basic surface cluster in a similar position as well, formed by K686, K693, K718, K721, R723 and R727. This could be taken as indication that also Fun30 may bind DNA at SHL2 and SHL-6.

It can even be speculated that Fun30 may be bound to the nucleosome as a dimer and that both Fun30 subunits could bind to the nucleosome. Nucleosome binding could be either in a symmetric fashion, like with SHL+6 and SHL-6 bound, or non-symmetrical.

A double interaction could also offer explanations for the molecular mechanism of Fun30. If both enzymes pump DNA in opposite directions and prevent backtracking, they would create a DNA loop between them, loosening DNA-histone-contacts enabling histone dimer exchange or nucleosome eviction, especially if assisted by histone chaperones like Nap1 or potentially binding the free octamer on its own, as suggested for SMARCAD1 (Markert et al., 2021). One could also speculate, that whether Fun30 is acting as monomer or dimer may dictate the remodeling output, like a single Fun30 would slide nucleosomes, while two Fun30 molecules would evict histones or nucleosomes.

The only way to find out the position of Fun30 on a nucleosome and perchance to detect a dimer or multiple Fun30 molecules is to solve a structure of Fun30 bound to a nucleosome. Using the AlphaFold prediction as template, one could design a truncated Fun30 containing mostly structured parts, for example a minimal Fun30 ATPase domain and the SAM-key to eliminate flexible regions that impair crystallization and are unlikely to be resolved by cryo-EM.

Notably, the SAM-key in the model is not facing towards the cleft for the DNA substrate between the ATPase lobes, but outwards.

Like its name-giving key the SAM-key can be divided into two parts: the SAM-like “handle”, that via a loop continues as the long protruding helix, the “key bit”. According to the nucleosome docking models, the key bit and the connecting loop could be extended towards or along (extra)nucleosomal DNA. In prominent position for interaction is the loop between SAM-like handle and key bit. Located there is a positively charged basic patch, that could interact with the DNA phosphate backbone (Fig. 22) or the nucleosome acidic patch like it is known for other remodelers (Dao and Pham, 2022).

When testing a deletion mutant lacking the charged residues of the loop (Fun30 Δ KRKRR), we did, however, not see impairment of nucleosome sliding, eviction and DNA-stimulated ATP hydrolysis (Fig. 23).

As this basic patch shows relatively poor evolutionary conservation (Fig. 5) and could be deleted without impairment, it may be irrelevant for remodeling function. It is however possible, that the loop may play a role in other context, for example with different substrates such as modified nucleosomes or a nucleosome array.

Based on its outward facing location and the presence of a SAM-like fold, the SAM-key may also contact another chromatin-bound factor. While so far no additional factor has been found to be necessary for remodeling by Fun30 and *in vitro* Fun30 on its own is able to catalyze nucleosome sliding, SAM-mediated macromolecular interactions may be important for regulation of Fun30 function *in vivo*.

Model: Fun30 SAM-key allosterically activates ATPase domain

In sum, our data shows that the SAM-key of Fun30 acts as an intrinsic, allosteric activator of its catalytic activity. Specifically, the SAM-key interacts with protrusion I, which is a regulatory hub in other chromatin remodelers as well. However, on its own, the SAM-key is not sufficient to stimulate ATP hydrolysis, this requires the presence of DNA.

Two principal models fit our experimental data: First, a Fun30 monomer may be the active form. The SAM-key makes intramolecular contact to the ATPase at protrusion I, as predicted in the AlphaFold model. Together with substrate binding this could self-activate Fun30, perhaps due to a conformational change. This would go in line with the fact that in the ATPase assay, Fun30 required a DNA stimulus for ATP

hydrolysis (Fig. 15) and SAM-key was not sufficient to stimulate ATPase activity of Fun30 or Fun30 Δ SAM (Fig. 25 A).

Second, a homo-dimer may be the active form of Fun30. The activation of Fun30 would then depend on binding of a second molecule of Fun30. This activation could be mediated by the SAM-key, if for example the SAM-key of the second molecule interacts with protrusion I of the first (Fig. 25 B). Our gel filtration experiments did not show a defect for dimerization in Fun30 Δ SAM (Fig. 12), however they did not contain substrate that might induce or stabilize dimerization.

In both models the SAM-key transduces some input signal from DNA/chromatin to regulate remodeling. Protrusion I has been shown to be a hub for controlling activity in other remodelers as well (Clapier et al., 2020). For example, in Ino80 the interaction of protrusion I with its regulatory module is key to transduce signal inputs including the length of entry DNA and adjust remodeler activity. Whether this is true also for Fun30-SMARCAD1-ETL SAM-key modules needs to be addressed in future studies.

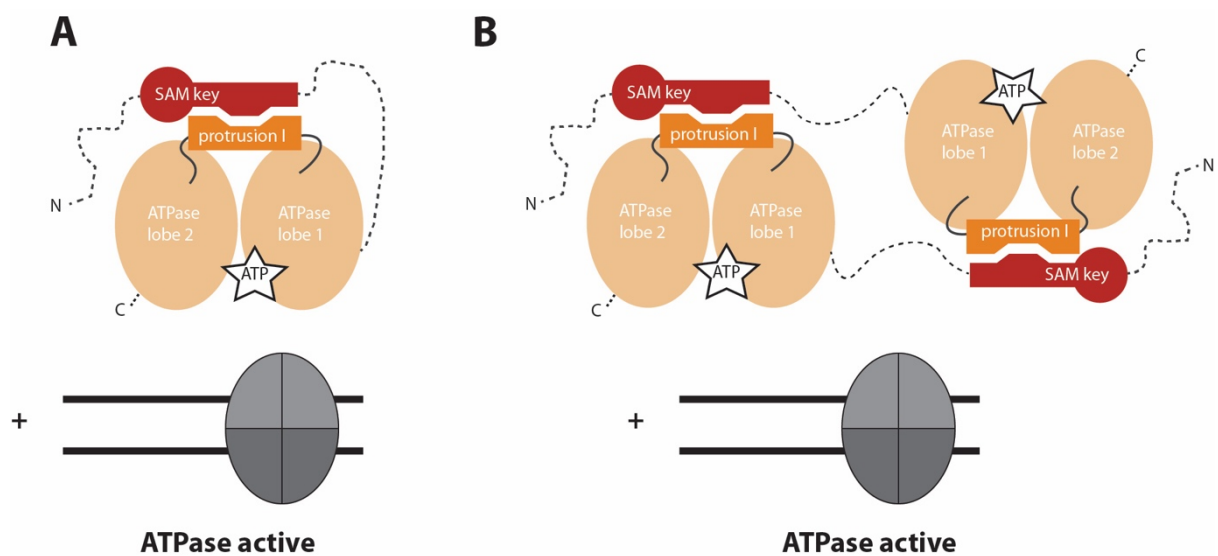


Figure 25: Regulation of Fun30 activity by the SAM-key in monomer or dimer

A: Model of regulation of Fun30 monomer activity: Domains from N-terminus (N), over SAM-key (red), ATPase lobe 1 (beige), protrusion I (orange) to ATPase lobe 2 (beige) and C-terminus (C). The SAM-key interact with protrusion I via the key helix and together with additional stimulation by DNA/substrate (here an end positioned nucleosome on DNA) the Fun30 monomer is ATPase active.

B: Model of regulation of Fun30 homo-dimer activity: Domains colored as in A. The SAM-key of the left Fun30 molecule interacts with protrusion I of the right Fun30 molecule (and vice versa). Dimerization is independent of the SAM-key, however only with SAM-key intermolecular interaction together with additional stimulation by DNA/substrate the Fun30 homo-dimer is ATPase active.

The location of protrusion I between the N-terminal ATPase lobe 1, which is required for ATP binding, and the C-terminal lobe 2, that is required for ATP hydrolysis could provide multiple regulatory mechanisms, likely involving conformational changes.

Looking at the process of ATP hydrolysis there are three key steps that could be influenced by allosteric regulation: i) The binding of ATP to ATPase lobe1, ii) the hydrolysis of ATP and coupling to the catalyzed reaction, in case of nucleosome remodelers pumping of DNA, and iii) the release of ADP and thereby enabling the next cycle.

Distinguishing between these options is not possible with the data obtained in this study and will require further investigation. One option to study this would be additional crosslinking mass spectrometry, looking

for conformational changes upon addition of only ADP or a non-hydrolysable ATP analogue like ATP γ S or AMP-PNP in presence of the substrate.

What still warrants further investigation is the open question what is the DNA stimulus of Fun30 ATPase activity. Our data indicate that a combination of ss- and ds-DNA works best, like at the junction at the site of resection, where Fun30 is located via Dpb11 and the 9-1-1 complex. This junction however, will likely be occupied *in vivo* by resection nucleases resecting into chromosomal DNA. So it is unclear, how accessible it would be for Fun30. Our results could also be explained by two actually separate stimuli being present at the same time, one being exposed ssDNA and the other being dsDNA, maybe interacting with the remodeler at different sites. To test for this option, one could try adding ssDNA to *in vitro* remodeling assays and checking for increase of sliding or eviction.

In all, our work shows that *in vitro* Fun30 can not only slide nucleosomes, but also evict both H2A-H2B dimers and H3-H4 tetramers, if assisted by a histone chaperone. Both these activities are ATP-dependent and are abrogated same as DNA-stimulated ATP hydrolysis upon deletion of the SAM-key or upon disturbing the hydrophobic interface of SAM-key and protrusion I. While the SAM-key is not required to bind to DNA or nucleosomes, it is required for catalytic activity. The mutants can be reactivated by addition of functional SAM-key *in trans*, speaking for allosteric activation by the SAM-key-protrusion-I-interaction. The two models of i) intramolecular activation within one Fun30 molecule or ii) intermolecular activation by a second Fun30 molecule, highlight the need for a Fun30 dimerization mutant to decipher the molecular details of this fascinating remodeler.

In vivo, the described activities in sliding nucleosomes, evicting histones or entire nucleosomes are likely important for Fun30 function, however what is the actual mechanism in the cell and whether the same activity is important for silencing and promoting resection warrants further research.

The molecular mechanism of Fun30 *in vivo* is difficult to solve, since a *fun30* Δ strain displays both reduced resection and eviction and with SWI/SNF and RSC two other evictors at DSBs could at least partially mask defects caused by *fun30* mutants (Peritore et al., 2021). Additionally, *in vivo fun30* Δ phenotypes can be suppressed by deleting its antagonist Rad9 (Bantele et al., 2017; Costelloe et al., 2012), which could be explained by a resection-promoting mechanism of Fun30 specifically remodeling/evicting Rad9-bound nucleosomes. To test *in vitro* whether Rad9-bound nucleosomes are the major substrate of Fun30, a complex reconstituted system of DNA end resection including ss-ds-DNA substrate, Rad9 bound to modified nucleosomes, RPA and best more factors like Dpb11 and the 9-1-1-complex will be required.

With our work, we also advanced the understanding of chromatin remodeling machines in general, by providing evidence for Fun30-SMARCAD1-ETL sharing the suggested conserved regulatory hub at protrusion I of the SNF2-type ATPase domain. Additionally, we showed that also in a single-subunit remodeler regulation of ATPase activity with a specific module and not only via substrate binding, is an important feature.

Our results indicate that a minimal nucleosome remodeler consists of a recruitment module, the conserved two-lobed ATPase domain and a module to control ATP hydrolysis for remodeling. Recently, also for single-subunit remodeler Chd1 a module out of chromodomains and the so-called bridge has been suggested to regulate coupling (Nodelman et al., 2021), further supporting that such a control module is a fundamental part of nucleosome remodelers.

Beyond the scopes of the project

Application of knowledge from Fun30 regulation to improve genome editing

For SMARCAD1 no structure is available, but AlphaFold predicts a structure highly similar to Fun30, including SAM-key interaction with protrusion I. Likely, also here a mutant that destroys the interface of SAM-key and protrusion I will affect the catalytic activity of the enzyme. Since SMARCAD1 is a crucial regulator of DSB resection in mammalian cells, it is also a highly interesting protein for genome editing. Over the past decade CRISPR/Cas9 technology has not only greatly improved and accelerated research but also entered clinical stages as a therapeutic strategy. One limitation is the efficiency of the genome editing that depends on endogenous repair. Particularly, if one wants to insert a specific sequence of choice using homologous recombination one needs to consider that recombination is under cell cycle control. Many human tissues like muscle, bone or most neurons mainly consist of differentiated cells that stay in a G₀-phase of the cell cycle, where HR is downregulated. To increase homology-directed and HR in this context is an important goal for the genome editing field. SMARCAD1 with its key role in repair pathway choice may provide a crucial factor in this endeavor. Understanding the regulation of Fun30 and SMARCAD1 may offer a way to manipulate DSB resection and genome editing as suggested by a first study (Bantele et al., 2017).

Application of knowledge from Fun30 regulation for development of disease and cancer treatments

Genomic instability is one of the established hallmarks of cancer (Hanahan, 2022; Hanahan and Weinberg, 2000; 2011) and defects in chromatin remodeling have been identified as reason for several disease syndromes (Gibbons and Higgs, 2000). That has put factors in the DNA damage response as well as chromatin remodelers high up on the list of potential drug targets (Kaur et al., 2019; Li et al., 2020), and Fun30-SMARCAD1-ETL belongs to both of these categories. Attempts to develop inhibitors against a chromatin remodeler will typically be generated against the highly conserved ATPase domain. This generates both a chance and a problem: On the one hand, every chromatin remodeler is an ATP-dependent machine, so inhibiting its catalytic subunit will abolish its function. However, due to conservation of the ATPase between different remodelers, specificity is a problem.

At this point the SAM-key is a unique element of Fun30-SMARCAD1-ETL remodelers. Therefore, the SAM-key-protrusion I interaction may offer new ways to interfere with its function and offer opportunities for the development of inhibitors. Interestingly, the interaction surface of Fun30 SAM-key protrusion I is hydrophobic in nature and activates ATP hydrolysis, while for the Ino80 post-HSA mostly positive charges appear to be oriented towards protrusion I and overall post-HSA domains seem to reduce ATP hydrolysis. This diversity in the interface and regulation could be used for developing inhibitors or activators specific for Fun30-SMARCAD1-ETL and not or less effective on other remodelers. In all, the discovery of the SAM-key domain of Fun30-SMARCAD1-ETL remodelers described for the first time in this thesis therefore does not only offer a new insight into the biology of this protein, but could also be a lead for future biotechnological and medical innovation.

Material and Methods

Microbiology methods

***E. coli* media and buffers**

LB medium (plates)	1%	tryptone
	0.5%	yeast extract
	1%	sodium chloride
	(1.5%	agar)
	for selection:	100 mg/mL ampicillin
		30 µg/mL kanamycin
		34 µg/mL chloramphenicol
Inoue transformation buffer	10 mM	PIPES pH 6.7
	250 mM	potassium chloride
	55 mM	manganese chloride
	15 mM	calcium chloride

Table 1: *E. coli* strains

Strain	Genotype	Reference/source
XL-1 blue	recA1 endA1 gyrA96 thi-1 supE44 relA1 hsdR17 lac [F' proAB lacIqZΔM15 Tn10 (Tetr)]	Stratagene
BL-21 pRIL	<i>E. coli</i> B F ⁻ ompT hsdS(rB- mB-) dcm ⁺ Tetr gal λ(DE3) endA Hte [argU ileY leuW Camr]	Agilent Technologies
Stellar	recA1 endA1 gyrA96 thi-1 supE44 relA1 phoA F ⁻ Φ80d lacZΔM15 Δ(lacZYA-argF) U169 Δ(mrr - hsdRMS - mcrBC) ΔmcrA λ-	Takara Bio

Table 2: *E. coli* plasmids

Plasmid	Description	Reference/source
pLAK080	pEC-A-3C-GST-Fun30-CO (codon optimized for yeast expression)	This study
pLAK081	pEC-A-3C-GST-Fun30-CO-K603R	This study
pLAK124	pEC-A-3C-GST-Fun30-CO-ΔSAM(Δ275-435)	This study

pLAK148	pET28a-1xWidom-601-nucleosome-positioning-sequence	This study
pLAK199	pEC-A-3C-GST-Fun30-CO-ICRR(I367R,C374R)	This study
pPH37	pEC-A-3C-GST-Fun30-CO-ΔKRKRR(338-342)	This study
pCD002	pGEX-6P-1-Fun30(275-436)	This study
pCFK1	pGEX-6P-1-Nap1	Christoph Kurat / (Kurat et al., 2017)

Cultivation and storage of *E. coli* cells

For short-term storage, *E. coli* cells were cultivated on agar plates and stored at 4 °C. For long-term storage, overnight cultures were supplemented with 25% glycerol (v/v) and kept at -80 °C. Overnight cultures or plates with *E. coli* cells were grown at 37 °C in LB medium with shaking (220 rpm) or on LB plates – without shaking – both supplemented with respective antibiotics for plasmid selection. Overnight culture volumes of 5 mL were used for inoculation of expression cultures or for preparation of plasmid DNA.

Preparation of chemically competent *E. coli* cells

Chemically competent *E. coli* cells were prepared according to the Inoue protocol (Inoue et al., 1990). In brief, cells were grown at 18 °C to an OD₆₀₀ of 0.55, cooled down to 4 °C before washing and resuspending in cold Inoue transformation buffer supplemented with 7.5% DMSO. Aliquots of 100 µL were prepared and snap-frozen in liquid nitrogen, then stored at -80°C.

Bacterial transformation

25 µL of Stellar® (Takara Bio) or 50 µL of XL-1-Blue or BL21 DE3 pRIL *E. coli* competent cells were thawed on ice. *E. coli* were incubated with 1 µL of plasmid solution (-200 ng/µL) for 15 min on ice. Cells were subjected to heat-shock at 42°C for 45 sec, recovered on ice for 5 min.

For Stellar and XL1-blue, cells were pelleted by centrifugation (Eppendorf Benchtop Microfuge 5418R, 3000 rpm, 3 min), the supernatant was discarded and cells resuspended in 150 µL of sterile water and plated on selective LB-agar plates.

For BL21 DE3 pRIL, cells were first mixed with 1 mL of non-selective LB-medium and incubated at 37°C, 1000 rpm for 1 h. After this recovery cells were pelleted, resuspended and plated on double-selective LB-agar plates.

Protein expression with *E. coli* cells

Protein expression in *E. coli* was performed as indicated for the respective protein in the section “Recombinant proteins”.

S. cerevisiae media and buffers

YP medium (plates)	1%	yeast extract
	2%	bacto-peptone
	2%	glucose for YPD / galactose for YPG / raffinose for YPR
	(2 %	agar)
for selection:	200 mg/L	geneticin G418
	500 mg/L	hygromycin B
	100 mg/L	nourseothricin
SC medium (plates)	0.67%	yeast nitrogen base
	0.133%	master mix -8
	2%	glucose / galactose / raffinose
	as required	Ade (22.5 mg/l), Leu (175 mg/l), His, Lys, Met, Arg, Ura, Trp (87.5 mg/l)
	(2%	agar)
5x SD (Synthetic Defined medium w/o 8 supplements)	3.3%	yeast nitrogen base
	0.664%	master mix -8
5'-FOA plates	20% (v/v)	5xSD
	2%	glucose
	0.00522%	Ade
	0.00875%	Lys
	0.00875%	Met
	0.00875%	Arg
	0.0119%	Ura
	0.00875%	His
	0.00875%	Leu
	0.00875%	Trp
	0.1%	5'-FOA
	2%	agar
	master mix -8	25 g (each)
25 g		myo-inositol
2.5 g		para-aminobenzoic acid
SORB buffer	100 mM	lithium acetate
	10 mM	Tris-HCl, pH 8.0
	1 mM	EDTA pH 8.0
	1 M	sorbitol

PEG buffer	100 mM	lithium acetate
	10 mM	Tris-HCl, pH 8.0
	1 mM	EDTA pH 8.0
	40% (w/v)	PEG-3350 (Sigma)

Table 3: *S. cerevisiae* strains

Strain	Genotype	Reference/source
Background strain		
W303	MatA ade2-1 ura3-1 his3-11,15 trp1-1 leu2-3,112 can1-100	(Rothstein, 1983)
ChIP strains		
YSB005	MatA ade3::pGAL::HO bar1Δ::TRP1 hmlΔ::pRS-1 hmrΔ::pRS-2	Susanne Bantele / This study
YSB168	YSB005 fun30Δ::kanMx4	Susanne Bantele / This study
YSB517	MatA ade3::pGAL::HO bar1Δ::TRP1 hmlΔ::pRS-1 hmrΔpRS-2	Susanne Bantele / This study
YSB525	MatA ade3::pGAL::HO bar1Δ::TRP1 hmlΔ::pRS-1 hmrΔpRS-2 fun30Δ::hphNT1	Susanne Bantele / This study
YSB541	Matalpha ade3::pGAL::HO bar1Δ::TRP1 hmlΔ::pRS-1 hmrΔ::pRS-2	Susanne Bantele / This study
YSB783	YSB517 fun30Δ::kanMX4	Susanne Bantele / This study
YSB784	W303 bar1Δ::TRP1 pep4Δ::LEU2 GAL4 pGAL 1-10 Fun30-3FLAG-CBP::HIS3	Susanne Bantele / This study
YSB870	YSB783 Ddc1-Fun30-527-C	Susanne Bantele / This study
YSB871	YSB783 Ddc1-Fun30-501-C	Susanne Bantele / This study
YSB872	YSB783 Ddc1-Fun30-422-C	Susanne Bantele / This study
YSB951	YSB783 Ddc1-Fun30 30-C	Susanne Bantele / This study
YSB952	YSB783 Ddc1-Fun30 120-C	Susanne Bantele / This study
YSB1046	YSB168 Ddc1-Fun30-3FLAG::hphNT1	Susanne Bantele / This study
YSB1052	YSB783 Fun30 278-389Δ	Susanne Bantele / This study
Camptothecin spotting		
YSB758	W303 fun30Δ::kanMX4	Susanne Bantele / This study
YSB865	YSB758 Ddc1-Fun30-527-C	Susanne Bantele / This study
YSB866	YSB758 Ddc1-Fun30-501-C	Susanne Bantele / This study
YSB867	YSB758 Ddc1-Fun30-422-C	Susanne Bantele / This study
YSB1038	YSB525 Fun30 247-281Δ	Susanne Bantele / This study
YSB1039	YSB525 Fun30 247-281Δ	Susanne Bantele / This study
YSB1040	YSB525 Fun30 278-389Δ	Susanne Bantele / This study
YSB1041	YSB525 Fun30 278-389Δ	Susanne Bantele / This study
YSB1042	YSB525 Fun30 338-389Δ	Susanne Bantele / This study
YSB1043	YSB525 Fun30 338-389Δ	Susanne Bantele / This study
YSB1044	YSB525 Fun30	Susanne Bantele / This study
YSB1045	YSB525 Fun30	Susanne Bantele / This study

Silencing assays		
ChrVII-L-Tel:URA3		
AEY1017	MATalpha ade2-1 ura3-1 his3-11,15 trp1-1 leu2-3,112 can1-100 ChrVII-L-TEL::URA3	(Meijsing and Ehrenhofer-Murray, 2001)
YSB246	MATalpha ade2-1 ura3-1 his3-11,15 trp1-1 leu2-3,112 can1-100 ChrVII-L-TEL::URA3 fun30Δ::hphNT1	Susanne Bantele / This study
YSB294	MATalpha ade2-1 ura3-1 his3-11,15 trp1-1 can1-100 ChrVII-L-TEL::URA3 fun30Δ::hphNT1 leu2::promoterFun30-Fun30-3FLAG-LEU2 (pSB59)	Susanne Bantele / This study
YSB297	URA3::ChrVII-L-TEL fun30Δ::hphNT1 leu2::promoterFun30-Fun30-SS20,28AA-3FLAG-LEU2 (pSB33)	Susanne Bantele / This study
YLAK163	MATalpha ade2-1 ura3-1 his3-11,15 trp1-1 can1-100 ChrVII-L-TEL::URA3 fun30Δ::hphNT1 leu2::promoterFun30-Fun30-CO-3xFLAG-LEU2 (pLAK132)	This study
YLAK167	MATalpha ade2-1 ura3-1 his3-11,15 trp1-1 can1-100 ChrVII-L-TEL::URA3 fun30Δ::hphNT1 leu2::promoterFun30-Fun30-K603R-CO-3xFLAG-LEU2 (pLAK133)	This study
YLAK169	MATalpha ade2-1 ura3-1 his3-11,15 trp1-1 can1-100 ChrVII-L-TEL::URA3 fun30Δ::hphNT1 leu2::promoterFun30-Fun30ΔSAM(275-436)-CO-3xFLAG-LEU2 (pLAK134)	This study
hmr:URA3		
UCC3511	MATalpha hmr::URA3 ade2-101 his3-200 leu2-1 lys2-801 trp1-63 ura3-52	(Singer et al., 1998)
YSB248	MATalpha hmr::URA3 ade2-101 his3-200 leu2-1 lys2-801 trp1-63 ura3-52 fun30Δ::hphNT1	Susanne Bantele / This study
YSB335	MATalpha URA3::hmr ade2-101 his3-200 leu2-1 lys2-801 trp1-63 ura3-52 fun30Δ::hphNT1 leu2::fun30-SS20,28AA-LEU2 (pSB38)	Susanne Bantele / This study
YLAK172	MATalpha hmr::URA3 ade2-101 his3-200 leu2-1 lys2-801 trp1-63 ura3-52 fun30Δ::hphNT1 leu2::promoterFun30-Fun30-CO-3FLAG-LEU2 (pLAK132)	This study
YLAK173	MATalpha hmr::URA3 ade2-101 his3-200 leu2-1 lys2-801 trp1-63 ura3-52 fun30Δ::hphNT1 leu2::promoterFun30-Fun30-K603R-CO-3FLAG-LEU2 (pLAK133)	This study
YLAK176	MATalpha hmr::URA3 ade2-101 his3-200 leu2-1 lys2-801 trp1-63 ura3-52 fun30Δ::hphNT1 leu2::promoterFun30-Fun30-ΔSAM(275-436)-CO-3FLAG-LEU2 (pLAK134)	This study

YLAK177	MAT α hmr::URA3 ade2-101 his3-200 leu2-1 lys2-801 trp1-63 ura3-52 fun30 Δ ::hphNT1 leu2::promoterFun30-Fun30- Δ SAM(275-436)-CO-3FLAG-LEU2 (pLAK134)	This study
Protein expression		
YBP392	MAT α bar1::TRP1 pep4::LEU2	Boris Pfander / This study
YSB784	Mata bar1 Δ ::TRP1 pep4 Δ ::LEU2 GAL4 pGAL 1-10 Fun30-CO-3FLAG-CBP::HIS3 (pKR347)	Susanne Bantele / This study
YLAK019	Mata bar1 Δ ::TRP1 pep4 Δ ::LEU2 GAL4 pGAL 1-10 Fun30- Δ SAM(275-436)-CO-3FLAG-CBP::HIS3 (pLAK008)	This study
YLAK020	Mata bar1 Δ ::TRP1 pep4 Δ ::LEU2 GAL4 pGAL 1-10 Fun30- Δ SAM(275-436)-CO-3FLAG-CBP::HIS3 (pLAK008)	This study
YLAK115	Mata bar1 Δ ::TRP1 pep4 Δ ::LEU2 GAL4 pGAL 1-10 Fun30-K603R-CO-3FLAG-CBP::HIS3 (pLAK057)	This study
YLAK116	Mata bar1 Δ ::TRP1 pep4 Δ ::LEU2 GAL4 pGAL 1-10 Fun30-K603R-CO-3FLAG-CBP::HIS3 (pLAK058)	This study
YLAK120	Mata bar1 Δ ::TRP1 pep4 Δ ::LEU2 GAL4 pGAL 1-10 Fun30-K603R- Δ SAM(275-436)-CO-3FLAG-CBP::HIS3 (pLAK059)	This study

Table 4: *S. cerevisiae* plasmids

Plasmid	Description	Reference/source
Protein expression		
pKR347	pRS303-based: Gal4-pGal1-10-Fun30-CO-3FLAG-CBP, HIS3, AmpR	Karl-Uwe Reußwig / this study
pLAK008	Gal4-pGal1-10-Fun30- Δ SAM(275-436)-CO-3FLAG-CBP, HIS3, AmpR	This study
pLAK056	Gal4-pGal1-10-Fun30- Δ SAM(275-436)-CO-3FLAG-CBP, HIS3, AmpR	This study
pLAK057	Gal4-pGal1-10-Fun30-K603R-CO-3FLAG-CBP, HIS3, AmpR	This study
pLAK058	Gal4-pGal1-10-Fun30-K603R-CO-3FLAG-CBP, HIS3, AmpR	This study
pLAK059	Gal4-pGal1-10-Fun30-K603R- Δ SAM(275-436)-CO-3FLAG-CBP, HIS3, AmpR	This study

Strain generation		
pBP82	pYM-20-based vector for 3FLAG-tagging of yeast genes: pYM-3FLAG-hph-NT1	Boris Pfander
pSB33	pRS304 pFun30o+t SS20,28AA AfeI	Susanne Bantele
pSB38	pRS305 pFun30o+t SS20,28AA	Susanne Bantele
pSB59	pRS305 pFun30o-3FLAG	Susanne Bantele
pSB213	pBP82 Fun30 527-C-3FLAG	Susanne Bantele
pSB214	pBP82 Fun30 501-C-3FLAG	Susanne Bantele
pSB215	pBP82 Fun30 422-C-3FLAG	Susanne Bantele
pSB235	pBP82 Fun30 30-C-3FLAG	Susanne Bantele
pSB236	pBP82 Fun30 120-C-3FLAG	Susanne Bantele
pSB265	pSB59 247-275Δ	Susanne Bantele
pSB266	pSB59 247-281Δ	Susanne Bantele
pSB267	pSB59 278-389Δ	Susanne Bantele
pSB268	pSB59 338-389Δ	Susanne Bantele
pSB286	pRS305 pFun30o-3FLAG 275-436Δ	Susanne Bantele
pLAK132	pRS305 pFun30-Fun30-CO-3FLAG, LEU2, AmpR	This study
pLAK133	pRS305 pFun30-Fun30-K603R-CO-3FLAG, LEU2, AmpR	This study
pLAK134	pRS305 pFun30-Fun30-ΔS-(Δaa275-435)-CO-3FLAG, LEU2, AmpR	This study

Cultivation and storage of *S. cerevisiae* cells

For short-term storage, *S. cerevisiae* cells were cultivated on agar plates and stored at 4 °C. For long-term storage, overnight cultures were supplemented with 15% glycerol (v/v) and kept at -80 °C. Liquid cultures or plates were grown at 30 °C, normally in YPD with shaking (220 rpm) or on respective agar plates – without shaking. Experiments were carried out in logarithmic growth phase (OD₆₀₀ 0.5-1.0).

Preparation of competent *S. cerevisiae* cells

Yeast cells from one single colony were inoculated in YPD and grown to an OD₆₀₀ between 0.5-1.0 (log-phase). Cells were pelleted at 3500 rpm for 2 min, washed once with sterile ddH₂O and once with sterile SORB buffer. The pellet was resuspended in SORB buffer supplemented with 1 mg/mL denatured herring sperm DNA (8 μL buffer per 1 mL yeast culture, ~1.5 x 10⁷ cells), then aliquoted (100 μL) and frozen and stored at -80°C.

Transformation of *S. cerevisiae* cells

100 μL of competent yeast cells (~19 x 10⁷ cells) were mixed with 10 μL of concentrated PCR product (see chapter Ethanol precipitation of DNA) or linearized integrative plasmid. 600 μL PEG buffer was

added and the reaction mixed for 30 min at room temperature (RT). DMSO (final 10%) was added and cells heat-shocked at 42°C for 15 min. Cells were pelleted by centrifugation (3 min, 3000 rpm, Eppendorf 5418R), supernatant removed and cells resuspended in 100 µL ddH₂O which was directly plated on selective plates for auxotrophic markers. For antibiotic resistance markers cells were first incubated with 1 mL of YPD at 30°C, 800 rpm for at least 3 h, before plating on the respective selective plate. Plates were incubated at 30°C and colonies grew after 2-3 days. Single transformed colonies were picked and streaked on selective plates and further analysed.

Genetic modification of *S. cerevisiae* cells

For stable integration of short (protein tags) or long (integrative plasmids) pieces of DNA into the yeast genome, a versatile toolbox of tags and resistance markers was used (Janke et al., 2004; Knop et al., 1999; Wach et al., 1994). In brief, with a certain set of primers designed specific for the gene of interest, but with common overhangs complementary to the set of plasmids (pYM series), containing the respective desired inserts and selective markers, one can exchange promoters, insert affinity-tags at N- or C-terminus or fully delete it from the genome by PCR. Additionally, another set of plasmids (pRS series, YIplac series) was used for integration of larger DNA fragments such as ORFs and genes. For haploid yeast cells, where there is just one gene copy, this enables fast and precise modifications of the genotype. Integrants were selected by auxotrophic or resistance markers and correct genomic modification was controlled by colony PCR, using primers designed to check the site and size of insertion.

Spotting assays: Survival assay and silencing assay

Pre-cultures were grown to stationary phase overnight. A serial dilution series was spotted on respective selective/drug-containing plates and YPD plates.

For survival assays on camptothecin (CPT), a 7-step serial dilution series (1:5 dilution) was prepared starting at OD₆₀₀ 1.0 and spotted on YPD plates with different concentrations of CPT (6, 10 or 12 µg/mL).

For silencing assays, a 6-step serial dilution series (1:5 dilution) was prepared starting at OD₆₀₀ 0.5 and spotted on YPD-, SC-Ura- and 5'-FOA-plates.

Molecular biology methods

Buffers and solutions

TE buffer	10 mM 1 mM	Tris-HCl pH 8.0 EDTA pH 8.0
HE buffer	10 mM 1 mM	HEPES-KOH pH 7.6 EDTA pH 8.0
DNA loading buffer (5x)	0.5% 0.25% 25% 25 mM	SDS orange G glycerol EDTA pH 8.0
TAE buffer	40 mM 20 mM 1 mM	Tris-HCl pH 7.6 acetic acid EDTA pH 8.0
TBE buffer	90 mM 90 mM 1 mM	Tris base boric acid EDTA (free acid)

Small scale plasmid DNA preparation

Single colonies from plates after transformation were used to inoculate 5 mL of selective LB-medium and grown overnight at 37 °C, 220 rpm. The next day, minipreps of DNA plasmids were conducted from 5 mL of stationary culture according to manufacturer's instructions with the AccuPrep® Plasmid Mini Extraction Kit (*Bioneer*, K-3030).

Ethanol precipitation of DNA

The DNA containing solution was mixed with 0.1 volumes 3 M sodium acetate pH 4.8 and 2.5 volumes absolute ethanol and incubated for at least 30 min at -20 °C. The precipitated DNA was pelleted by centrifugation (15 min, max speed), dried (at least 30 min, RT), and resuspended in an appropriate amount of water.

Restriction digests

A DNA sample (2 µg) was digested in a 30 µL reaction with 5 U of the respective restriction enzyme(s) (New England Biolabs) according to the manufacturer's instructions, usually for one to two hours at 37 °C. Afterwards, digested DNA was analysed by agarose gel electrophoresis.

Agarose gel electrophoresis

DNA loading buffer was added to DNA samples (final conc. 1x), mixed and separated on 1% (or up to 2% according to specific construct) agarose gels containing ethidium bromide (0.5 µL / 10 mL gel) in TAE buffer. Bands were visualized using a Gel Doc™ XR+ (BioRad) gel documentation system with ImageLab™ software (v 5.2.1).

Agarose gel extraction

Bands of interest were excised from agarose gels and purified using NucleoSpin Gel and PCR Clean-up kit (Macherey Nagel; 740609.50) following the manufacturer's instructions.

Standard polymerase chain reaction (PCR)

Routinely, the PCR programs "CASTORP" and "Phusion" were used for tasks as amplification of cassettes for introducing tags or deletions into yeast cells. For checking correct integration into the yeast genome, these programs were used as well.

standard PCR reaction

2 μ L	template
3.2 μ L	primer 1 (10 μ M)
3.2 μ L	primer 2 (10 μ M)
1.75 μ L	dNTPs (10 mM, NEB-N0447L))
10 μ L	HF-buffer (NEB-B0518S)
1 μ L	DMSO (NEB-B0518S)
0.5 μ L	Phusion polymerase
28.35 μ L	water

PCR program CASTORP

- (1) 95 °C for 4 min
 - (2) 95 °C for 1 min
 - (3) 45 °C for 35 sec
 - (4) 72 °C for 1:40 min
- repeat steps (2)-(4) for 10 cycles
- (5) 95 °C for 1 min
 - (6) 54 °C for 30 sec
 - (7) 72 °C for 1:40 min
- repeat steps (5)-(7) for 20 cycles and
increase extension time by 20 sec each cycle
- (8) hold at 4 °C

PCR program Phusion

- (1) 98 °C for 30 sec
 - (2) 98 °C for 30 sec
 - (3) 58 °C for 30 sec
 - (4) 72 °C for 2 min
- repeat steps (2) to (4) for 35 cycles
- (5) 72 °C for 5 min
 - (6) hold at 4 °C

Sequencing

Sanger-sequencing service was provided by Eurofins genomics, using the *overnight Mix2Seq Kit*. The sequence of complete ORFs was confirmed after cloning. Sequences were analyzed with the SnapGene software v6.1.1 (GSL Biotech LLC).

Sequence and ligation independent cloning (SLIC)

Sequence and ligation independent cloning (SLIC) is a technique to seamlessly insert a sequence of interest into any plasmid of choice without the use of restriction endonucleases or DNA ligases. The method exploits annealing of complementary 5'-overhangs from PCR fragments introduced via primers and generated using exonuclease activity of specific polymerase enzymes with plasmid ends. To finalize the cloning, the endogenous repair of the resulting nicks in *E. coli* is used.

For SLIC, gene-specific primers (~20nt) were designed with the SnapGene software with 15bp extensions complementary to vector ends at the required insertion site and the desired gene amplified in PCR with these primers. The PCR product was checked for correct size by agarose gel electrophoresis using a 1% agarose in 1x TAE gel (run at 100 V for 30 min in 1x TAE). Desired bands were cut out and gel purified using the NucleoSpin Gel and PCR Clean-up kit (Macherey Nagel; 740609.50) according to the manufacturer's instructions. The desired vector was linearized by either restriction digest or PCR (using two primers to start polymerization into opposite directions from the insertion site and amplifying the entire vector). Using the In-Fusion HD Enzyme Premix (Takara Bio; 102518), 10 µL reactions were assembled according to table 5 and mixed before 15 min incubation at 50°C. 1-2µL of the reaction were used for standard transformation.

Table 5: SLIC reactions

Reagent	Amount	Explanations
Purified PCR fragment	~50 ng (10-200 ng*)	* <0.5 kb: 10-50 ng; 0,5 to 10 kb: 50-100 ng; >10 kb: 50-200 ng
Linearized vector	50-200 ng**	** <10 kb: 50-100 ng; >10 kb: 50-200 ng
5x In-Fusion HD Enzyme Premix	1 µL	
ddH ₂ O	Add to 10 µL	

Ligation independent cloning (LIC)

Ligation independent cloning (LIC) is another technique to seamlessly insert a sequence of interest into a specific set of plasmids (pEC-series) without the use of restriction endonucleases or DNA ligases. The method exploits annealing of complementary 5'-overhangs from PCR fragments introduced via primers and generated using exonuclease activity of T4 DNA polymerase enzymes at temperatures below the optimum. To finalize the cloning, the endogenous repair of the resulting nicks in *E. coli* is used.

For LIC, gene-specific primers (~20nt) were designed with specific extensions for the used vectors with tags cleavable by 3C-protease (PreScission®) according to the bold sequences in this schematic:

5' – **C CAG GGG CCC GAC TCG ATG** (gene of interest) taa gca gtc ggt ggc ggt ctg – 3'
 3' – g gtc ccc ggg ctg agc tac (-----) **ATT CGT CAG CCA CCG CCA GAC** – 5'

The extensions were complementary to vector ends at the insertion site after vector processing. The desired gene was amplified in standard PCR with these primers. 2 µg of the desired vector was linearized by restriction digest with 20 U of ZraI. Vector and PCR product were checked for correct size/linearization by agarose gel electrophoresis using a 1% agarose in 1x TAE gel (run at 100 V for 30 min in 1x TAE). Desired bands were cut out and gel purified using the NucleoSpin Gel and PCR Clean-up kit (Macherey Nagel; 740609.50) according to the manufacturer's instructions. The insert and linearized vector were processed in separate reactions according to tables 6 and 7, incubation for 30 min at RT, then 20 min at 75°C.

Table 6: Insert processing for LIC

Reagent	Amount	Manufacturer
Purified PCR fragment	~600 ng	-
T4 DNA Polymerase Buffer (NEB 2.1) (10x)	2 μ L	NEB – B7202S
dATP (25 mM)	2 μ L	NEB – N0440S
DTT (100 mM)	1 μ L	-
T4 DNA Polymerase	0.4 μ L	NEB – M0203L
ddH ₂ O	Add to 20 μ L	-

Table 7: Vector processing for LIC

Reagent	Amount	Manufacturer
Purified linearized vector	~450 ng	-
T4 DNA Polymerase Buffer (NEB 2.1) (10x)	3 μ L	NEB – B7202S
dTTP (25 mM)	3 μ L	NEB – N0443S
DTT (100 mM)	1.5 μ L	-
T4 DNA Polymerase	0.6 μ L	NEB – M0203L
ddH ₂ O	Add to 30 μ L	-

For the LIC reaction, 2 μ L of processed insert and 1 μ L of processed vector were combined, incubated for 10 min at RT, then 1 μ L of EDTA (25 mM) was added and another 10 min incubation at RT. 2 μ L of the reaction were used for standard transformation procedure.

Site-directed mutagenesis

Site-directed mutagenesis is used to specifically introduce a desired point mutation at a specific position by using two complementary primers with the desired change and amplifying the entire rest of the plasmid.

For site-directed mutagenesis two complementary ssDNA oligos, which harboured the desired mutated codon(s) in the centre, and 15 bp complementary sequence to each end were designed. In a PCR (BioRad *C1000 Touch™ Thermal Cycler*) with the Pfu TURBO polymerase (Agilent) with the reaction composition and program listed below mutations were introduced. After PCR the template plasmid was digested by addition of DpnI (NEB-R0176L) (20 U) and incubation at 37°C for at least 1 h. 1 μ L of the reaction was transformed into Stellar® competent cells using standard heat shock transformation method and cells were plated on selective plates. After growing colonies overnight at 37°C, clones were used to inoculate 2 mL selective medium, subjected to plasmid miniprep and plasmids confirmed by sequencing.

mutagenesis PCR reaction		mutagenesis PCR program	
0.5 µL	template (-25 ng/µL)	(1)	95 °C for 3 min
0.63 µL	primer 1 (10 µM)	(2)	95 °C for 30 sec
0.63 µL	primer 2 (10 µM)	(3)	55 °C for 60 sec
0.63 µL	dNTPs (10 mM)	(4)	68 °C for 2 min / kb plasmid
2.5 µL	10x Pfu buffer	repeat steps (2)-(4) for 20 cycles	
0.5 µL	Pfu Turbo polymerase (2.5 U/µL)	(5)	hold at 4 °C
19.6 µL	water		

100W0 DNA amplification and purification

The 147 bp Widom 601-nucleosome positioning sequence (Lowary and Widom, 1998)) is used to assemble nucleosomes onto a specific site on a DNA fragment. By using 100 bp overhang on one side and no overhang on the other (=100W0) there is enough space to slide the nucleosome but not assemble a second on the same DNA molecule.

Large scale PCR amplification of 100W0 from plasmid pLAK148 was performed with oligos BP8196 and BP8198 (for 100 bp overhang) using the master mix indicated below and program Phusion SHRT. PCR reactions were pooled, spun down and purified using a 1 mL HiTrap Q HP column (Cytiva). DNA was eluted with a gradient from 100% buffer A (TE + 50 mM NaCl) to 100% buffer B (TE + 1 M NaCl) over 20 column volumes. Fractions containing the DNA were pooled, subjected to ethanol precipitation and finally resuspend in HE buffer, then stored at -20°C.

Large scale PCR master mix (160x 50 µL)		Program Phusion SHRT	
320 µL	template pLAK148	(1)	98°C 30 sec
280 µL	dNTP-mix	(2)	98°C 10 sec
512 µL	oligo BP8196	(3)	52°C 15 sec
512 µL	oligo BP8198	(4)	72°C 5 sec
1600 µL	HF buffer (10x)	repeat steps (2) to (4) for 35x cycles	
4704 µL	H ₂ O	(5)	72°C 1 min
80 µL	Phusion polymerase	(6)	4°C forever

Sequence of the 247 bp 100W0 construct, 147 bp Widom-601-sequence in bold and underlined:

5'-

tatggctagcatgactggtggacagcaaatgggtcgcggatccgaattcgagctccgtcgacaagcttgcggccgcacaattcagctactacgggccccctg
gagaatcccgggtgccgaggccgctcaattggctcgtagacagctctagcaccgcttaaacgcacgtacgcgctgtcccccgctttaaccgccaaggg
gattactccctagtctccaggcacgtgtcagatatatacatcctgt

- 3'

Chromatin Immunoprecipitation (ChIP) and qPCR analysis

Chromatin immunoprecipitation (ChIP) allows to retain DNA that is in close proximity/bound by a certain target protein using formaldehyde crosslinking, shearing of the genome and a pulldown using an antibody against the target protein. By using specific and non-specific primers for a known binding site and quantitative PCR (qPCR) analysis, the enrichment of the protein at a certain locus compared to a random position in the genome.

For chromatin immunoprecipitation of Fun30 (FL and truncated versions), cells were grown in YP-Raffinose to an OD₆₀₀ of 0.5 and – as indicated for the individual experiments – cell cycle arrest was induced using nocodazole (5 µg/mL culture) (G2/M phase arrest) for 90 min at 30 °C. Arrests were confirmed using a microscope. A double-strand break at the MAT locus was introduced by inducing the HO endonuclease from the galactose promoter by addition of galactose to the cultures (final concentration 2%). 100 mL samples were crosslinked with formaldehyde (final concentration 1%) for 16 min at indicated timepoints and the reaction was quenched with glycine (final concentration 450 mM). Cells were harvested by centrifugation, washed in ice-cold PBS and snap-frozen.

For lysis, cell pellets were resuspended in 800 µL lysis buffer (50 mM HEPES KOH pH 7.5, 150 mM NaCl, 1 mM EDTA, 1% Triton X-100, 0.1% Na-deoxycolate, 0.1% SDS) and grinded with zirconia beads using a bead beating device (Retsch, MM301). The chromatin was sonified to shear the DNA to a size of 200-500 bp using Bioruptor (Diagenode). Subsequently, the extracts were cleared by centrifugation, 1% was taken as input sample and 40% were incubated for 90 min with anti RFA antibody (AS07-214, Agrisera) followed by 30 min with Dynabeads ProteinA (Invitrogen). The beads were washed 3x in lysis buffer, 2x in lysis buffer with 500 mM NaCl, 2x in wash buffer (10 mM Tris-Cl pH 8.0, 0.25 M LiCl, 1 mM EDTA, 0.5% NP-40, 0.5% Na-deoxycholate) and 2x in TE pH 8.0. DNA-protein complexes were eluted in 1% SDS, proteins were removed with Proteinase K (3 h, 42°C) and crosslinks were reversed (8 h or overnight, 65°C). The DNA was subsequently purified using phenol-chloroform extraction and ethanol precipitation and quantified by quantitative PCR (Roche LightCycler480 System, KAPA SYBR FAST 2x qPCR Master Mix, KAPA Biosystems) at indicated positions with respect to the DNA double-strand break. As control, 2-3 control regions on other chromosomes were quantified.

Biochemistry methods

Recombinant protein

Histone octamer expression, purification and labeling

Genes encoding wild type *S. cerevisiae* histones were codon optimized and synthesized (Genscript) for the bacterial expression. H2A, H2B genes were cloned into pETDuet™ and H3, H4 were cloned into pCDFDuet™ vectors (#71146, #71340, Novagen). The mutants H2A_46C and H4_64C were generated using QuickChange mutagenesis (#200515 Agilent). The combination of 2 vectors pETDuet_H2A_46C-H2B + pCDFDuet_H3-H4 and pETDuet_H2A-H2B + pCDFDuet_H3-H4_64C were co-transformed in *E. coli* BL21(DE3) codon plus RIL (Agilent) and grown in ZYP-5052 auto-induction media (Studier FW, 2005) at 37 °C up to OD600 = 0.8. The temperature was lowered to 18 °C and expression continued further for 16 hours. All subsequent steps were performed at 4 °C. The cells were harvested by centrifugation (4000 x g, 15 min), resuspended in buffer A (20 mM HEPES-NaOH, pH 7.6, 10 % (v/v) glycerol, 1 mM EDTA) + 0.8M NaCl, 1 mM Dithiothreitol (DTT), supplemented with 1 vial protease inhibitor cocktail (#39102.03 Serva) and lysed by sonication. The cell lysate was cleared by centrifugation (23666 x g, 45 min) and applied to 2x HiTrap Heparin HP (#17040701 Cytiva) 5 mL columns equilibrated in buffer A + 0.8M NaCl, 1mM DTT. The columns were washed with 10 CV buffer A + 0.8M NaCl, 1 mM DTT and histone octamers were eluted with a 0.8M – 2M NaCl linear gradient. Peak fractions were pooled, spin concentrated with a MWCO 10000 Amicon Ultra Centrifugal Filter unit (#UFC901024 Merck). The concentrated protein complex was applied to a HiPrep 26/10 (#17508701 Cytiva) desalting column equilibrated with buffer A to remove DTT, peak fractions were collected and concentration was measured. DyLight™ 550 Maleimide (#62290 ThermoFisher) was added to the protein such that there were approximately 20 moles of dye for each mole of protein. The reaction was allowed to proceed over night at 4°C protected from light. Upon completion of the reaction the conjugate and free dye were separated on a Superdex 200 increase 10/300 GL (#28990944 Cytiva) gel filtration column equilibrated in buffer A + 2 M NaCl, 1 mM DTT. Peak fractions containing histone octamers were pooled, spin concentrated, frozen in aliquots in liquid nitrogen and stored at -80 °C.

Nucleosome assembly

For nucleosome assembly the established protocol (Dyer et al., 2004; Luger et al., 1999) was slightly adapted. In short, dialysis buttons (3,500 MWCO, Slide-A-Lyzer® Mini dialysis unit, Thermo Scientific) were prepared and equilibrated according to the manufacturer's instructions. Nucleosome assembly reactions were combined according to the schematic below, mixing DNA and NaCl first, then filling with HE and adding the histone octamer last. The optimal ratio of DNA/octamer was determined for the different octamer preparations by titration. After mixing the reaction was transferred to the dialysis buttons and dialysis in RB-high was performed at 4°C for 1 hour. A setup of peristaltic pumps exchanged RB-high completely with RB-low over 12-16 h, slowly removing dialysis buffer and dripping in the 4-fold volume of RB-low. After a final dialysis with RB-low over 4 hours, the reaction was transferred to low binding tubes (Sigma, T4816). The efficiency of the assembly was tested by native PAGE, followed by ethidium bromide staining. Nucleosome concentration was estimated using a free DNA control on the gel and calculating the volume of the reaction after dialysis and the amount of free DNA left inside.

Bacterial expression and purification of 6xHis-GST-Fun30

A plasmid harboring the respective Fun30 construct (e.g. pLAK080 for Fun30 WT) with N-terminal 6xHis-GST-3C-cleavage site was transformed into *E. coli* BL21DE3 pRIL. The cells were cultivated at 37°C, 220 rpm in double selective LB-medium (100 µg/mL ampicillin (Amp) and 34 µg/mL chloramphenicol (Chl)) to an OD₆₀₀ of approximately 1.0. Addition of IPTG (1 mM final, Roth, 2316.4) induced overexpression of the construct, which was performed overnight at 18°C. Cells were harvested by centrifugation, washed in ice-cold PBS and snap-frozen or directly processed. Unless specified, all further steps were performed on ice/at 4°C. Cells were lysed in lysis buffer (50 mM HEPES KOH pH 7.5, 500 mM NaCl, 10% glycerol, 0.5 mM CHAPS, 2 mM β-mercaptoethanol, 1x cOmplete protease inhibitor cocktail EDTA-free (Roche) and 10 µg/mL leupeptin, 1 µg/mL pepstatin A, 1 mM benzamidine, 2 µg/mL aprotinin, 1 mM AESBF) with a combination of lysozyme (1 mg/mL) and sonication (3 x 5 min, 2 sec on, 2 sec off; Bandelin *Sonopuls UW 2070*). Lysate was cleared with SmdNase (750 U/mL lysate) and centrifugation. Cleared lysate was incubated with Ni-NTA-agarose (1 mL bed volume/L culture, QIAGEN) for one hour. Beads were washed (lysis buffer) and proteins eluted (lysis buffer + 1 M imidazole). Eluate was diluted (100 mM imidazole final), incubated with glutathione sepharose 4 FF (1.5 mL bed volume/L culture, Cytiva) for two hours. Beads were washed (lysis buffer) and protein eluted by cleaving off the tags using His-3C-protease (lysis buffer + 17U/mL His-3C (homemade)). Eluate was concentrated to 500 µL (Amicon Ultra 4, 10,000 MWCO) and run on a gelfiltration. Here, a superdex 200 (S200 Increase 10/300 GL, Cytiva, 24 mL column volume) column was used, 500 µL fractions were collected and the fractions analyzed by SDS-PAGE and Coomassie staining. The fractions were aliquoted, snap-frozen and stored at -80°C.

Yeast expression and purification of Fun30-3xFLAG-CBP

The respective yeast strain with integrated Fun30 overexpression construct (e.g. YSB784 for Fun30 FL) was grown in 6 L YP-medium + 2% raffinose at 30°C to an OD₆₀₀ of 0.5 and Fun30-3xFLAG-CBP expression was induced by adding galactose (final concentration 2%) and continued for 3 hours at 30°C. Harvest and purification was performed at 4°C on ice unless indicated otherwise. The cells were pelleted and washed with wash buffer (25 mM HEPES KOH pH 7.6, 1 M Sorbitol). Cells were resuspended in 20 mL lysis buffer (400 mM NaCl, 25 mM HEPES KOH pH 7.6, 0.05% NP-40, 10% glycerol, 2 mM β-mercaptoethanol) with protease inhibitors (0.2 mM PMSF, 4 µg/mL aprotinin, 2 mM benzamidine, 2 µg/mL pepstatin A, 2 µg/mL leupeptin and 1x cOmplete™ protease inhibitor cocktail EDTA-free (04693132001, Roche)) and dropwise frozen in liquid nitrogen as “popcorn”. Lysis of the popcorn was performed in a cryo-mill (Spex sample prep) with liquid nitrogen cooling. The whole cell extract was thawed and cleared by centrifugation followed by incubation with 1.5 mL equilibrated slurry of anti-FLAG-M2-affinity gel (A2220, Sigma) for 2 hours. The affinity gel was washed 6 times with 15 CV of lysis buffer and then the protein was eluted twice with 2 mL 0.5 mg/mL 3xFLAG peptide (F4799, Sigma) in lysis buffer and incubation for 30 min. Fun30-3xFLAG-CBP was further purified using a 1 mL MonoQ 5/50 GL column. For this the elution was diluted to 100 mM NaCl by adding lysis buffer without salt and run over a 100 mM to 1 M NaCl gradient over 20 CV. Fun30 containing fractions were snap-frozen in liquid nitrogen and stored at -80°C.

Bacterial expression and purification of Nap1

A plasmid harboring the respective Nap1 construct (pCFK1) with N-terminal GST-3C-cleavage site was transformed into *E. coli* BL21DE3 cells also carrying the pRIL plasmid (for rare yeast tRNAs). The cells were grown at 37°C, 220 rpm in double selective LB-medium (100 µg/mL ampicillin (Amp) and 34 µg/mL chloramphenicol (Chl)) to an OD₆₀₀ of approximately 1.0. Addition of IPTG (1 mM final) induced overexpression of the construct, which was performed for 2 hours at 37°C. Cells were harvested by centrifugation, washed in ice-cold PBS and snap-frozen. Unless specified, all further steps were performed on ice at 4°C. Cell pellets were lysed in Nap1 lysis buffer (100 mM K₂PO₄ pH 7.6, 150 mM KOAc, 5 mM MgCl₂, 0.5 mM CHAPS, 1 mM DTT, 1x cOmplete protease inhibitor cocktail EDTA-free (Roche) and 10µg/mL leupeptin, 1µg/mL pepstatin A, 1mM benzamidine, 2µg/mL aprotinin, 1mM AESBF) with a combination of lysozyme (1 mg/mL) and sonication (3x5min). Lysate was cleared with SmDNase and centrifugation. Cleared lysate was incubated with glutathione sepharose 4 FF (1.5 mL bed volume/L culture, Cytiva) for two hours. Beads were washed (lysis buffer) and protein eluted by cleaving off the tags using His-3C-protease (lysis buffer + 17 U/mL His-3C (homemade)). Eluate was dialyzed for 2 hours (3500 MWCO, G2 cassette, Slide-a-Lyzer™, Thermo Scientific) with dialysis buffer (20 mM Tris pH 7.5, 100 mM NaCl, 0.5 mM EDTA, 10% glycerol, 1 mM DTT, 0.1 mM PMSF). Nap1 was further purified using MonoQ column (Cytiva) using a 20 CV gradient from 0.1 M to 1 M NaCl (20 mM Tris-HCl pH 7.5, 100 mM NaCl, 0.5 mM EDTA, 10 % glycerol and 1 mM DTT) and the fractions analyzed by SDS-PAGE and Coomassie staining.

Analytical biochemistry methods

Buffers and solutions

HU buffer	8 M	urea
	5%	SDS
	200 mM	Tris-HCl pH 6.8
	1.5%	DTT
	traces	bromophenol blue
MOPS buffer	50 mM	MOPS
	50 mM	Tris base
	0.1%	SDS
	1 mM	EDTA pH 8.0
	adjust to pH 7.7	
MES buffer	50 mM	MES
	50 mM	Tris base
	0.1%	SDS
	1 mM	EDTA pH 8.0
SDS buffer	25 mM	Tris base
	192 mM	glycine
	0.1%	SDS

transfer buffer	48 mM	Tris base
	39 mM	glycine
	0.0375%	SDS
	20%	methanol
superblotto	2.5%	skim milk powder in TBS
	0.5%	bovine serum albumin
	0.5%	Nonidet™ P-40 substitute (Sigma)
	0.1%	Tween-20
western wash buffer	0.2%	Nonidet™ P-40 substitute in TBS
PBS	10 mM	phosphate buffer pH 7.4
	137 mM	sodium chloride
	2.7 mM	potassium chloride
inhibitors	2 mM	sodium fluoride
	2 mM	β-glycerophosphate
	1 mM	DTT
	1 x	cOmplete protease inhibitor cocktail EDTA-free (Roche) (1 tablet per 50 mL buffer)
2x Laemmli	160 mM	Tris-HCl pH 6.8
	20%	glycerol
	7%	SDS
	500 mM	β-mercaptoethanol
	traces	bromophenol blue
RB-high	10 mM	HEPES KOH pH 7.6
	1 mM	EDTA
	2 M	NaCl
	1 mM	DTT
RB-low:	10 mM	HEPES KOH pH 7.6
	1 mM	EDTA
	100 mM	NaCl
	1 mM	DTT

TCA precipitation

Yeast cells (1 OD₆₀₀ = ~2 x 10⁷ cells) were harvested by centrifugation (1 min max speed) and supernatant was removed. Pellets were resuspended in 1 mL cold ddH₂O (on ice), then 150 μL cold TCA precipitation buffer (1.85 M NaOH, 7.5% β-mercaptoethanol) was added, the reaction mixed by inverting 3 times and incubated on ice for 15 min. 150 μL cold TCA (55%) was added, the reaction mixed by inverting 3 times and incubated on ice for 10 minutes. Then reactions were centrifuged (2 min,

full speed) and the supernatant discarded. The procedure was repeated once to remove traces of TCA from the sample. Samples were then resuspended in 50 μ L HU buffer (8 M Urea, 5% (w/v) SDS, 200 mM Tris (pH 6.8), 1.5 % DTT, traces bromophenol blue) by shaking at 65°C, 1400 rpm, before analyzing via SDS-PAGE and/or Western blot.

SDS-PAGE

NuPAGE™ Bis-Tris 4-12% gradient gels (Invitrogen) were used according to the manufacturer's instructions. In brief, gels were run with either 1x MOPS buffer (for larger proteins like Fun30) at 200V for 45 minutes or 1x MES buffer (for smaller proteins like histones) at 200V for 30 minutes.

Alternatively, 10% or 17% SDS-gels were prepared using the BioRad mini gel system with 0.75mm spacers: In brief, the respective separating gel mix was filled to approximately 80% of the gel, covered with a layer of 2-propanol until polymerized, then 2-propanol was discarded and stacking gel was filled on top with a 15-fold comb. For the gel mixtures see the following tables 8 and 9:

Table 8: Separating gel for 4 BioRad mini gels with 0.75mm spacers.

Reagent	10%	17%
40% acrylamide	5 mL	8.4 mL
2% bis-acrylamide	1.32 mL	0.72 mL
1.5 M Tris HCl pH 8.8	5 mL	5 mL
10% SDS	200 μ L	200 μ L
H ₂ O	8.7 mL	5.72 mL
TEMED	25 μ L	25 μ L
10% APS	100 μ L	100 μ L

Table 9: Stacking gel for 4 BioRad mini gels with 0.75mm spacers.

Reagent	-
40% acrylamide	640 μ L
2% bis-acrylamide	350 μ L
1.0 M Tris HCl pH 6.8	625 μ L
10% SDS	50 μ L
H ₂ O	3.35 mL
TEMED	20 μ L
10% APS	40 μ L

These gels were run at 180V for 60 min in 1x SDS running buffer (3g/L Tris, 14.4g/L glycine, 1g/L SDS).

Coomassie staining

For Coomassie staining the GelCode™ Blue reagent (*Thermo Fisher Scientific*, 24590) was used according to manufacturer's instructions. In brief, gels were fixed (50% methanol, 7% acetic acid) for 15 minutes, rehydrated in dH₂O (2x 15 minutes), stained for one hour with GelCode™ Blue and destained in dH₂O overnight.

Silver staining

Silver staining was conducted using solutions and steps listed below. Gels were fixed for 10 min and re-hydrated with ddH₂O for 10 min. Sensitizing was conducted for 1 min and gels were rinsed with ddH₂O twice for 20 sec. Gels were stained in the dark for 10 min, rinsed with ddH₂O and developing was conducted until bands were clearly visible, before developing solution was exchanged with stop solution.

<u>solution</u>	<u>concentration</u>	<u>chemical</u>
Fixing	40%	methanol
	5%	formaldehyde
Sensitizing	0.02%	Na ₂ S ₂ O ₃
Staining	0.1%	AgNO ₃
Developing	3%	Na ₂ CO ₃
	0.0185%	formaldehyde
	0.000016%	Na ₂ S ₂ O ₃
Stop	50%	ethanol
	15%	acetic acid

<u>step</u>	<u>duration</u>
Soaking in fixing solution	10 min
2x washing with water	2x 5 min
Rinsing with sensitizing solution	1 min
2x washing with water	2x 20 s
Soaking in staining solution (dark)	10 min
Rinsing in water and developing solution	---
Soaking in developing solution	1-5 min
Soaking in stop solution	10-inf

Western blotting & development

Western blotting uses the transfer of proteins separated by gel electrophoresis onto a membrane and probing for the presence of targets with specific antibodies.

Membrane transfer after electrophoresis was conducted via wet blotting (Hoefer Tank) in transfer buffer (48 mM Tris, 39 mM glycine, 20% methanol, 0.0375% v/v SDS) onto an AmershamTM ProtranTM nitrocellulose blotting membrane (GE Healthcare) for 90 minutes at 90 V, 400 mA at 4°C.

Antibodies were diluted in a blocking buffer, consisting of 2.5% milk, 0.5% BSA (*Sigma*, 05479), 0.5% Nonidet™ P 40 substitute and 0.1% Tween 20 in TBS.

Mouse anti-FLAG HRP (M2, directly coupled, *Sigma*, A8592) was used in a working concentration of 1:5000.

Rabbit anti-H3 primary antibody (*Abcam*, ab1791) was used in a working concentration of 1:5000. As secondary antibody goat anti-rabbit HRP (*Jackson Immuno Research*, 111-035-045) was used in 1:5000 working concentration.

The membrane was incubated with 5 mL of primary antibody dilution overnight at 4°C. Western wash buffer was buffer. The membrane was washed three times with wash buffer (0.2% Nonidet™ P 40 substitute in TBS) for 5 min at room temperature followed by incubation with 5 mL of secondary antibody solution for 2.5 h at room temperature. The membrane was washed three times with wash buffer again before signal detection was done with the Pierce™ ECL Western Detection Reagents (*Thermo Scientific*, 32106), using 2 mL per reagent per membrane. The results were detected and documented with the *Fujifilm LAS-3000* CCD camera system.

Table 10: Antibodies

Antibody	Host organism	Supplier	Order#	Clone#
anti-RFA	rabbit	Agrisera	AS07-214	polyclonal
anti-H3	rabbit	Abcam	ab1791	polyclonal
anti-rabbit HRP-coupled	goat	Jackson Immuno Research	111-035-045	polyclonal
anti-FLAG HRP-coupled	mouse	Sigma	A8592	Monoclonal, clone M2

Assays

Limited proteolysis

Limited proteolysis uses the characteristic cleavage pattern of folded proteins after limited digestion by proteases to judge protein folding and stability.

Respective proteins were digested with different dilutions of the five proteases chymotrypsin, elastase, Glu C, subtilisin and trypsin (*Promega*), to achieve coverage of different cleavage sites and to analyze patterns. Protein and protease dilutions were made in protease dilution buffer (20 mM HEPES pH 7.5, 50 mM NaCl, 10 mM MgSO₄). 1 µL of diluted protease was added to 600 ng protein in a total volume of 5 µL. For trypsin, chymotrypsin and subtilisin the dilutions used were 0.02 mg/mL, 0.005 mg/mL and 0.001 mg/mL. For GluC and elastase dilutions were 1 mg/mL, 0.1 mg/mL and 0.01 mg/mL. Cleavage occurred during 30 minutes incubation on ice. To stop the reaction 5 µL 2x Laemmli buffer were added. After 5 minutes at 95°C the samples were loaded onto a self-made 10% gel to perform electrophoresis followed by silver staining.

ATPase assay

ATPase activity of Fun30 WT and mutants was analyzed using an absorbance-based (A₃₄₀) assay: An ATP regeneration system (phosphoenolpyruvate, lactate dehydrogenase/pyruvate kinase) replenishes any ATP that is hydrolyzed to ADP + P_i, oxidizing one molecule of NADH per regenerated molecule ATP. NAD⁺ absorbance spectrum is shifted compared to NADH, so the decrease of absorbance at 340nm (NADH) can be used to calculate the oxidation of NADH and thus the hydrolysis of ATP. Measurements were performed at a *Tecan* infinite M200 Pro plate reader using the *i-control v2.0* software in transparent 384-well plates (Greiner BioOne, 781186).

For the assay, DNA stimulus (below), NADH (Sigma, N8129), ATP regeneration system and enzyme (final concentration 100 nM) were mixed in reaction buffer (below) inside a 384-well plate with a total volume of 30 μ L per well. Reactions were spun down. ATP (Thermo Scientific, R1441) was added with equimolar MgCl₂ (final concentration 1 mM) to start the assay. Before the start the plate was mixed for 30 sec 300 rpm orbital shaking. Operating temperature of the plate reader was 26°C, kinetic A₃₄₀-measurements were taken every 10 sec within a total of 60 min. ATP consumption was measured in form of NADH decrease. Evaluation of the data was performed with Microsoft Excel: A timeframe from 1000-2500 sec (or at least 500 sec with linear decline of the A₃₄₀-curve) was selected to calculate the slope using the SLOPE function of Microsoft Excel. From the slope value, the turnover rate k_{cat} – the number of ATP molecules hydrolyzed per second per remodeler enzyme – was calculated using the law of Lambert-Beer.

Using the extinction coefficient of NADH 6220 M⁻¹ cm⁻¹ and the pathlength 0.272727 cm for a volume of 30 μ L in one well of the 384-well plate: First the reaction speed (v_{max}) was calculated using the equation $v_{max} = \text{slope} / (6220 \text{ M}^{-1} \text{ cm}^{-1} \times 0.272727 \text{ cm})$. Then turnover rate k_{cat} [s⁻¹] was calculated by dividing v_{max} by the protein concentration used in the assay (10⁻⁷ M) and correcting by the actual concentration used in the assay obtained from quantification of the input into the ATPase assay from a Coomassie-stained gel with BSA protein standard as described below in “Quantification of protein concentration”.

To find out the best stimulus for Fun30 ATPase activity a plethora of constructs were tested: Herring sperm DNA (Invitrogen, 15634-017), the M13 phage plasmid (NEB) and ss and dsDNA fragments were used as stimuli.

component	concentration in assay
DNA stimulus	40-1000 ng/ μ L
Enzyme	100 nM
MgCl ₂	3 mM
NADH	1.5 mM
ATP/MgCl ₂	1 mM
ATP regeneration system:	
Phosphoenolpyruvate (Roche, 10108294001)	3 mM
Lactate dehydrogenase/pyruvate kinase (Sigma, P0294)	15.5 U/mL
β -mercaptoethanol	10 mM

DNA stimuli:

Herring sperm DNA (Invitrogen, 15634-017)

ssDNA

BP5196 (120 nt):

5'CACCTGTTGTAATCGTCTAGAATGGATTATAAAGATGACGATGACAAGGATTATAAAGATGACGATGACAAGGATTATAAAGATGACGATGACAAGATCGAGCTCGAATTCATCGATGAT3'

M13 ssDNA plasmid (7249 nt)

dsDNA

100W0 DNA (247 bp)

25x 601 array DNA 20(W50)₂₅20 from pTB127 (4920 bp)

Quantification of protein concentration

A serial dilution of bovine serum albumin (BSA) in ddH₂O was created and BSA standards were analyzed alongside protein samples via SDS PAGE and Coomassie staining. Intensities of bands were measured using the Fiji-distribution of ImageJ (Schindelin et al., 2012; Schneider et al., 2012). In the FIJI software intensity plots for the entire lane (rectangular selection for control lane, all subsequent lanes selected with identical rectangle) were made and the peaks corresponding to the respective bands selected for retrieving the integral/area under the curve. The values were evaluated in Microsoft Excel by generating a linear regression of BSA standard concentrations and calculating the sample concentration using the linear regression equation. Nucleosome concentration after assembly was estimated using a free DNA control on the gel and calculating the volume of the reaction after dialysis and the amount of free DNA left inside.

***In vitro* nucleosome Co-IP**

Co-IP experiments perform an immunoprecipitation experiment using one protein as bait that is pulled down and looking for another protein as prey, to see interaction between the two proteins.

For Co-IP experiments, Fun30 constructs with still intact 6xHis-GST-tag or a tag-only construct as bait protein (final conc. 360 nM) was mixed with H2A-46C-D550 labeled nucleosome (60 nM) in a total volume of 30 μ L pulldown buffer (50 mM HEPES/KOH pH 7.6, 1 mM EDTA, 150 mM NaCl, 0.1% Tween-20, 10% glycerol, 1 mM DTT, 10 μ g/mL leupeptin, 1 μ g/mL pepstatinA, 1mM PMSF) and incubated for 30 min on ice. Equilibrated glutathione Sepharose 4 FF (5 μ L bed volume) was added and incubated for 2h at 4°C with rotation.

Supernatant was removed (25 μ L) and mixed with 25 μ L of 2x Laemmli. Beads were washed 3x with 400 μ L buffer. Beads were mixed with equal volume of 2x Laemmli and boiled at 95°C for 5 min. Equal amounts of supernatant and pulldown were loaded on gels and analyzed with fluorescence imaging (Typhoon FLA 9000, GE, in the Cy3-channel for labeled histone H2A) and with Western blot (against histone H3).

Native PAGE based assays

Native polyacrylamide gel electrophoresis is an electrophoresis method that does not denature proteins before separating them through the gel matrix. This can be used to detect binding between two proteins/protein and DNA or changes in protein/macromolecule shape that change its running properties.

Native PAGE gels and gel electrophoresis

To analyze gelshifts with 100W0 DNA or 100W0 nucleosomes, 5% native gels were prepared according to the list below. Gels were poured without stacking gel, polymerized for 30 min at RT, then submerged in 0.2xTBE at 4°C overnight.

Reagent	Volume for 1 native gel (BioRad mini gel, 1.5 mm spacers)
30% acrylamide-bisacrylamide mix (59:1)	1.67 mL
10x TBE	200 μ L
H ₂ O	8.1 mL
TEMED	10 μ L
10% APS	50 μ L

Native gels were pre-run without samples for 90 min and thereafter run with samples at 4°C in 0.2x TBE at 180V for 90 minutes before imaging fluorescent labels and/or staining with ethidium bromide (1:10 000 in H₂O).

DNA & nucleosome binding assay

Unless indicated otherwise, all steps were performed on ice or at 4°C.

For DNA binding, 100W0 DNA substrate was used.

For nucleosome binding, 100W0 nucleosomes were used.

DNA/nucleosomes were diluted (final concentration 100 nM) and mixed in reaction buffer (15 mM HEPES pH 7.6, 100 mM KOAc, 2 mM MgCl₂, 75 μ g/mL BSA, 1 mM DTT). Lastly, respective amount of Fun30 protein was added to a total sample volume of 10 or 15 μ L and the reaction incubated for 30 min at 30°C.

To check for reversibility, 1 μ g herring sperm DNA was added thereafter and incubation continued for additional 5 min.

5% native gels were pre-run in cold 0.2x TBE buffer for 90 min at 180 V, 400 mA prior to preparing the gel shift samples. Samples were mixed with native loading buffer (final conc. 5% sucrose, traces bromophenol blue) before loading and gels were run with 0.2x TBE at 180 V for 90 min. Fluorescence (labeled histone) was imaged by Typhoon Imager (FLA 9000, GE, Cy3 channel), afterwards the gel was stained with ethidium bromide (1:10 000 solution, 10 min) and the DNA was imaged.

Nucleosome sliding assay

Unless specified all steps are performed on ice.

10 μ L reaction volume containing 100 nM 100W0 mononucleosomes with labelled histones (*H2A 46-C-D550 and H4 64-C-D550*), respective amount of remodeler (5 nM, 25 nM and 100 nM in titrations) in reaction buffer (15 mM HEPES pH 7.6, 100 mM KOAc, 2 mM MgCl₂, 75 μ g/mL BSA, 1 mM DTT) is mixed. The reaction is started by addition of ATP/Mg mix (1 mM final) and eviction is performed for 120 min at 30°C, 300 rpm. Then 1 μ g of herring sperm DNA is added to chelate the remodeler for 5 minutes at 30°C. The resulting gelshifts are analyzed by native gel electrophoresis.

5% native gels were pre-run in cold 0.2x TBE buffer for 90 min at 180 V, 400 mA prior to loading the samples. Samples were mixed with native loading buffer (final conc. 5% sucrose, traces bromophenol blue) before loading and gels were run with 0.2x TBE at 180 V for 90 min. Fluorescence (labeled histone) was imaged by Typhoon Imager (FLA 9000, GE, Cy3 channel), afterwards the gel was stained with ethidium bromide (1:10 000 solution, 10 min) and the DNA was imaged.

Nap1-assisted nucleosome eviction assay

Unless specified all steps were performed on ice. 10 μ L reaction volume containing 100 nM 100W0 mononucleosomes with labelled histones (*H2A 46-C-D550 and H4 64-C-D550*), respective amount of remodeler (5 nM, 25 nM and 100 nM in titrations) and excess Nap1 (5 μ M) were mixed in reaction

buffer (15 mM HEPES pH 7.6, 100 mM KOAc, 2 mM MgCl₂, 75 µg/mL BSA, 1 mM DTT). The reaction was started by addition of ATP/Mg mix (1 mM final) and eviction was performed for 120 min at 30°C, 300 rpm. Then 1 µg of herring sperm DNA was added to chelate the remodeler for 5 minutes at 30°C. The resulting gelshifts were analyzed by native gel electrophoresis. 5% native gels were pre-run in cold 0.2x TBE buffer for 90 min at 180 V, 400 mA prior to loading the samples. Samples were mixed with native loading buffer (final conc. 5% sucrose, traces bromophenol blue) before loading and gels were run with 0.2x TBE at 180 V for 90 min. Fluorescence (labeled histone) was imaged by Typhoon Imager (FLA 9000, GE, Cy3 channel), afterwards the gel was stained with ethidium bromide (1:10 000 solution, 10 min) and the DNA was imaged.

Biophysical methods

NanoDSF

NanoDSF (differential scanning fluorometry) uses tryptophan fluorescence to monitor protein unfolding. Fluorescence intensity and the fluorescence maximum both depend on the close surroundings of the tryptophan (Lakowicz, 2006).

Therefore, changes in protein structure during unfolding can be detected by monitoring the ratio of the fluorescence intensities at 350 nm and 330 nm during application of a temperature gradient to small volumes of protein sample in glass capillaries.

Protein samples were diluted to a concentration of 0.1-0.2 mg/mL and triplicate measurements in glass capillaries (Prometheus™ NT.48 Capillaries, Nanotemper Technologies, PR-C002) were performed on a Prometheus NT.48 (Nanotemper Technologies) over a temperature gradient from 20-90°C with a rate of +1°C/min. Results were evaluated with the PR.ThermControl software (v2.1.2).

Mass photometry

Mass photometry enables accurate determination of molecule mass of single molecules in solution without the need for labels. It is based on the principles of interference reflection microscopy (Verschueren, 1985) and interferometric scattering microscopy (Ortega-Arroyo and Kukura, 2012). Controlled illumination, a novel spatial-filtering strategy in the detection beam path as well as careful image analysis (Cole et al., 2017) can be used to detect the minute amount of light scattered by single molecules during binding to a glass surface and this light scattering correlates directly with the molecular mass (Young et al., 2018).

Mass photometry was performed on a Model Number One^{MP} (Refeyn) and analysis with the software Discover^{MP} (v2.5.0). A CultureWell™ gasket (Grace Bio-Labs, 103250) was attached to a clean glass coverslip by applying gentle pressure. 19 µL of buffer were put in one well, then the focus was adjusted before addition of 1 µL of 1 µM protein (fractions after gelfiltration, final protein concentration 50 nM). The solution was mixed and a video of surface binding events was acquired for 60 sec. To determine molecular weight of the measured molecules, the datasets were compared to a mass calibration made by the facility in the software using NativeMark Unstained Protein Standard (ThermoFisher, LC0725) and assigning the observed peaks to the molecular weights 1048, 720, 480, 242, 146 and 66 kDa.

Cross-linking mass spectrometry

Cross-linking mass spectrometry (XL-MS) allows identification of structural regions of close proximity on amino acid level. Protein samples are combined with crosslinking reagents that form covalent bonds

(crosslinks). Upon protein digestion the resulting crosslinked peptide pairs can be identified by tandem mass spectrometry.

For crosslinking, BS3, a lysine-specific crosslinker was used. 20 µg of Fun30 protein was crosslinked with 100x molar excess of BS3 for 30 min at 25°C, 300 rpm before stopping the reaction by adding Tris pH 7.5 (final concentration 100 mM) and mixing for 15 min at 25°C, 300 rpm. The crosslinked peptides were handed over to the XL-MS core facility for digestion, mass spectrometry and data processing.

For the mass spectrometry, crosslinked proteins were diluted 1:1 with digestion buffer (8 M Urea, 40 mM CAA, 10 mM TCEP, 50 mM Tris) and incubated for 20 min at 37 °C followed by a 1:4 dilution with water. Crosslinked proteins were digested overnight at 37 °C by addition of 0.5 µg of LysC and 1 µg of trypsin (Promega). The digestion was stopped by addition of 1% of TFA followed by desalting of the peptides using Sep-Pak C18 1cc vacuum cartridges (Waters). Desalted peptides were vacuum-dried. Vacuum-dried peptides were dissolved at a concentration of 100 ng/µL in buffer A (0.1% formic acid). Peptides (100 ng) were separated and measured at a flow rate of 250 nL/min using the Thermo Easy-nLC 1200 (Thermo Fisher Scientific) coupled to the Orbitrap Exploris 480 mass spectrometer (Thermo Fisher Scientific). Peptides were separated on a 30-cm analytical column (inner diameter: 75 microns; packed in-house with ReproSil-Pur C18-AQ 1.9-micron beads, Dr. Maisch GmbH) using an increasing percentage of buffer B (80% acetonitrile, 0.1% formic acid). A linear gradient from 5% to 30% buffer B over 40 minutes, to 95% B over 10 minutes was used, and elution strength was held at 95% B for 5 minutes. The mass spectrometer was operated in data-dependent mode with survey scans from m/z 300 to 1650 Th (resolution of 60k at $m/z = 200$ Th). Up to 15 of the most abundant precursors were selected and fragmented using stepped Higher-energy C-trap Dissociation (HCD with a normalized collision energy of value of 19, 27, 35). The MS2 spectra were recorded with a dynamic m/z range (resolution of 30k at $m/z = 200$ Th). AGC target for MS1 and MS2 scans were set to 3×10^6 and 105, respectively, within a maximum injection time of 100 and 60 ms for the MS1 and MS2 scans. Charge state 2 was excluded from fragmentation.

The acquired raw data was processed using Proteome Discoverer (version 2.5.0.400, Thermo Fisher) with the XlinkX/PD nodes integrated. “NonCleavable” was set as acquisition strategy. The database search was performed against a FASTA containing the sequence(s) of the protein(s) under investigation as well as a contaminant database. DSS/BS3 was set as a crosslinker, Cysteine carbamidomethylation was set as fixed modification and methionine oxidation and protein N-term acetylation were set as dynamic modifications. Trypsin/P was specified as protease and up to two missed cleavages were allowed. Identifications were accepted with a minimal score of 40 and a minimal delta score of 4. Filtering at 1% false discovery rate (FDR) at peptide level was applied by the XlinkX Validator node with setting simple.

***In silico* methods**

AlphaFold2 prediction

The respective protein sequences were submitted to AlphaFold2 (Jumper et al., 2021) either fully for Fun30 (1-1131), Fun30ΔSAM (1-968), SMARCAD1 (1-1026) or only regions of interest as for the Fun30 SAM-key region (275-436) and the SMARCAD1 SAM-key region (203-488). The *in trans* complementation scenario was modelled using the AlphaFold2 multimer algorithm, providing the respective constructs Fun30ΔSAM and SAM-key as separate polypeptide chains. Models were visualized using UCSF ChimeraX (Pettersen et al., 2021).

Structural alignment of Fun30 AlphaFold2 model with nucleosome-remodeler co-structures

An AlphaFold2 (Jumper et al., 2021) model of *S. cerevisiae* Fun30 was obtained from the AlphaFold Protein Structure Database (Varadi et al., 2022). Extended regions with a low confidence score were rejected (residues 1-275, 410-560, 1126-1131). Structures were visualized and superimposed using UCSF ChimeraX (Pettersen et al., 2021).

For docking of the Fun30 model at the dyad, the nucleosomal DNA at SHL 2 of the RSC bound nucleosome structure (PDB: 6TDA) was manually aligned with the dyad of a nucleosome core particle (PDB: 7OHC). Subsequently, the DNA of the RSC-bound nucleosome (PDB: 6TDA) and the nucleosome core particle (PDB: 7OHC) were fit into the cryo-EM map of the nucleosome core particle (EMD-12900), resulting in an improved alignment of SHL 2 of PDB: 6TDA with the dyad of PDB: 7OHC. The Fun30 AlphaFold model was aligned with the Sth1 ATPase (PDB: 6TDA) and the Fun30 model was visualized together with the nucleosome core particle (PDB: 7OHC).

For docking of the Fun30 model at SHL 2, the Fun30 AlphaFold model was superimposed with the Sth1 ATPase (PDB: 6TDA) by alignment of the ATPase N-lobes (Fun30 residues 561-802). The Fun30 model was visualized together with the nucleosome (PDB: 6TDA).

For comparison of the Fun30 model with Ino80 bound at SHL -6, a nucleosome bound INO80 model was generated based on PDB: 8AV6 and EMD-15211. In brief, the structure of a nucleosome-bound INO80 complex (PDB: 8AV6) was fitted into the low-resolution cryo-EM map of INO80 bound to a nucleosome and extranucleosomal DNA (EMD-15211) (Kunert et al., *in press*). The model was extended by fitting of extranucleosomal DNA as well as the post-HSA/HSA helix into the low-resolution cryo-EM map. For docking of the Fun30 model at SHL -6, the Fun30 AlphaFold model was superimposed with the Ino80 ATPase (Model based on PDB: 8AV6 and EMD-15211) by alignment of the ATPase N-lobes (Fun30 residues 561-802). The Fun30 model was visualized together with the nucleosome.

Visualization of XL-MS data

Experimentally obtained crosslinks were visualized onto a 2D representation of the protein using xiNet (Combe et al., 2015) or onto the 3D model (AlphaFold) using PyMol v2.5.2 (DeLano, 2000) with the plugin PyXlinkViewer (Schiffrin et al., 2020).

For the 3D-mapping of the crosslinks onto the model, likely mobile regions without predicted secondary structure (± 2 residues) were excluded. The threshold for BS3-crosslinks was set to 35Å, allowing some flexibility taking into account that AlphaFold models may reflect an in-between situation of nucleotide-bound and apo-state of the enzyme.

References

- Abbott, D. W., Ivanova, V. S., Wang, X., Bonner, W. M., and Ausió, J. (2001). Characterization of the Stability and Folding of H2A.Z Chromatin Particles. *Journal of Biological Chemistry* 276, 41945–41949. doi:10.1074/jbc.M108217200.
- Adkins, N. L., Niu, H., Sung, P., and Peterson, C. L. (2013). NUCLEOSOME DYNAMICS REGULATE DNA PROCESSING. *Nat Struct Mol Biol* 20, 836–842. doi:10.1038/nsmb.2585.
- Adkins, N. L., Swygert, S. G., Kaur, P., Niu, H., Grigoryev, S. A., Sung, P., et al. (2017). Nucleosome-like, Single-stranded DNA (ssDNA)-Histone Octamer Complexes and the Implication for DNA Double Strand Break Repair*. *The Journal of biological chemistry* 292, 5271–5281. doi:10.1074/jbc.m117.776369.
- Ait-Saada, A., Khorosjutina, O., Chen, J., Kramarz, K., Maksimov, V., Svensson, J. P., et al. (2019). Chromatin remodeler Fft3 plays a dual role at blocked DNA replication forks. *Life Sci Alliance* 2. doi:10.26508/lsa.201900433.
- Alberts, B., Johnson, A., Lewis, J., Raff, M., Roberts, K., and Walter, P. (2002). *Molecular Biology of the Cell*. 4 ed. New York: Garland Science.
- ALLFREY, V. G., FAULKNER, R., and MIRSKY, A. E. (1964). ACETYLATION AND METHYLATION OF HISTONES AND THEIR POSSIBLE ROLE IN THE REGULATION OF RNA SYNTHESIS. *Proceedings of the National Academy of Sciences of the United States of America* 51, 786–794. doi:10.1073/pnas.51.5.786.
- Altschul, S. F., Gish, W., Miller, W., Myers, E. W., and Lipman, D. J. (1990). Basic local alignment search tool. *Journal of molecular biology* 215, 403–410. doi:10.1016/S0022-2836(05)80360-2.
- Andrews, A. J., and Luger, K. (2011). Nucleosome structure(s) and stability: variations on a theme. *Annu Rev Biophys* 40, 99–117. doi:10.1146/annurev-biophys-042910-155329.
- Angus-Hill, M. L., Schlichter, A., Roberts, D., Erdjument-Bromage, H., Tempst, P., and Cairns, B. R. (2001). A Rsc3/Rsc30 zinc cluster dimer reveals novel roles for the chromatin remodeler RSC in gene expression and cell cycle control. *Molecular Cell* 7, 741–751. doi:10.1016/s1097-2765(01)00219-2.
- Annunziato, A. (2008). DNA Packaging: Nucleosomes and Chromatin. *Nature Education* 1, 26. Available at: <https://www.nature.com/scitable/topicpage/dna-packaging-nucleosomes-and-chromatin-310/>.
- Arya, R., and Bassing, C. H. (2017). V(D)J Recombination Exploits DNA Damage Responses to Promote Immunity. *Trends in genetics : TIG* 33, 479–489. doi:10.1016/j.tig.2017.04.006.
- Awad, S., Ryan, D., Prochasson, P., Owen-Hughes, T., and Hassan, A. H. (2010). The Snf2 homolog Fun30 acts as a homodimeric ATP-dependent chromatin-remodeling enzyme. *Journal of Biological Chemistry* 285, 9477–9484. doi:10.1074/jbc.M109.082149.
- Aylon, Y., and Kupiec, M. (2004). DSB repair: the yeast paradigm. *DNA Repair* 3, 797–815. doi:10.1016/j.dnarep.2004.04.013.
- Badis, G., Chan, E. T., van Bakel, H., Pena-Castillo, L., Tillo, D., Tsui, K., et al. (2008). A library of yeast transcription factor motifs reveals a widespread function for Rsc3 in targeting nucleosome exclusion at promoters. *Molecular Cell* 32, 878–887. doi:10.1016/j.molcel.2008.11.020.

- Baker, K. M., Wei, G., Schaffner, A. E., and Ostrowski, M. C. (2003). Ets-2 and components of mammalian SWI/SNF form a repressor complex that negatively regulates the BRCA1 promoter. *The Journal of biological chemistry* 278, 17876–17884. doi:10.1074/jbc.M209480200.
- Baker, R. W., Reimer, J. M., Carman, P. J., Turegun, B., Arakawa, T., Dominguez, R., et al. (2021). Structural insights into assembly and function of the RSC chromatin remodeling complex. *Nat Struct Mol Biol* 28, 71–80. doi:10.1038/s41594-020-00528-8.
- Bannister, A. J., and Kouzarides, T. (2011). Regulation of chromatin by histone modifications. *Cell Res* 21, 381–395. doi:10.1038/cr.2011.22.
- Bantele, S. C. S., and Pfander, B. (2019). Nucleosome Remodeling by Fun30SMARCAD1 in the DNA Damage Response. *Frontiers in Molecular Biosciences* 6. doi:10.3389/fmolb.2019.00078.
- Bantele, S. C. S., Lisby, M., and Pfander, B. (2019). Quantitative sensing and signalling of single-stranded DNA during the DNA damage response. *Nature Communications* 10, 944. doi:10.1038/s41467-019-08889-5.
- Bantele, S. C., Ferreira, P., Gritenaite, D., Boos, D., and Pfander, B. (2017). Targeting of the Fun30 nucleosome remodeller by the Dpb11 scaffold facilitates cell cycle-regulated DNA end resection. *eLife Sciences* 6, 836.
- Barrera, F. N., Poveda, J. A., González-Ros, J. M., and Neira, J. L. (2003). Binding of the C-terminal sterile alpha motif (SAM) domain of human p73 to lipid membranes. *The Journal of biological chemistry* 278, 46878–46885. doi:10.1074/jbc.M307846200.
- Becker, P. B., and Workman, J. L. (2013). Nucleosome remodeling and epigenetics. *Cold Spring Harbor Perspectives in Biology* 5, a017905. doi:10.1101/cshperspect.a017905.
- Bennett, G., and Peterson, C. L. (2015). SWI/SNF recruitment to a DNA double-strand break by the NuA4 and Gcn5 histone acetyltransferases. *DNA Repair* 30, 38–45. doi:10.1016/j.dnarep.2015.03.006.
- Bennett, G., Papamichos-Chronakis, M., and Peterson, C. L. (2013). DNA repair choice defines a common pathway for recruitment of chromatin regulators. *Nature Communications* 4, 2084–2010.
- Boyer, L. A., Logie, C., Bonte, E., Becker, P. B., Wade, P. A., Wolffe, A. P., et al. (2000). Functional delineation of three groups of the ATP-dependent family of chromatin remodeling enzymes. *The Journal of biological chemistry* 275, 18864–18870. doi:10.1074/jbc.M002810200.
- Brahma, S., Udugama, M. I., Kim, J., Hada, A., Bhardwaj, S. K., Hailu, S. G., et al. (2017). INO80 exchanges H2A.Z for H2A by translocating on DNA proximal to histone dimers. *Nature Communications* 8, 15616. doi:10.1038/ncomms15616.
- Bunting, S. F., and Nussenzweig, A. (2013). End-joining, translocations and cancer. *Nat Rev Cancer* 13, 443–454. doi:10.1038/nrc3537.
- Byeon, B., Wang, W., Barski, A., Ranallo, R. T., Bao, K., Schones, D. E., et al. (2013). The ATP-dependent chromatin remodeling enzyme Fun30 represses transcription by sliding promoter-proximal nucleosomes. *The Journal of biological chemistry* 288, 23182–23193. doi:10.1074/jbc.M113.471979.

- Cadet, J., and Wagner, J. R. (2013). DNA base damage by reactive oxygen species, oxidizing agents, and UV radiation. *Cold Spring Harbor Perspectives in Biology* 5, a012559. doi:10.1101/cshperspect.a012559.
- Cejka, P., and Symington, L. S. (2021). DNA End Resection: Mechanism and Control. *Annu Rev Genet* 55, 285–307. doi:10.1146/annurev-genet-071719-020312.
- Chai, B., Huang, J., Cairns, B. R., and Laurent, B. C. (2005). Distinct roles for the RSC and Swi/Snf ATP-dependent chromatin remodelers in DNA double-strand break repair. *Genes Dev* 19, 1656–1661. doi:10.1101/gad.1273105.
- Chen, X., Cui, D., Papusha, A., Zhang, X., Chu, C.-D., Tang, J., et al. (2012). The Fun30 nucleosome remodeler promotes resection of DNA double-strand break ends. *Nature* 489, 576–580.
- Chen, X., Niu, H., Yu, Y., Wang, J., Zhu, S., Zhou, J., et al. (2016). Enrichment of Cdk1-cyclins at DNA double-strand breaks stimulates Fun30 phosphorylation and DNA end resection. *Nucleic Acids Research* 44, 2742–2753.
- Cheng, X., Côté, V., and Côté, J. (2021). NuA4 and SAGA acetyltransferase complexes cooperate for repair of DNA breaks by homologous recombination. *PLoS Genet* 17, e1009459. doi:10.1371/journal.pgen.1009459.
- Clapier, C. R., and Cairns, B. R. (2009). The biology of chromatin remodeling complexes. *Annu Rev Biochem* 78, 273–304.
- Clapier, C. R., Chakravarthy, S., Petosa, C., Fernández-Tornero, C., Luger, K., and Müller, C. W. (2008). Structure of the Drosophila nucleosome core particle highlights evolutionary constraints on the H2A-H2B histone dimer. *Proteins* 71, 1–7. doi:10.1002/prot.21720.
- Clapier, C. R., Iwasa, J., Cairns, B. R., and Peterson, C. L. (2017). Mechanisms of action and regulation of ATP-dependent chromatin-remodelling complexes. *Nature Reviews Molecular Cell Biology* 18, 407–422. doi:10.1038/nrm.2017.26.
- Clapier, C. R., Kasten, M. M., Parnell, T. J., Viswanathan, R., Szerlong, H., Sirinakis, G., et al. (2016). Regulation of DNA Translocation Efficiency within the Chromatin Remodeler RSC/Sth1 Potentiates Nucleosome Sliding and Ejection. *Molecular Cell* 62, 453–461. doi:10.1016/j.molcel.2016.03.032.
- Clapier, C. R., Verma, N., Parnell, T. J., and Cairns, B. R. (2020). Cancer-Associated Gain-of-Function Mutations Activate a SWI/SNF-Family Regulatory Hub. *Molecular Cell* 80, 712–725.e5. doi:10.1016/j.molcel.2020.09.024.
- Cole, D., Young, G., Weigel, A., Sebesta, A., and Kukura, P. (2017). Label-Free Single-Molecule Imaging with Numerical-Aperture-Shaped Interferometric Scattering Microscopy. *ACS Photonics* 4, 211–216. doi:10.1021/acsp Photonics.6b00912.
- Combe, C. W., Fischer, L., and Rappsilber, J. (2015). xiNET: cross-link network maps with residue resolution. *Mol Cell Proteomics* 14, 1137–1147. doi:10.1074/mcp.O114.042259.
- Costelloe, T., Louge, R., Tomimatsu, N., Mukherjee, B., Martini, E., Khadaroo, B., et al. (2012). The yeast Fun30 and human SMARCD1 chromatin remodelers promote DNA end resection. *Nature* 489, 581–584.

- Dao, H. T., and Pham, L. T. D. (2022). Acidic patch histone mutations and their effects on nucleosome remodeling. *Biochem Soc Trans* 50, 907–919. doi:10.1042/BST20210773.
- DeLano, W. L. The PyMOL Molecular Graphics System. V2.5.2 Schrödinger, LLC.
- Densham, R. M., Garvin, A. J., Stone, H. R., Strachan, J., Baldock, R. A., Daza-Martin, M., et al. (2016). Human BRCA1–BARD1 ubiquitin ligase activity counteracts chromatin barriers to DNA resection. *Nat Struct Mol Biol* 23, 647–655. doi:10.1038/nsmb.3236.
- Downs, J. A., Allard, S., Jobin-Robitaille, O., Javaheri, A., Auger, A., Bouchard, N., et al. (2004). Binding of chromatin-modifying activities to phosphorylated histone H2A at DNA damage sites. *Molecular Cell* 16, 979–990.
- Downs, J. A., Lowndes, N. F., and Jackson, S. P. (2000). A role for *Saccharomyces cerevisiae* histone H2A in DNA repair. *Nature* 408, 1001–1004. doi:10.1038/35050000.
- Durand-Dubief, M., Will, W. R., Petrini, E., Theodorou, D., Harris, R. R., Crawford, M. R., et al. (2012). SWI/SNF-like chromatin remodeling factor Fun30 supports point centromere function in *S. cerevisiae*. *PLoS Genet* 8, e1002974. doi:10.1371/journal.pgen.1002974.
- Dyer, P. N., Edayathumangalam, R. S., White, C. L., Bao, Y., Chakravarthy, S., Muthurajan, U. M., et al. (2004). Reconstitution of nucleosome core particles from recombinant histones and DNA. *Methods in enzymology* 375, 23–44. doi:10.1016/s0076-6879(03)75002-2.
- Eapen, V. V., Sugawara, N., Tsabar, M., Wu, W.-H., and Haber, J. E. (2012). The *Saccharomyces cerevisiae* chromatin remodeler Fun30 regulates DNA end resection and checkpoint deactivation. *Molecular and Cellular Biology* 32, 4727–4740.
- Eltsov, M., Maclellan, K. M., Maeshima, K., Frangakis, A. S., and Dubochet, J. (2008). Analysis of cryo-electron microscopy images does not support the existence of 30-nm chromatin fibers in mitotic chromosomes in situ. *Proceedings of the National Academy of Sciences of the United States of America* 105, 19732–19737. doi:10.1073/pnas.0810057105.
- Eustermann, S., Schall, K., Kostrewa, D., Lakomek, K., Strauss, M., Moldt, M., et al. (2018). Structural basis for ATP-dependent chromatin remodelling by the INO80 complex. *Nature* 556, 386–390. doi:10.1038/s41586-018-0029-y.
- Flaus, A., Martin, D. M. A., Barton, G. J., and Owen-Hughes, T. (2006). Identification of multiple distinct Snf2 subfamilies with conserved structural motifs. *Nucleic Acids Research* 34, 2887–2905.
- Forné, I., Ludwigsen, J., Imhof, A., Becker, P. B., and Mueller-Planitz, F. (2012). Probing the conformation of the ISWI ATPase domain with genetically encoded photoreactive crosslinkers and mass spectrometry. *Mol Cell Proteomics* 11, M111.012088. doi:10.1074/mcp.M111.012088.
- Frey, F., Sheahan, T., Finkl, K., Stoehr, G., Mann, M., Benda, C., et al. (2016). Molecular basis of PRC1 targeting to Polycomb response elements by PhoRC. *Genes Dev* 30, 1116–1127. doi:10.1101/gad.279141.116.
- Fussner, E., Ching, R. W., and Bazett-Jones, D. P. (2011). Living without 30nm chromatin fibers. *Trends in biochemical sciences* 36, 1–6. doi:10.1016/j.tibs.2010.09.002.
- Gibbons, R. J., and Higgs, D. R. (2000). Molecular-clinical spectrum of the ATR-X syndrome. *Am J Med Genet* 97, 204–212. doi:10.1002/1096-8628(200023)97:3<204::AID-AJMG1038>3.0.CO;2-X.

- Goellner, E. M., Putnam, C. D., Graham, W. J., Rahal, C. M., Li, B.-Z., and Kolodner, R. D. (2018). Identification of Exo1-Msh2 interaction motifs in DNA mismatch repair and new Msh2-binding partners. *Nat Struct Mol Biol* 25, 650–659. doi:10.1038/s41594-018-0092-y.
- Green, J. B., Gardner, C. D., Wharton, R. P., and Aggarwal, A. K. (2003). RNA recognition via the SAM domain of Smaug. *Molecular Cell* 11, 1537–1548. doi:10.1016/s1097-2765(03)00178-3.
- Greinert, R., Volkmer, B., Henning, S., Breitbart, E. W., Greulich, K. O., Cardoso, M. C., et al. (2012). UVA-induced DNA double-strand breaks result from the repair of clustered oxidative DNA damages. *Nucleic Acids Research* 40, 10263–10273. doi:10.1093/nar/gks824.
- Haber, J. E. (2012). Mating-type genes and MAT switching in *Saccharomyces cerevisiae*. *Genetics* 191, 33–64. doi:10.1534/genetics.111.134577.
- Han, Y., Reyes, A. A., Malik, S., and He, Y. (2020). Cryo-EM structure of SWI/SNF complex bound to a nucleosome. *Nature* 579, 452–455. doi:10.1038/s41586-020-2087-1.
- Hanahan, D. (2022). Hallmarks of Cancer: New Dimensions. *Cancer Discov* 12, 31–46. doi:10.1158/2159-8290.CD-21-1059.
- Hanahan, D., and Weinberg, R. A. (2000). The hallmarks of cancer. *Cell* 100, 57–70. doi:10.1016/s0092-8674(00)81683-9.
- Hanahan, D., and Weinberg, R. A. (2011). Hallmarks of cancer: the next generation. *Cell* 144, 646–674. doi:10.1016/j.cell.2011.02.013.
- Hansen, J. C. (2002). Conformational dynamics of the chromatin fiber in solution: determinants, mechanisms, and functions. *Annu Rev Biophys Biomol Struct* 31, 361–392. doi:10.1146/annurev.biophys.31.101101.140858.
- Hansen, J. C. (2012). Human mitotic chromosome structure: what happened to the 30-nm fibre? *The EMBO Journal* 31, 1621–1623. doi:10.1038/emboj.2012.66.
- Hauk, G., McKnight, J. N., Nodelman, I. M., and Bowman, G. D. (2010). The chromodomains of the Chd1 chromatin remodeler regulate DNA access to the ATPase motor. *Molecular Cell* 39, 711–723. doi:10.1016/j.molcel.2010.08.012.
- He, S., Wu, Z., Tian, Y., Yu, Z., Yu, J., Wang, X., et al. (2020). Structure of nucleosome-bound human BAF complex. *Science (New York, N.Y.)* 367, 875–881. doi:10.1126/science.aaz9761.
- Holm, L. (2022). Dali server: structural unification of protein families. *Nucleic Acids Research*. doi:10.1093/nar/gkac387.
- Inoue, H., Nojima, H., and Okayama, H. (1990). High efficiency transformation of *Escherichia coli* with plasmids. *Gene* 96, 23–28. doi:10.1016/0378-1119(90)90336-p.
- Janke, C., Magiera, M. M., Rathfelder, N., Taxis, C., Reber, S., Maekawa, H., et al. (2004). A versatile toolbox for PCR-based tagging of yeast genes: new fluorescent proteins, more markers and promoter substitution cassettes. *Yeast* 21, 947–962. doi:10.1002/yea.1142.
- Jin, C., and Felsenfeld, G. (2007). Nucleosome stability mediated by histone variants H3.3 and H2A.Z. *Genes Dev* 21, 1519–1529.

- Jumper, J., Evans, R., Pritzel, A., Green, T., Figurnov, M., Ronneberger, O., et al. (2021). Highly accurate protein structure prediction with AlphaFold. *Nature* 596, 583–589. doi:10.1038/s41586-021-03819-2.
- Jungblut, A., Hopfner, K.-P., and Eustermann, S. (2020). Megadalton chromatin remodelers: common principles for versatile functions. *Current Opinion in Structural Biology* 64, 134–144. doi:10.1016/j.sbi.2020.06.024.
- Kalocsay, M., Hiller, N. J., and Jentsch, S. (2009). Chromosome-wide Rad51 Spreading and SUMO-H2A.Z-Dependent Chromosome Fixation in Response to a Persistent DNA Double-Strand Break. *Molecular Cell* 33, 335–343. doi:10.1016/j.molcel.2009.01.016.
- Karl, L. A., Peritore, M., Galanti, L., and Pfander, B. (2022). DNA Double Strand Break Repair and Its Control by Nucleosome Remodeling. *Frontiers in Genetics* 0. doi:10.3389/fgene.2021.821543.
- Kaur, J., Daoud, A., and Eblen, S. T. (2019). Targeting Chromatin Remodeling for Cancer Therapy. *Curr Mol Pharmacol* 12, 215–229. doi:10.2174/1874467212666190215112915.
- Kelley, L. A., Mezulis, S., Yates, C. M., Wass, M. N., and Sternberg, M. J. E. (2015). The Phyre2 web portal for protein modeling, prediction and analysis. *Nat Protoc* 10, 845–858. doi:10.1038/nprot.2015.053.
- Kemble, D. J., McCullough, L. L., Whitby, F. G., Formosa, T., and Hill, C. P. (2015). FACT Disrupts Nucleosome Structure by Binding H2A-H2B with Conserved Peptide Motifs. *Molecular Cell* 60, 294–306. doi:10.1016/j.molcel.2015.09.008.
- Kemble, D. J., Whitby, F. G., Robinson, H., McCullough, L. L., Formosa, T., and Hill, C. P. (2013). Structure of the Spt16 middle domain reveals functional features of the histone chaperone FACT. *The Journal of biological chemistry* 288, 10188–10194. doi:10.1074/jbc.C113.451369.
- Kennedy, S. R., Loeb, L. A., and Herr, A. J. (2012). Somatic mutations in aging, cancer and neurodegeneration. *Mech Ageing Dev* 133, 118–126. doi:10.1016/j.mad.2011.10.009.
- Kim, C. A., and Bowie, J. U. (2003). SAM domains: uniform structure, diversity of function. *Trends in biochemical sciences* 28, 625–628. doi:10.1016/j.tibs.2003.11.001.
- Knoll, K. R., Eustermann, S., Niebauer, V., Oberbeckmann, E., Stoehr, G., Schall, K., et al. (2018). The nuclear actin-containing Arp8 module is a linker DNA sensor driving INO80 chromatin remodeling. *Nat Struct Mol Biol* 25, 823–832. doi:10.1038/s41594-018-0115-8.
- Knop, M., Siegers, K., Pereira, G., Zachariae, W., Winsor, B., Nasmyth, K., et al. (1999). Epitope tagging of yeast genes using a PCR-based strategy: more tags and improved practical routines. *Yeast* 15, 963–972. doi:10.1002/(SICI)1097-0061(199907)15:10B<963::AID-YEA399>3.0.CO;2-W.
- Kunert, F., Metzner, F.J., Jung, J., Höpfler, M., Woike, S., Schall, K., Kostrewa, D., Moldt, M., Chen, J., Bantele S.C.S., Pfander, B., Eustermann, S., Hopfner K. (*in press*). Structural mechanism of extranucleosomal DNA readout by the INO80 complex. *Science Advances*
- Kurat, C. F., Yeeles, J. T. P., Patel, H., Early, A., and Diffley, J. F. X. (2017). Chromatin Controls DNA Replication Origin Selection, Lagging-Strand Synthesis, and Replication Fork Rates. *Molecular Cell* 65, 117–130. doi:10.1016/j.molcel.2016.11.016.
- Kuryan, B. G., Kim, J., Tran, N. N. H., Lombardo, S. R., Venkatesh, S., Workman, J. L., et al. (2012). Histone density is maintained during transcription mediated by the chromatin remodeler RSC and

- histone chaperone NAP1 in vitro. *Proceedings of the National Academy of Sciences of the United States of America* 109, 1931–1936. doi:10.1073/pnas.1109994109.
- Lademann, C. A., Renkawitz, J., Pfander, B., and Jentsch, S. (2017). The INO80 Complex Removes H2A.Z to Promote Presynaptic Filament Formation during Homologous Recombination. *Cell Rep* 19, 1294–1303. doi:10.1016/j.celrep.2017.04.051.
- Lakowicz, J. R. *Principles of Fluorescence Spectroscopy*. 3rd ed. 2006. Springer New York, NY doi:10.1007/978-0-387-46312-4.
- Lee, J., Choi, E. S., Seo, H. D., Kang, K., Gilmore, J. M., Florens, L., et al. (2017). Chromatin remodeller Fun30Fft3 induces nucleosome disassembly to facilitate RNA polymerase II elongation. *Nature Communications* 8, 14527–13. doi:10.1038/ncomms14527.
- Lewis, T. S., Sokolova, V., Jung, H., Ng, H., and Tan, D. (2021). Structural basis of chromatin regulation by histone variant H2A.Z. *Nucleic Acids Research* 49, 11379–11391.
- Li, L.-Y., Guan, Y.-D., Chen, X.-S., Yang, J.-M., and Cheng, Y. (2020). DNA Repair Pathways in Cancer Therapy and Resistance. *Front Pharmacol* 11, 629266. doi:10.3389/fphar.2020.629266.
- Li, X., Liu, K., Li, F., Wang, J., Huang, H., Wu, J., et al. (2012). Structure of C-terminal tandem BRCT repeats of Rtt107 protein reveals critical role in interaction with phosphorylated histone H2A during DNA damage repair. *The Journal of biological chemistry* 287, 9137–9146. doi:10.1074/jbc.M111.311860.
- Liang, B., Qiu, J., Ratnakumar, K., and Laurent, B. C. (2007). RSC Functions as an Early Double-Strand-Break Sensor in the Cell's Response to DNA Damage. *Current Biology* 17, 1432–1437. doi:10.1016/j.cub.2007.07.035.
- Lieleg, C., Ketterer, P., Nuebler, J., Ludwigsen, J., Gerland, U., Dietz, H., et al. (2015). Nucleosome spacing generated by ISWI and CHD1 remodelers is constant regardless of nucleosome density. *Molecular and Cellular Biology* 35, 1588–1605. doi:10.1128/MCB.01070-14.
- Lindahl, T. (1993). Instability and decay of the primary structure of DNA. *Nature* 362, 709–715. doi:10.1038/362709a0.
- Liu, L., and Jiang, T. (2017). Crystal structure of the ATPase-C domain of the chromatin remodeller Fun30 from *Saccharomyces cerevisiae*. *Acta Crystallogr F Struct Biol Commun* 73, 9–15. doi:10.1107/S2053230X16019269.
- Liu, X., Li, M., Xia, X., Li, X., and Chen, Z. (2017). Mechanism of chromatin remodelling revealed by the Snf2-nucleosome structure. *Nature* 544, 440–445. doi:10.1038/nature22036.
- Lodato, N. J., Rampersaud, A., and Waxman, D. J. (2018). Impact of CAR Agonist Ligand TCPOBOP on Mouse Liver Chromatin Accessibility. *Toxicol Sci* 164, 115–128. doi:10.1093/toxsci/kfy070.
- Lorch, Y., Maier-Davis, B., and Kornberg, R. D. (2006). Chromatin remodeling by nucleosome disassembly in vitro. *103*, 3090–3093.
- Lowary, P. T., and Widom, J. (1998). New DNA sequence rules for high affinity binding to histone octamer and sequence-directed nucleosome positioning. *Journal of molecular biology* 276, 19–42. doi:10.1006/jmbi.1997.1494.

- Ludwigsen, J., Pfennig, S., Singh, A. K., Schindler, C., Harrer, N., Forné, I., et al. (2017). Concerted regulation of ISWI by an autoinhibitory domain and the H4 N-terminal tail. *eLife Sciences* 6. doi:10.7554/eLife.21477.
- Luger, K., Mäder, A. W., Richmond, R. K., Sargent, D. F., and Richmond, T. J. (1997). Crystal structure of the nucleosome core particle at 2.8 Å resolution. *Nature* 389, 251–260. doi:10.1038/38444.
- Luger, K., Rechsteiner, T. J., and Richmond, T. J. (1999). Preparation of nucleosome core particle from recombinant histones. *Methods in enzymology* 304, 3–19. doi:10.1016/s0076-6879(99)04003-3.
- Maeshima, K., Hihara, S., and Eltsov, M. (2010). Chromatin structure: does the 30-nm fibre exist in vivo? *Curr Opin Cell Biol* 22, 291–297. doi:10.1016/j.ceb.2010.03.001.
- Markert, J., Zhou, K., and Luger, K. (2021). SMARCAD1 is an ATP-dependent histone octamer exchange factor with de novo nucleosome assembly activity. *Science Advances* 7. doi:10.1126/sciadv.abk2380.
- McBryant, S. J., Park, Y.-J., Abernathy, S. M., Laybourn, P. J., Nyborg, J. K., and Luger, K. (2003). Preferential binding of the histone (H3-H4)₂ tetramer by NAP1 is mediated by the amino-terminal histone tails. *The Journal of biological chemistry* 278, 44574–44583. doi:10.1074/jbc.M305636200.
- McGinty, R. K., and Tan, S. (2015). Nucleosome structure and function. *Chem Rev* 115, 2255–2273. doi:10.1021/cr500373h.
- Meijsing, S. H., and Ehrenhofer-Murray, A. E. (2001). The silencing complex SAS-I links histone acetylation to the assembly of repressed chromatin by CAF-I and Asf1 in *Saccharomyces cerevisiae*. *Genes Dev* 15, 3169–3182. doi:10.1101/gad.929001.
- Mimitou, E. P., Yamada, S., and Keeney, S. (2017). A global view of meiotic double-strand break end resection. *Science* 355, 40–45. doi:10.1126/science.aak9704.
- Morgan, A., LeGresley, S., and Fischer, C. (2021). Remodeler Catalyzed Nucleosome Repositioning: Influence of Structure and Stability. *International Journal of Molecular Sciences* 2021, Vol. 22, Page 76 22, 76. doi:10.3390/ijms22010076.
- Morillo-Huesca, M., Clemente-Ruiz, M., Andújar, E., and Prado, F. (2010). The SWR1 histone replacement complex causes genetic instability and genome-wide transcription misregulation in the absence of H2A.Z. *PLoS One* 5, e12143. doi:10.1371/journal.pone.0012143.
- Morrison, A. J., Highland, J., Krogan, N. J., Arbel-Eden, A., Greenblatt, J. F., Haber, J. E., et al. (2004). INO80 and gamma-H2AX interaction links ATP-dependent chromatin remodeling to DNA damage repair. *Cell* 119, 767–775.
- Mueller-Planitz, F., Klinker, H., Ludwigsen, J., and Becker, P. B. (2013). The ATPase domain of ISWI is an autonomous nucleosome remodeling machine. *Nat Struct Mol Biol* 20, 82–89. doi:10.1038/nsmb.2457.
- Nakagawa, T., Bulger, M., Muramatsu, M., and Ito, T. (2001). Multistep Chromatin Assembly on Supercoiled Plasmid DNA by Nucleosome Assembly Protein-1 and ATP-utilizing Chromatin Assembly and Remodeling Factor. *Journal of Biological Chemistry* 276, 27384–27391. doi:10.1074/jbc.M101331200.

- Nakamura, T. M., Du, L.-L., Redon, C., and Russell, P. (2004). Histone H2A Phosphorylation Controls Crb2 Recruitment at DNA Breaks, Maintains Checkpoint Arrest, and Influences DNA Repair in Fission Yeast. *Molecular and Cellular Biology* 24, 6215–6230. doi:10.1128/MCB.24.14.6215-6230.2004.
- Neves-Costa, A., Will, W. R., Vetter, A. T., Miller, J. R., and Varga-Weisz, P. (2009). The SNF2-family member Fun30 promotes gene silencing in heterochromatic loci. *PLoS One* 4, e8111. doi:10.1371/journal.pone.0008111.
- Nishino, Y., Eltsov, M., Joti, Y., Ito, K., Takata, H., Takahashi, Y., et al. (2012). Human mitotic chromosomes consist predominantly of irregularly folded nucleosome fibres without a 30-nm chromatin structure. *The EMBO Journal* 31, 1644–1653. doi:10.1038/emboj.2012.35.
- Niu, Q., Wang, W., Wei, Z., Byeon, B., Das, A. B., Chen, B.-S., et al. (2020). Role of the ATP-dependent chromatin remodeling enzyme Fun30/Smardc1 in the regulation of mRNA splicing. *Biochemical and Biophysical Research Communications* 526, 453–458. doi:10.1016/j.bbrc.2020.02.175.
- Nodelman, I. M., Shen, Z., Levendosky, R. F., and Bowman, G. D. (2021). Autoinhibitory elements of the Chd1 remodeler block initiation of twist defects by destabilizing the ATPase motor on the nucleosome. *Proceedings of the National Academy of Sciences of the United States of America* 118, e2014498118. doi:10.1073/pnas.2014498118.
- O'Driscoll, M. (2012). Diseases associated with defective responses to DNA damage. *Cold Spring Harbor Perspectives in Biology* 4, a012773. doi:10.1101/cshperspect.a012773.
- Ohouo, P. Y., Bastos de Oliveira, F. M., Liu, Y., Ma, C. J., and Smolka, M. B. (2013). DNA-repair scaffolds dampen checkpoint signalling by counteracting the adaptor Rad9. *Nature* 493, 120–124. doi:10.1038/nature11658.
- Ohshima, H., Yermilov, V., Yoshie, Y., and Rubio, J. (1999). “DNA Damage Induced by Reactive Nitrogen Species,” in *Advances in DNA Damage and Repair* (Boston, MA), pp329–339. doi:https://doi.org/10.1007/978-1-4615-4865-2_27.
- Ortega-Arroyo, J., and Kukura, P. (2012). Interferometric scattering microscopy (iSCAT): new frontiers in ultrafast and ultrasensitive optical microscopy. *Phys Chem Chem Phys* 14, 15625–15636. doi:10.1039/c2cp41013c.
- Oudet, P., Gross-Bellard, M., and Chambon, P. (1975). Electron microscopic and biochemical evidence that chromatin structure is a repeating unit. *Cell* 4, 281–300. doi:10.1016/0092-8674(75)90149-x.
- Papamichos-Chronakis, M., Watanabe, S., Rando, O. J., and Peterson, C. L. (2011). Global regulation of H2A.Z localization by the INO80 chromatin-remodeling enzyme is essential for genome integrity. *Cell* 144, 200–213. doi:10.1016/j.cell.2010.12.021.
- Park, Y.-J., Chodaparambil, J. V., Bao, Y., McBryant, S. J., and Luger, K. (2005). Nucleosome assembly protein 1 exchanges histone H2A-H2B dimers and assists nucleosome sliding. *The Journal of biological chemistry* 280, 1817–1825. doi:10.1074/jbc.M411347200.
- Paull, T. T., Rogakou, E. P., Yamazaki, V., Kirchgessner, C. U., Gellert, M., and Bonner, W. M. (2000). A critical role for histone H2AX in recruitment of repair factors to nuclear foci after DNA damage. *Current Biology* 10, 886–895. doi:10.1016/s0960-9822(00)00610-2.

- Peritore, M., Reuswig, K.-U., Bantele, S. C. S., Straub, T., and Pfander, B. (2021). Strand-specific ChIP-seq at DNA breaks distinguishes ssDNA versus dsDNA binding and refutes single-stranded nucleosomes. *Molecular Cell* 81, 1841–1853.e4. doi:10.1016/j.molcel.2021.02.005.
- Pettersen, E. F., Goddard, T. D., Huang, C. C., Meng, E. C., Couch, G. S., Croll, T. I., et al. (2021). UCSF ChimeraX: Structure visualization for researchers, educators, and developers. *Protein science : a publication of the Protein Society* 30, 70–82. doi:10.1002/pro.3943.
- Pfeiffer, P. (1998). The mutagenic potential of DNA double-strand break repair. *Toxicol Lett* 96-97, 119–129. doi:10.1016/s0378-4274(98)00058-7.
- Ponting, C. P. (1995). SAM: a novel motif in yeast sterile and Drosophila polyhomeotic proteins. *Protein science : a publication of the Protein Society* 4, 1928–1930. doi:10.1002/pro.5560040927.
- Prasad, R., D'Arcy, S., Hada, A., Luger, K., and Bartholomew, B. (2016). Coordinated Action of Nap1 and RSC in Disassembly of Tandem Nucleosomes. *Molecular and Cellular Biology* 36, 2262–2271. doi:10.1128/MCB.00195-16.
- Redon, C., Pilch, D., Rogakou, E., Sedelnikova, O., Newrock, K., and Bonner, W. (2002). Histone H2A variants H2AX and H2AZ. *Current opinion in genetics & development* 12, 162–169. doi:10.1016/s0959-437x(02)00282-4.
- Reyes, A. A., Marcum, R. D., and He, Y. (2021). Structure and Function of Chromatin Remodelers. *Journal of molecular biology* 433, 166929.
- Rothstein, R. J. (1983). One-step gene disruption in yeast. *Methods in enzymology* 101, 202–211.
- Rowbotham, S. P., Barki, L., Neves-Costa, A., Santos, F., Dean, W., Hawkes, N., et al. (2011). Maintenance of Silent Chromatin through Replication Requires SWI/SNF-like Chromatin Remodeler SMARCAD1. *Molecular Cell* 42, 285–296. doi:10.1016/j.molcel.2011.02.036.
- Safaric, B., Chacin, E., Scherr, M. J., Rajappa, L., Gebhardt, C., Kurat, C. F., et al. (2022). The fork protection complex recruits FACT to reorganize nucleosomes during replication. *Nucleic Acids Research* 50, 1317–1334. doi:10.1093/nar/gkac005.
- Saha, A., Wittmeyer, J., and Cairns, B. R. (2002). Chromatin remodeling by RSC involves ATP-dependent DNA translocation. *Genes Dev* 16, 2120–2134. doi:10.1101/gad.995002.
- Santisteban, M. S., Kalashnikova, T., and Smith, M. M. (2000). Histone H2A.Z Regulates Transcription and Is Partially Redundant with Nucleosome Remodeling Complexes. *Cell* 103, 411–422. doi:10.1016/S0092-8674(00)00133-1.
- Schiffrin, B., Radford, S. E., Brockwell, D. J., and Calabrese, A. N. (2020). PyXlinkViewer: A flexible tool for visualization of protein chemical crosslinking data within the PyMOL molecular graphics system. *Protein science : a publication of the Protein Society* 29, 1851–1857. doi:10.1002/pro.3902.
- Schindelin, J., Arganda-Carreras, I., Frise, E., Kaynig, V., Longair, M., Pietzsch, T., et al. (2012). Fiji: an open-source platform for biological-image analysis. *Nature methods* 9, 676–682. doi:10.1038/nmeth.2019.
- Schneider, C. A., Rasband, W. S., and Eliceiri, K. W. (2012). NIH Image to ImageJ: 25 years of image analysis. *Nature methods* 9, 671–675. doi:10.1038/nmeth.2089.

- Schultz, J., Ponting, C. P., Hofmann, K., and Bork, P. (1997). SAM as a protein interaction domain involved in developmental regulation. *Protein science : a publication of the Protein Society* 6, 249–253. doi:10.1002/pro.5560060128.
- Scully, R., Panday, A., Elango, R., and Willis, N. A. (2019). DNA double-strand break repair-pathway choice in somatic mammalian cells. *Nature Reviews Molecular Cell Biology* 20, 698–714. doi:10.1038/s41580-019-0152-0.
- Shen, X., Ranallo, R., Choi, E., and Wu, C. (2003). Involvement of actin-related proteins in ATP-dependent chromatin remodeling. *Molecular Cell* 12, 147–155. doi:10.1016/s1097-2765(03)00264-8.
- Shim, E. Y., Hong, S. J., Oum, J.-H., Yanez, Y., Zhang, Y., and Lee, S. E. (2007). RSC mobilizes nucleosomes to improve accessibility of repair machinery to the damaged chromatin. *Molecular and Cellular Biology* 27, 1602–1613.
- Shim, E. Y., Ma, J.-L., Oum, J.-H., Yanez, Y., and Lee, S. E. (2005). The Yeast Chromatin Remodeler RSC Complex Facilitates End Joining Repair of DNA Double-Strand Breaks†. *Molecular and Cellular Biology* 25, 3934–3944. doi:10.1128/mcb.25.10.3934-3944.2005.
- Shroff, R., Arbel-Eden, A., Pilch, D., Ira, G., Bonner, W. M., Petrini, J. H., et al. (2004). Distribution and dynamics of chromatin modification induced by a defined DNA double-strand break. *Current Biology* 14, 1703–1711. doi:10.1016/j.cub.2004.09.047.
- Singer, M. S., Kahana, A., Wolf, A. J., Meisinger, L. L., Peterson, S. E., Goggin, C., et al. (1998). Identification of high-copy disruptors of telomeric silencing in *Saccharomyces cerevisiae*. *Genetics* 150, 613–632. doi:10.1093/genetics/150.2.613.
- Sinha, R. P., and Häder, D. P. (2002). UV-induced DNA damage and repair: a review. *Photochem Photobiol Sci* 1, 225–236. doi:10.1039/b201230h.
- Smith, S., and Stillman, B. (1991). Stepwise assembly of chromatin during DNA replication in vitro. *The EMBO Journal* 10, 971–980. doi:10.1002/j.1460-2075.1991.tb08031.x.
- Sonntag, von, C. (2006). *Free-Radical-Induced DNA Damage and Its Repair*. ed.S. Schreck Berlin Heidelberg New York: Springer Available at: <https://link.springer.com/book/10.1007/3-540-30592-0>.
- Steglich, B., Strålfors, A., Khorosjutina, O., Persson, J., Smialowska, A., Javerzat, J.-P., et al. (2015). The Fun30 chromatin remodeler Fft3 controls nuclear organization and chromatin structure of insulators and subtelomeres in fission yeast. *PLoS Genet* 11, e1005101. doi:10.1371/journal.pgen.1005101.
- Stielow, B., Zhou, Y., Cao, Y., Simon, C., Pogoda, H.-M., Jiang, J., et al. (2021). The SAM domain-containing protein 1 (SAMD1) acts as a repressive chromatin regulator at unmethylated CpG islands. *Science Advances* 7. doi:10.1126/sciadv.abf2229.
- Strålfors, A., Walfridsson, J., Bhuiyan, H., and Ekwall, K. (2011). The FUN30 chromatin remodeler, Fft3, protects centromeric and subtelomeric domains from euchromatin formation. *PLoS Genet* 7, e1001334. doi:10.1371/journal.pgen.1001334.
- Szerlong, H., Hinata, K., Viswanathan, R., Erdjument-Bromage, H., Tempst, P., and Cairns, B. R. (2008). The HSA domain binds nuclear actin-related proteins to regulate chromatin-remodeling ATPases. *Nat Struct Mol Biol* 15, 469–476. doi:10.1038/nsmb.1403.

- Takata, H., Hanafusa, T., Mori, T., Shimura, M., Iida, Y., Ishikawa, K., et al. (2013). Chromatin compaction protects genomic DNA from radiation damage. *PLoS One* 8, e75622. doi:10.1371/journal.pone.0075622.
- Taneja, N., and Grewal, S. I. S. (2017). Shushing histone turnover: It's FUN protecting epigenome-genome. *Cell Cycle* 16, 1731–1732. doi:10.1080/15384101.2017.1360651.
- Terui, R., Nagao, K., Kawasoe, Y., Taki, K., Higashi, T. L., Tanaka, S., et al. (2018). Nucleosomes around a mismatched base pair are excluded via an Msh2-dependent reaction with the aid of SNF2 family ATPase Smarcd1. *Genes Dev* 32, 806–821. doi:10.1101/gad.310995.117.
- Tremethick, D. J. (2007). Higher-order structures of chromatin: the elusive 30 nm fiber. *Cell* 128, 651–654. doi:10.1016/j.cell.2007.02.008.
- Troshin, P. V., Procter, J. B., and Barton, G. J. (2011). Java bioinformatics analysis web services for multiple sequence alignment--JABAWS:MSA. *Bioinformatics* 27, 2001–2002. doi:10.1093/bioinformatics/btr304.
- Tsukuda, T., Fleming, A. B., Nickoloff, J. A., and Osley, M. A. (2005). Chromatin remodelling at a DNA double-strand break site in *Saccharomyces cerevisiae*. *Nature* 438, 379–383. doi:10.1038/nature04148.
- Tsunaka, Y., Kajimura, N., Tate, S.-I., and Morikawa, K. (2005). Alteration of the nucleosomal DNA path in the crystal structure of a human nucleosome core particle. *Nucleic Acids Research* 33, 3424–3434. doi:10.1093/nar/gki663.
- van Attikum, H., Fritsch, O., and Gasser, S. M. (2007). Distinct roles for SWR1 and INO80 chromatin remodeling complexes at chromosomal double-strand breaks. *The EMBO Journal* 26, 4113–4125.
- van Attikum, H., Fritsch, O., Hohn, B., and Gasser, S. M. (2004). Recruitment of the INO80 complex by H2A phosphorylation links ATP-dependent chromatin remodeling with DNA double-strand break repair. *Cell* 119, 777–788.
- Varadi, M., Anyango, S., Deshpande, M., Nair, S., Natassia, C., Yordanova, G., et al. (2022). AlphaFold Protein Structure Database: massively expanding the structural coverage of protein-sequence space with high-accuracy models. *Nucleic Acids Research* 50, D439–D444. doi:10.1093/nar/gkab1061.
- Verschueren, H. (1985). Interference reflection microscopy in cell biology: methodology and applications. *Journal of Cell Science* 75, 279–301. doi:10.1242/jcs.75.1.279.
- Wach, A., Brachat, A., Pöhlmann, R., and Philippsen, P. (1994). New heterologous modules for classical or PCR-based gene disruptions in *Saccharomyces cerevisiae*. *Yeast* 10, 1793–1808. doi:10.1002/yea.320101310.
- Wagner, F. R., Dienemann, C., Wang, H., Stützer, A., Tegunov, D., Urlaub, H., et al. (2020). Structure of SWI/SNF chromatin remodeler RSC bound to a nucleosome. *Nature* 579, 448–451. doi:10.1038/s41586-020-2088-0.
- Wang, W., Daley, J. M., Kwon, Y., Krasner, D. S., and Sung, P. (2017). Plasticity of the Mre11-Rad50-Xrs2-Sae2 nuclease ensemble in the processing of DNA-bound obstacles. *Genes Dev* 31, 2331–2336.
- Watanabe, S., Radman-Livaja, M., Rando, O. J., and Peterson, C. L. (2013). A Histone Acetylation Switch Regulates H2A.Z Deposition by the SWR-C Remodeling Enzyme. *Science* 340, 195–199. doi:10.1126/science.1229758.

- White, C. L., Suto, R. K., and Luger, K. (2001). Structure of the yeast nucleosome core particle reveals fundamental changes in internucleosome interactions. *The EMBO Journal* 20, 5207–5218. doi:10.1093/emboj/20.18.5207.
- Wiest, N. E., Houghtaling, S., Sanchez, J. C., Tomkinson, A. E., and Osley, M. A. (2017). The SWI/SNF ATP-dependent nucleosome remodeler promotes resection initiation at a DNA double-strand break in yeast. *Nucleic Acids Research* 45, 5887–5900. doi:10.1093/nar/gkx221.
- Xia, X., Liu, X., Li, T., Fang, X., and Chen, Z. (2016). Structure of chromatin remodeler Swi2/Snf2 in the resting state. *Nat Struct Mol Biol* 23, 722–729. doi:10.1038/nsmb.3259.
- Ye, Y., Wu, H., Chen, K., Clapier, C. R., Verma, N., Zhang, W., et al. (2019). Structure of the RSC complex bound to the nucleosome. *Science (New York, N.Y.)* 366, 838–843. doi:10.1126/science.aay0033.
- Young, G., Hundt, N., Cole, D., Fineberg, A., Andrecka, J., Tyler, A., et al. (2018). Quantitative mass imaging of single biological macromolecules. *Science (New York, N.Y.)* 360, 423–427. doi:10.1126/science.aar5839.
- Zhang, H., Roberts, D. N., and Cairns, B. R. (2005). Genome-wide dynamics of Htz1, a histone H2A variant that poises repressed/basal promoters for activation through histone loss. *Cell* 123, 219–231.
- Zhou, B. B., and Elledge, S. J. (2000). The DNA damage response: putting checkpoints in perspective. *Nature* 408, 433–439. doi:10.1038/35044005.

Appendix

Abbreviations

2D	2-dimensional
3C	3C protease cleavage site
3D	3-dimensional
5'-FOA	5'-fluoroorotic acid
9-1-1	Rad9-Hus1-Rad1 complex (in yeast: Rad17-Mec3-Ddc1)
A	adenine
ADP	adenosine diphosphate
AP	affinity purification
Arp	actin related protein
ATP	adenosine-5'-triphosphate
ATP _γ S	adenosine-5'-(3-thiotriphosphate)
BS3	Bis(sulfosuccinimidyl)suberat
BSA	bovine serum albumin
C	cytosine
CDK	cyclin-dependent kinase
Chr	chromosome
ChIP	chromatin Immunoprecipitation
CPT	camptothecin
CRISPR	clustered regularly interspaced short palindromic repeats
CUE	coupling of ubiquitin to ER degradation
DDR	DNA damage response
DMSO	dimethyl sulfoxide
DNA	deoxyribonucleic acid
ds	double-stranded
DSB	double-strand break
DTT	dithiothreitol
EDTA	ethylenediaminetetraacetic acid
Etbr	ethidiumbromide
G	guanine
GST	glutathione S-transferase
HEPES	4-(2-hydroxyethyl)-1-piperazineethanesulfonic acid
HR	homologous recombination
HRP	horseradish peroxidase
IEX	ion exchange chromatography
IMAC	Immobilized metal affinity chromatography
IP	immunoprecipitation
IR	ionizing radiation
LB	lysogeny broth
MES	2-(N-morpholino)ethanesulfonic acid
MOPS	3-(N-morpholino)propanesulfonic acid
MS	mass spectrometry

NHEJ	non-homologous end joining
OD	optical density
PAGE	Polyacrylamide gel electrophoresis
PBS	phosphate-buffered saline
PCR	polymerase chain reaction
PEG	polyethylene glycol
pLDDT	predicted Local Distance Difference Test (1-100, higher = better)
PTM	post-translational modification
qPCR	quantitative PCR
ROS	reactive oxygen species
RPA	replication protein A
S-CDK	Cdc28 in complex with Clb5/6
SC	synthetic complete
SDS	sodium dodecyl sulfate
ss	single-stranded
SWI/SNF	Switch/Sucrose non-fermentable
T	thymine
TBS	Tris-buffered saline
Tris	tri(hydroxymethyl)aminomethane
Ura	uracil
UV	ultra violet
WT	wildtype
YP	yeast extract/peptone
γH2A	histone H2A phosphorylated on serine 129 (<i>S. cerevisiae</i>)

Prefixes and units

G	giga (10 ⁹)	nt	nucleotide(s)	h	hour(s)
M	mega (10 ⁶)	bp	base pair(s)	min	minute(s)
k	kilo (10 ³)	kb	kilobases	sec	second(s)
m	milli (10 ⁻³)	Da	Dalton	L	liter(s)
μ	micro (10 ⁻⁶)	°C	degrees Celsius	g	gram
n	nano (10 ⁻⁹)	V	Volt	M	molar

Amino acid abbreviations

amino acid	one-letter code	three-letter code
alanine	A	Ala
cysteine	C	Cys
aspartic acid	D	Asp
glutamic acid	E	Glu
phenylalanine	F	Phe
glycine	G	Gly
histidine	H	His
isoleucine	I	Ile

lysine	K	Lys
leucine	L	Leu
methionine	M	Met
asparagine	N	Asn
proline	P	Pro
glutamine	Q	Gln
arginine	R	Arg
serine	S	Ser
threonine	T	Thr
valine	V	Val
tryptophan	W	Trp
tyrosine	Y	Tyr

Acknowledgements

First and foremost, I would like to express my deep gratitude to Prof. Boris Pfander, my supervisor, mentor and guide through the PhD jungle. Thank you for always having an open ear for my ideas, giving advice, discussing my own and other people's data and supporting my scientific development. You created a wonderful work group with an inspiring atmosphere of support and attention and I am sure you are going to continue to do great science (and win volleyball tournaments)! Thank you for the great time in Martinsried and I wish you all the best for the new chapter of the lab in Cologne!

I thank my PhD committee with Prof. Julian Stinglele, PD Dr. Gregor Witte, Prof. Klaus Förstemann, Prof. Johannes Stigler and particularly my doctoral supervisor at the LMU, Prof. Elena Conti. Furthermore, I thank the members of my thesis advisory committee Prof. Christoph Kurat, Prof. Elena Conti, Prof. Petr Cejka and also non-TAC Prof. Karl-Peter Hopfner for open discussions, valuable input and support at all stages of my project.

Similar thanks go out to the R4-seminar-group, with the Duderstadt, Stinglele, Kurat and Hamperl labs, that I had the pleasure to co-organize: It was a great forum for discussing research and exchanging ideas and experience with all of you! I want to especially highlight here Lional and Barbara from the Duderstadt lab, whose advice on histone octamer and protein purification was invaluable. And also you, Erika and Priyanka from the Kurat lab, thank you for exchanging proteins and protocols with me and I keep my fingers crossed for your projects! A big thank you also to Till Bartke and Benjamin Foster for helping me get started with histones and nucleosomes, I learnt a lot from you and it has been a pleasure working with you!

Thank you to all the members of the junior group wing at the Max Planck Institute of Biochemistry, to our helpers in the media kitchen Massimo, Beate and Benji for supplying media, buffers and plates. And a big thank you to our lab manager Bianca for being so reachable, efficient and quick with any administrative task and in general keeping everything running in LM.

Regarding the Max Planck Institute of Biochemistry, I want to thank for the collaborative atmosphere and openness, for example enabling me easy access to the Conti-department plate reader. I would also like to acknowledge the outstanding scientific support by the core facilities, especially the biochemistry core facility headed by Stephan Uebel, thank you for advice on biophysical measurements and for help with setting up an oxygen-free bubble to work in.

Thanks to the protein production headed by Dr. Sabine Suppmann for providing advice and protein, and the proteomics core facility headed by Dr. Barbara Steigenberger, with helpful suggestions and analysis of XL-MS experiments. Thank you to Dr. Daniel Bollschweiler for introducing me to mass photometry. Also, thanks to Jérôme Basquin and his team from the Crystallization facility, we tried very hard, the SAM-key was just too soluble, but your advice and introduction to AlphaFold and PyMol have been invaluable to me and my project.

Thank you to the IMPRS coordination office with Hans-Jörg Schäffer, Ingrid Wolf and Marta Cipińska, for always having an open ear and for organizing such a rich program.

Another thank you goes also to Dr. Elizabeth Schroeder-Reiter for the great job she is doing in coordinating the IRTG-1064 and for bringing together chromatin aficionados for scientific and non-scientific events, especially the Serenissima-Retreat 2022 was an amazing experience.

And of course, a really big thank you goes to all the past and present members of the Pfander lab, #Sharkaromyces! It was a lot of fun to work side by side with you all! Thank you to our technicians Uschi and Sandra for their invaluable support. Thanks to my students Ermioni, Paul and Tobi, it was really rewarding teaching you, I learnt a lot myself and you helped me with my project. Kalle, thank you for being my bench neighbour in the Pfander-lab outpost, and for sharing your vast experience with me in your wonderful, calm and concentrated way. Julia, thank you for always being kind and helpful and keeping me company in the first half of the day and thank you for organizing lab and most importantly lab events. Susi, thank you for starting the FUN project and for spreading your enthusiasm in the lab. Martina, thanks for being a wonderful office mate, the bringer of cakes and the heart and soul of the volleyball-team. Your plants made life in the lab greener and made my summers there like in a jungle. Lorenzo, thank you for being available whenever I needed help or advice with biochemistry or really anything. I really enjoyed us working side-by-side in the biochem-cave. Thanks for so many great discussions (scientific and non-scientific, some even philosophic), funny memories and for sharing my enthusiasm for “Ina and the birds”! Thanks to you both, for giving the lab a little Italian touch!

Last, but not least, I want to thank my friends and family that supported me throughout this journey. Thank you to my in-laws Sabine and Heribert, for making me part of the family from the first moment. Thank you, Simone, for your spontaneous ideas and funny car and dinner conversations. A very warm and special thank you Irmina, Mama and Papa, for your love, your constant support, believing in me and always being there for me. Thanks for trying to understand what I am doing, and, even if you did not get it all, being proud of me.

Ina, I am lacking the words to tell you, how much I want to thank you and how much you mean to me. I try nevertheless: When I started this special journey of pursuing a PhD you were already by my side and I could hardly imagine life without you, so not long after starting, I asked you to marry me. When you said yes then and when you repeated it at our two wedding days, you made me incredibly happy. Thank you not only for your love and affection, for understanding and supporting me but also for challenging me and making me grow. A special thanks for bringing the birds into our lives and thank you for so many wonderful memories. I really look forward to spending our future together. Together we can do anything. I love you.